UNIVERSITEIT VAN PRETORIA
UNIVERSITY OF PRETORIA
YUNIBESITHI YA PRETORIA

Microbial fuel cells: The effect of granular activated carbon and graphite as growth substrates on bioelectrogenesis by *Geobacter sulfurreducens*

Xandra van Heerden

2019

UNIVERSITEIT VAN PRETORIA
UNIVERSITY OF PRETORIA
YUNIBESITHI YA PRETORIA

Microbial fuel cells: The effect of granular activated carbon and graphite as growth substrates on bioelectrogenesis by *Geobacter sulfurreducens*

Xandra van Heerden

Submitted in partial fulfilment of the requirements for the degree of *Philosophiae Doctor* (Chemical Engineering) in the Faculty of Engineering, the Built Environment and Information Technology, University of Pretoria, Pretoria, South Africa

2019

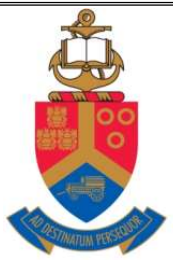

UNIVERSITEIT VAN PRETORIA
UNIVERSITY OF PRETORIA
YUNIBESITHI YA PRETORIA

Microbial fuel cells: The effect of granular activated carbon and graphite as growth substrates on bioelectrogenesis by *Geobacter sulfurreducens*

By: Xandra van Heerden
Supervisor: Dr Heinrich Badenhorst
Department: Chemical Engineering
Degree: PhD (Chemical Engineering)

Synopsis

There is an increasing demand for environmentally sustainable alternative energy sources as the supply of fossil fuels dwindles and the concern about our carbon footprint continues to increase. Bioelectrogenesis is a process that directly converts biomass into electricity. Bioelectrochemical systems hold great potential to breach the gap into sustainable and green energy. Bioelectrochemical systems can be thought of as fuel cells with regenerative, living microbial catalysts.

The aim of this investigation was to study the effect of the addition of carbon particles to the anodic chamber of a microbial fuel cell (MFC) containing *Geobacter sulfurreducens* in order to change the conditions of the MFC. The effect of the crystallinity of the carbon on the efficiency of the cell was evaluated. A crystalline carbon in the form of graphite particles was added to the initial growth media to increase the electrical conductivity of the anolyte. An amorphous carbon, granular activated carbon (GAC) particles, was added to the growth media to increase microbial growth. It was then decided which parameter needed to be prioritised if only one carbon substrate were to be added. A mixture of the two carbon substrates was added to the growth media to investigate what, if both the microbial growth and the conductivity in the MFC were increased, the effect would be on bioelectrogenesis. The effect of various growth periods of *G. sulfurreducens* prior to inoculation into the MFCs was also investigated. The

experiments was thus limited to screening the effects of the bacteria growth media and growth time for the different carbon substrates and mixtures thereof.

An increased growth period, 4 months, appeared to be more advantageous for bioelectrogenesis. The addition of GAC particles proved to be advantageous to the microbial growth as the growth was improved nearly 6 fold compared to the control MFC containing *G. sulfurreducens* only. FE-SEM imaging and BET analyses confirmed that a large and rough surface area is ideal due to the ample attachment sites available for microbes. The biofilm thickens after only 3 weeks of growth.

It was evident that the addition of GAC particles to the system was beneficial for bioelectrogenesis. The maximum power density of the MFC containing GAC particles with a 4 months growth period was increased by 6 times compared to the MFC containing pure *G. sulfurreducens*. The average total energy generated by the MFC containing GAC particles was also 41 % higher than that of the pure *G. sulfurreducens* control MFC. The overall outputs were improved by the mere addition of GAC particles to the growth media.

The addition of the graphite particles to the system had to the opposite effect. The microbial growth was inhibited, which directly caused the bioelectrogenesis to be extremely low. The average energy density of the graphite containing MFC is almost equal to the blank MFC, i.e., the MFC containing no microbial community. This suggests that growth must be prioritised over conductivity. Without microbial growth, increased conductivity does not help the system.

The energy density of the MFC comprising the 1:1 mixture of graphite and GAC particles as growth substrate increased the average energy density of the control MFC by 134 %. The addition of the mixture of the two carbon substrates showed a synergistic effect since adding only pure GAC to the MFC increased the average energy density by 41 % compared to the control MFC, and by the addition of pure graphite particles to the MFC had the opposite effect of producing lower energy density than the control MFC. Therefore, mixing the two neat carbon sources and adding the mixture to the MFC, caused the synergistic effect of increasing the energy density of the MFC by more than triple than that of the MFC containing only pure GAC. With the mixture of GAC and graphite particles, both parameters were improved, i.e., microbial growth was improved compared with the control MFC and the conductivity in the

system was increased, increasing the electron transfer efficiency and consequently the bioelectrogenesis.

One of the industrial applications of MFC systems where the impact can be maximised, is in waste water treatment, since the outcomes include both power generation and the removal of organic compounds in waste streams. It is well documented that numerous microbial fuel cells generate power by oxidation of compounds in wastewater. One study predicts, assuming 100 % efficiency, that the wastewater from a town of 150 000 people could be used to generate approximately 2.3 MW of power; but realistically, a power of 0.5 MW can be expected. From this review it is mentioned that up to 80 % of the chemical oxygen demand (COD) of the wastewater can be removed by using an MFC and that the power generated could be used on site to power additional wastewater treatment.

The second most promising application is the use of MFC systems in the biomedical industry as implantable devices. Currently most implanted biomedical devices are powered by batteries, which need to be recharged or replaced, necessitating additional surgeries for the patients. A method for continual electricity generation within the body would revolutionise biomedical devices. The use of MFCs as power sources for implantable devices in humans is a promising focus point. MFCs offer advantages over existing technologies such as lithium-ion batteries in implantable devices such as the heart pacemakers. The MFC would ideally use a biological metabolite fuel source (i.e. glucose or lactate) which is available in physiological fluids such as blood. It is unlikely that MFCs can replace the enzymatic glucose sensors that are currently used, but it was found that a well-designed MFC system, operating in a continuous flow regime, is implanted into the large intestines and utilises the natural flora of microbes within the intestines, could provide adequate power for cardiac pacing. This is one of the most promising future research areas. There are several variables that impact MFC power outputs, therefore extensive future research is still required. The one major problem that needs to be addressed is the longevity of many types of MFCs, most of which would currently be capable of meeting demands for biomedical devices implanted for short-term applications only.

Keywords: Microbial fuel cell, *Geobacter sulfurreducens*, Granular activated carbon, graphite, bioelectrogenesis

UNIVERSITEIT VAN PRETORIA
UNIVERSITY OF PRETORIA
YUNIBESITHI YA PRETORIA

Acknowledgements

"For from Him and through Him and for Him
are all things. To Him be the glory forever! Amen."
~ Romans 11:36 ~

"This also comes from the Lord Almighty,
whose plan is wonderful, whose wisdom is magnificent."
~ Isaiah 28:29 ~

To my **Heavenly Father**, for giving the strength and wisdom and for His guidance and grace.

My dearest husband, **Jacques van Heerden**, for his continued encouragement, his constant support, committed love and personal sacrifices so that I could pursue my dreams.
"The best and most beautiful things in this world cannot be seen or even heard but must be felt with the heart." ~ Helen Keller ~

My supervisor, **Dr Heinrich Badenhorst**, for the opportunity to work with him, for his guidance, encouragement and academic advice.
"If your actions inspire others to dream more, learn more, do more and become more, you are a leader" ~ John Quincy Adams ~

To **Prof. Johan Labuschagné**, a special thank you for all his advice and continued support throughout my studies. Without him, I would not have come this far.
"A mentor is someone who sees more talent and ability within you, than you see in yourself, and helps bring it out of you." ~ Bob Proctor ~

To Researcher, **Mr Paul Sonnendecker**, for his assistance in the design and manufacturing of the microbial fuel cell and the assistance with all the equipment. To **Prof. Philip Crouse**, for the use of his equipment and document editing. Without them this research could not be possible.

"Unselfish and noble actions are the most radiant pages in the biography of souls."

~ David Thomas ~

To the Centre for Microbial Ecology and Genomics (CMEG), Genomic Research Institute, **Prof. Don Cowan** and **Dr Jean-Baptiste Ramond**, for the expertise and guidance with the field of microbiology and for the use of their equipment.

"I can no other answer make, but, thanks, and thanks." ~ William Shakespeare ~

To the **National Research Foundation,** the **SARChI Chair in Carbon Technology and Materials, Prof. Ncholu Manyala** and **Dr Heinrich Badenhorst**, for the financial support throughout the duration of my doctoral studies.

"Education is the most powerful weapon which you can use to change the world."

~ Nelson Mandela ~

Lastly, I would like to thank my **whole family** and dearest friend, **Suzette Seymore**, for all their encouragement and motivation during my doctoral studies.

"A word of encouragement during a failure is worth more than an hour of praise after success." ~ Unknown ~

"Commit your work to the Lord, and your plans will be established."

~ Proverbs 16:3 ~

UNIVERSITEIT VAN PRETORIA
UNIVERSITY OF PRETORIA
YUNIBESITHI YA PRETORIA

Declaration

DECLARATION BY CANDIDATE:

I, the undersigned, declare that the thesis that I hereby submit for degree of *Philosophiae Doctor*, at the University of Pretoria, is my contribution to research work done under the guidance of my supervisor with assistance of others in generating the experimental data and has not previously been submitted for a degree or examination at this or any other institution of higher education.

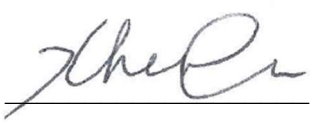

Xandra van Heerden

Contents

Synopsis ii

Acknowledgements v

Declaration vii

Contents viii

List of figures xi

List of tables xiv

1. Introduction 1-1

2. Literature 2-1

2.1 Introduction to electrochemical devices 2-1

2.1.1 Electrochemical devices 2-1

2.1.2 Batteries 2-1

2.1.3 Fuel cells 2-1

2.1.4 Bioelectrochemical systems 2-1

2.2 Bioelectrogenesis 2-3

2.2.1 Electrogenic bacteria 2-3

2.2.2 Microbiology 2-3

2.2.3 How does bioelectrogenesis work 2-4

2.2.4 Inoculums 2-5

2.3 Microbial fuel cells 2-6

2.3.1 Historical perspective 2-6

2.3.2 Electron transfer in microbial fuel cells 2-7

2.3.3 Different configurations 2-9

2.3.4 Design parameters 2-11

2.3.5 Mass transfer 2-14

2.3.6 Thermodynamics and electromotive force 2-14

2.3.7 Factors influencing cell voltage 2-16

2.3.8 Measurements 2-19
2.3.9 Applications 2-23
2.3.10 Comparative performance data 2-25
3. Materials and experimental setup 3-1
3.1 Materials used 3-1
3.1.1 Microorganism 3-1
3.1.2 Growth media 3-1
3.1.3 Carbon particles as growth substrates 3-2
3.1.4 MFC construction material 3-4
3.1.5 Instrumentation and software 3-4
3.2 Cultivation 3-4
3.3 MFC configuration 3-5
3.3.1 MFC design 3-5
3.3.2 Electrolyte 3-8
3.3.3 Electrical system and electrochemical monitoring 3-8
3.3.4 Electrical parameters and measurements 3-1
3.4 Characterisation 3-2
3.4.1 PCR amplification and DNA sequencing of 16S rRNA gene fragments 3-2
3.4.2 Turbidity 3-4
3.4.3 Dry cell mass/growth curves 3-4
3.4.4 Brunauer-Emmet-Teller (BET) surface area analysis 3-5
3.4.5 Field emission scanning electron microscope (FE-SEM) 3-6
4. Results 4-1
4.1 PCR amplification and DNA Sequencing of 16S rRNA gene Fragments 4-1
4.2 Growth of *Geobacter sulfurreducens* 4-3
4.3 Brunauer-Emmet-Teller (BET) surface area analysis 4-5
4.4 Field emission scanning electron microscope (FE-SEM) 4-5

4.5 Bioelectricity generation 4-25
5. Discussion 5-1
5.1 Microbial community 5-1
5.2 Microbial growth 5-1
5.3 Bioelectricity generation 5-6
5.4 Modelling, prediction and up-scaling 5-21
6. Conclusions and recommendations 6-1
7. References 7-1
8. Appendix A 8-1
8.1 Mechanical design 8-1
9. Appendix B 9-1
9.1 Product sheet 9-1
10. Appendix C 10-1
10.1 Certificate of analysis: Granular activated carbon 10-1
10.2 Certificate of analysis: Graphite 10-2
11. Appendix D 11-1

List of figures

Figure 3-1: Full assembly illustration of MFC design employed for experiments (drawn with SolidWorks software 2017). *3-6*
Figure 3-2: A sectioned view and a front view of the MFC enabling a perfect view of the anodic (bottom) compartment, where the G. sulfurreducens and carbon substrates reside(drawn with SolidWorks software 2017). *3-6*
Figure 3-3: Exploded view of the MFC design. Top images illustrate the complete MFC; since the two compartments are identical the bottom image is an exploded view of one of the compartments of the cell (drawn with SolidWorks software 2017). *3-7*
Figure 3-4: External electrical circuit including three MFC cells running and sampling simultaneously, connected to 5 resisters connected to a PicoScope measuring cell potential (drawn with Microsoft Visio). *3-9*
Figure 3-5: All MFCs connected in parallel per experiment; *3-11*
Figure 4-1: DNA sequence of Geobacter sulfurreducens PCA chromosome, complete genome. *4-1*
Figure 4-2:DNA sequence of Geobacter sulfurreducens strain AM-1 genome. *4-2*
Figure 4-3: Sequence ladder at 1500 kb for G. sulfurreducens. *4-3*
Figure 4-4: Growth curve for pure G. sulfurreducens and with added carbon growth substrates added over a period of 3 weeks. *4-4*
Figure 4-5: Turbidity progression of Geobacter sulfurreducens growth media over a period of 3 weeks. *4-4*
Figure 4-6: Pure granular activated carbon (GAC) flakes, untreated. *4-6*
Figure 4-7: Pure granular activated carbon (GAC) flakes, untreated. *4-7*
Figure 4-8: Pure natural graphite flakes, untreated. *4-8*
Figure 4-9: Pure natural graphite flakes, untreated – magnified. *4-9*
Figure 4-10: Pure natural graphite flakes – magnification of layers. *4-10*
Figure 4-11: The growth substrate, GAC after a growth period of 2 – magnification of biofilm. *4-12*
Figure 4-12: Microbial growth on GAC surface after 2 weeks of growth (arrow indicate crystal formed from freeze-drying process). *4-13*
Figure 4-13: Microbial growth visible in the pores and edges of the GAC particles after 2 weeks of growth. *4-14*

Figure 4-14: Microbial growth visible on the surface of the GAC particles after 2 weeks of growth – arrows indicate crystals formed from freeze drying process. 4-15
Figure 4-15: Graphite particles after 2 weeks of microbial growth. 4-16
Figure 4-16: Magnification of graphite particles after 2 weeks of microbial growth – include magnification of crystals formed due to freeze-drying process. 4-17
Figure 4-17: Magnification of basal plane of graphite particles after 2 weeks of microbial growth – no microbes visible, only crystals. 4-18
Figure 4-18: Magnification of basal plane of graphite after 2 weeks of growth. A: evidence of a single microbial cell. B: Damaged basal plane, no evidence of growth. 4-19
Figure 4-19: Graphite particles after 2 weeks of microbial growth. Layered structure and smooth basal plane excellently illustrated. 4-20
Figure 4-20: Microbial growth on GAC particles after 3 weeks of growth – A: on GAC edge and B: on flat plane 4-21
Figure 4-21: Magnification of microbial growth on GAC particles after 3 weeks of growth 4-22
Figure 4-22: Graphite growth substrate after a growth period of 3 weeks 4-23
Figure 4-23: Graphite growth substrate after a growth period of 3 weeks. A: illustrating crystals and possible single microbe (depicted by red arrow). B: illustrating the layered structure typical for graphite, with smooth basal plane (blue arrow) 4-24
Figure 4-24: Cell potential measured (A); Power density generated (B) by blank cell. 4-25
Figure 4-25: Cell potential (mV) after 1 month growth period. 4-26
Figure 4-26: Power density (mW/m^3) generated after a growth period of 1 month 4-26
Figure 4-27: Power density (mW/m^3) generated after a 3 month growth period. A: Full experimental run; B: Zoom-in to illustrate initial 25 h. 4-27
Figure 4-28: Power density (mW/m^3) generated after a 4 months growth period. A: Full experimental run; B: Zoom-in to illustrate initial 40 h. 4-28
Figure 4-29: Power density (mW/m^3) generated by G. sulfurreducens grown on a mixture of graphite and GAC particles to a ratio of 1:1 after a 4 month growth period (3 repeats). ... 4-29
Figure 4-30: Power density (mW/m^3) generated by all different MFC setups with 4 months growth period. A: all data points; B: every 5th data point plotted. 4-30
Figure 4-31: Power density (mW/m^3) generated by pure G. sulfurreducens after different growth periods. 4-31
Figure 4-32: Power density (mW/m^3) generated by G. sulfurreducens with graphite particles after different growth periods.). 4-31

Figure 4-33: Power density (mW/m^3) generated by G. sulfurreducens with GAC particles after different growth periods. A: First 60 h; B: first 40 h..... 4-32
Figure 5-1: Illustration of surface area increase and decrease due to microbial growth. ... 5-3
Figure 5-2: Power density (mW/m^3) generated by pure G. sulfurreducens after different growth periods (every 5th data point).... 5-7
Figure 5-3: Modified power density (mW/m^3) generated by pure G. sulfurreducens after different growth periods (every 5th data point); The linear lines indicate power depletion rates..... 5-8
Figure 5-4: Power density (mW/m^3) generated by G. sulfurreducens with graphite particles after different growth periods (every 5th data point).. 5-10
Figure 5-5: Power density (mW/m^3) generated by G. sulfurreducens with GAC particles after different growth periods (first 40 h). The linear lines indicate power depletion rates..... 5-11
Figure 5-6: Power density (mW/m^3) generated after a growth period of 1 month (Every 5th data point plotted). The linear lines indicate power depletion rates.... 5-13
Figure 5-7: Schematic illustrating the mechanism of complete circuit (internal and external) (A); the result of bubble in cathodic chamber leading to broken internal ionic circuit (B). 5-15
Figure 5-8: Power density (mW/m^3) generated by G. sulfurreducens on GAC particles ('○') and on a mixture of graphite and GAC particles to a ratio of 1:1 ('✱') after a 4 month growth period for the first 80 h.. 5-17
Figure 5-9: Constants using linear regression to express the effect of carbon substrates and their mixtures on the various outcomes described in this investigation. 5-22
Figure 5-10: Prediction model for energy density from system. 5-23
Figure 5-11: Prediction model for maximum power density from system..... 5-24
Figure 5-12: Prediction model for average power density from system. 5-25
Figure 5-13: Prediction model for longevity from system..... 5-26
Figure 5-14: All prediction models of carbon substrates on various parameters. Data points are predicted values, not true experimental data points..... 5-27

List of tables

Table 2-1: Comparison of the construction and performance of some recent MFCs. 2-26
Table 3-1: Certificate of analysis for granular activated carbon (GAC). 3-3
Table 3-2: Certificate of analysis for natural crystalline graphite 3-3
Table 4-1: Absorbance measurements for sample A. 4-2
Table 4-2: Absorbance measurements for sample B. 4-3
Table 4-3: BET analysis for carbon growth substrates, pure and after microbial growth. .. 4-5
Table 4-4: Summary of power density normalised to anodic chamber volume. 4-33
Table 4-5: Energy density (MJ/m^3) generated by the various systems. 4-34
Table 5-1: Energy densities of conventional sources. 5-20
Table 5-2: Summary of models from linear regression. 5-21

1. Introduction

The global primary energy consumption has increased by an average of 1.8 % annually over the last decade. This magnitude of increase has slightly declined in the past three years with the global primary energy consumption increasing 1 % per year according to the BP Statistical Review of World Energy 2017. The persistent effort to improve energy efficiency is causing global energy consumption to decelerate. Due to the uncontrolled use and depletion of fossil fuels the interest in alternative and renewable energy sources has greatly increased. (Davis and Higson, 2007, Dudley and Dale, 2017)

Bioelectrogenesis is a process that directly converts biomass into electricity. Bioelectrochemical systems, such as microbial fuel cells (MFCs), hold great potential to breach the gap into sustainable and green energy. Bioelectrochemical systems can be thought of as fuel cells with regenerative, living microbial catalysts. (Chouler et al., 2016, Aviles et al., 2017)

In high power producing MFCs, the anode has been found to be the limiting factor. The anode and the anodic chamber therefore are extremely important components for the investigation. Additional factors that influence the power output are the microbial attachment to the anode, electron transfer, and substrate oxidation. These parameters can be influenced by the anode. It is vital to select the appropriate anode material or to modify the surface for increased conductivity. The microbial growth also needs to be optimised for optimal microbial attachment and electron transfer. (Ghasemi et al., 2013)

The aim of this investigation was to study the effect of the addition of carbon particles to the anodic chamber of a microbial fuel cell (MFC) containing *Geobacter sulfurreducens* in order to change the conditions of the MFC. The effect of the crystallinity of the carbon on the efficiency of the cell was evaluated. A crystalline carbon in the form of graphite particles was added to the initial growth media to increase the electrical conductivity of the anolyte. An amorphous carbon, granular activated carbon (GAC) particles, was added to the growth media to increase microbial growth. It was then decided which parameter needed to be prioritised if only one carbon substrate were to be added. A mixture of the two carbon substrates was added to the growth media to investigate what, if both the microbial growth and the conductivity in the MFC were increased, the effect would be on bioelectrogenesis. The effect of various growth periods of *G. sulfurreducens* prior to inoculation into the MFCs was also investigated. The

experiments was thus limited to screening the effects of the bacteria growth media and growth time for the different carbon substrates and mixtures thereof.

A few experimental difficulties were encountered during the course of the investigation. The design and manufacture of the MFC was challenging; the first design was such that the electrodes were in a perpendicular position relative to the working-surface which led to all the microbes settling out allowing no or only a small surface of direct contact to the electrode. The second problem with the design was finding a method of inoculating the MFC with the growth media in an anoxic atmosphere. In addition to the architecture of the MFC, it was difficult to find the correct growth conditions for the anaerobic microbe, *Geobacter sulfurreducens*. The final experimental difficulty encountered was acquiring the correct equipment for measuring such low cell potentials.

The MFC design was finalised, by choosing the electrodes to be positioned parallel relative to the working-surface which allows for the continued direct contact with the electrode after the inevitable settling of microbes. A glove-box was acquired which allowed for working in an anoxic atmosphere and all necessary instrumentation was acquired as well.

The bioelectrogenesis was measured by recording the cell potential generated per MFC, which was then manipulated to determine the power and energy densities. The growth was correlated by measuring the dry mass over the initial growth period to determine the growth curves, and qualitatively correlated using FE-SEM and BET analyses.

2. Literature

2.1 Introduction to electrochemical devices

2.1.1 Electrochemical devices

Electrochemical devices convert chemical energy directly into electrical energy, bypassing the thermodynamic limitations of combustion-based power cycles. Using an external circuit the energy production can be finely controlled in electrochemical devices. (Gileadi, 1993)

2.1.2 Batteries

A *battery* consist of more than one electrochemical cell enclosed in a battery housing, in which the fuel is contained internally, allowing a reaction to occur at each anode and cathode. (Gileadi, 1993)

2.1.3 Fuel cells

By the reversal of the electrolysis of water, i.e. by the recombination of hydrogen and oxygen to produce water and electrical current, the first fuel cell was built by William Grove in 1839 (Bullen et al., 2006). In a *fuel cell*, the fuel is stored and supplied from outside the reaction chambers and waste fuel is removed (Gileadi, 1993).

An oxidation reaction takes place at the anode, releasing electrons, which travel to the cathode via an external circuit, where a reduction reaction occurs. Fuel cells conventionally operate using relatively simple inorganic chemistries. E.g., by using methanol as fuel, energy, water and carbon dioxide are produced. Lower order alcohols and alkanes are frequently reformed to produce hydrogen before the cell process and then supplied to the fuel cell. (Bullen et al., 2006) Theoretically, by direct oxidation and reduction of compounds at the electrode surfaces, fuel cells circumvent the inadequacies of internal combustion engines (Bond and Lovley, 2003).

2.1.4 Bioelectrochemical systems

Bioelectrochemical systems convert chemical to electrical energy by means of electrochemical reactions involving biochemical pathways taking advantage of the metabolic processes of microorganisms (Bullen et al., 2006, Chouler et al., 2016). To date, there have been numerous bioelectrochemical systems: (1) cells that use a primary fuel such as organic waste to generate a fuel source like hydrogen, which is then used as a secondary fuel for a conventional

hydrogen/oxygen fuel cell, known as a “secondary” or “indirect” biofuel cell; (2) direct electricity generation from the redox reaction or reaction chain from the organic fuel using either enzymes or whole microorganisms, known as a “primary” or “direct” biofuel cell; and, (3) the combination of photochemically active and biological systems to convert the energy harvested from sunlight to electrical energy. (Davis and Higson, 2007, Kim et al., 2006)

2.1.4.1 Enzymatic biofuel cells

Enzymatic biologically catalysed devices utilise biological molecules as catalysts for achieving their redox reaction as either purified or derived enzymes to catalyse a specific reaction (Bullen et al., 2006, Osman et al., 2011). Enzymatic biofuel cells typically possess orders of magnitude higher power densities than microbial biofuel cells (although still lower than conventional fuel cells) but can only partially oxidise the fuel and have limited lifetimes (typically 7–10 days) owing to the fragile nature of the enzyme. The active lifetimes of enzymes can be extended to up to 20 days by electron surface immobilisation. (Osman et al., 2011) Recently, however, active lifetimes have been extended beyond 1 year through encapsulation in micellar polymers. These polymers physically confine the enzymes which prevents the denaturing by providing a biocompatible hydrophobic nest and buffered pH micro-chemical environment. An additional advantage of enzymes is specificity, which can eliminate the need for a membrane. (Minteer et al., 2007)

2.1.4.2 Microbial fuel cells

Microbially catalysed systems use whole living organisms, such as bacteria, as the source of complete enzyme pathways to oxidise organic and inorganic matter to generate current and usable energy. As a result of operating with living systems, these microbially catalysed systems are generally robust, can function on various feedstock, and are poison-resistant. These systems can oxidise substrates entirely to carbon dioxide and water. (Bullen et al., 2006, Bond and Lovley, 2003) The current advantage to microbial fuel cells is that they typically have long lifetimes, of up to five years. They are, however, limited by low power densities. (Minteer et al., 2007)

2.2 Bioelectrogenesis

2.2.1 Electrogenic bacteria

Bioelectrogenesis is known as a process in which organic material is oxidised with quantitative electron transfer from microorganisms to solid conductive materials to harvest clean electricity. Electricigens or electrogenic bacteria are found in various environments, including sediments of rivers, lakes or seas. Anaerobic microorganisms such as *Geobacter* species can breathe iron and mineral compounds from sediments and soil, similarly to humans and animals breathing oxygen. An extreme diversity of the composition of microorganism communities have so far been revealed by community analysis. Existing and new data from Logan and co-workers suggest that many new types of bacteria capable of anodophilic electron transfer (electron transfer to an anode) or interspecies electron transfer (transfer of electrons between bacteria in any form) may still be discovered. (Logan et al., 2006)

Electrical current generation has been demonstrated in four of the five *Proteobacteria* classes, as well as the *Firmicutes* and *Acidobacteria* phyla. The oxygenic phototrophic cyanobacterium *Synechocystis* sp. PCC 6803 produced electrically conductive appendages called nanowires and the yeast *Pichia anomala* produced current through redox enzymes on its outer membrane. Both *Shewanella* and *Geobacter* species produce nanowires and are highly conductive. *Shewanella oneidensis* MR-1 exhibit nonlinear electrical transport properties along their length, due to their nanowires. (Logan, 2009)

2.2.2 Microbiology

Microbial growth is dependent on many factors, including but not limited to, the substrate, metabolites and microbial concentrations, and an adaptation or change in the biofilm structure or microbial community. All of these factors will influence the electrochemical characteristics of microbes. The biofilm porosity affects the transfer of metabolites to the electrode surface. (Alterman et al., 2006)

The microorganisms are structured in a biofilm as part of the electrolyte. Any alteration of the microbial community will influence the structure and properties such as the electrochemical characteristics and losses in microbial fuel cells (Alterman et al., 2006).

2.2.3 How does bioelectrogenesis work

Bioelectrogenesis work by allowing bacteria to do what they are known for: oxidise and reduce organic molecules. Bacterial respiration is essentially a redox reaction in which electrons move around. When there are moving electrons, there is the potential of harnessing an electromotive force. (Alterman et al., 2006)

There are at least three possible mechanisms for exocellular electron transfer which result in power generation. The most studied mechanism is power generation due to cell respiration utilising solid metal oxides. Many strains of bacteria can release electrons from a terminal oxidase in the respiratory chain to Fe(III) outside the cell, producing Fe(II). The second mechanism occurs when the cells transfer electrons directly to another cell without intermediates, like hydrogen. It was observed that the fermentative bacterium *Pelotomaculum thermopropionicum* was linked to the methanogen *Methanothermobacter thermautotrophicus* by an electrically conductive nanowire, providing evidence of interspecies electron transfer. The evidence that electrons can be both released and accepted by microorganisms suggest that electron exchange between cells is a natural occurring phenomenon in microbial communities. (Logan, 2009)

The third possible mechanism has not been experimentally examined but relates to a possible role of electron transfer for cell-cell communication. It is well known that bacteria within biofilm communicate through quorum sensing chemicals. Bacteria such as *Pseudomonas aeruginosa* generate quorum signals with fatty acyl-homoserine lactones (acyl-HSLs), and recently *Rhodopseudomonas palustris* strains have shown to produce quorum signal *p*-coumaroyl-HSL. The pathogen *P. aeruginosa* produces pyocyanin, which is a chemical that is a signal for the upregulation of quorum sensing-controlled genes. Pyocyanin can be utilised as an electron mediator, allowing power generation in MFCs. Pyocyanin produced by one microorganism can be used by another microorganism for power generation in MFCs. Other microorganisms capable of power generation in MFCs include the opportunistic pathogen, *Ochrobactrum anthropic*; the yeast, *P. anomala*, among others. (Logan, 2009)

Living cells in the biofilm consume the electron donors which are transferred from the bulk solution. The cellular metabolism comprises enzyme reactions, from which some will yield electrons. During biological metabolism the electron relay occurs in the microbes and a fraction

of these electrons are collected by the anode via extracellular cytochromes. (Alterman et al., 2006)

The outer membrane c-type cytochrome, OmcS and several other c-type cytochromes are known to be involved in Fe(III) reduction, but their role in electron transfer to electrodes still requires investigation. The outer membrane c-type cytochromes, OmcB, are believed to function as electron transfer components in the chain of redox proteins leading to Fe(III) reduction. The c-type cytochromes OmcG and OmcH inhibits Fe(III) reduction due to OmcB being less expressive in the mutants. OmcF is a monoheme outer membrane c-type membrane of *Geobacter sulfurreducens* and the OmcF-deficient mutant was impaired in Fe(III) reduction because the OmcB transcript was dramatically decreased in the mutant. The depletion of the OmcF also inhibits electricity production. (Kim et al., 2008)

Direct electron transfer (DET) between an enzyme and electrode has only been observed with a number of enzymes, for example: cytochrome *c;* laccase; hydrogenase; and, numerous peroxidases including microperoxidases (Kim et al., 2006).

For metabolic energy to be generated, microorganisms should transport electrons from a substrate (the electron donor, for example acetate or fumarate) at a low potential through the electron transport chain to the final electron acceptor (for example oxygen or nitrate) at higher potentials. In MFCs the final electron acceptor is usually the anode and its potential determines the energy gain for the microorganism.

The ratio of NADH to NAD^+ gives an example of how an electron carrier could affect exocellular electron transfer. Some microorganisms have characteristic NADH to NAD^+ ratios which are dependent on redox conditions. The accumulation of NADH affects cellular processes. Higher accumulation of NADH could allow exocellular electron transfer at more-negative anode potentials. (Logan, 2009)

2.2.4 **Inoculums**

There are several types of microorganisms that produce electrical current in MFCs, but many of these strains exhibit low power densities when grown as pure cultures. Highest power

densities are achieved by inoculating the anode chamber with a rich and diverse source of bacteria, like wastewater or sludge. (Logan, 2009)

Geobacter sulfurreducens is the most intensively studied electricigen because it produces high current densities, the complete genome sequence and genetic system are available and the extracellular electron transfer to Fe(III) oxide have been extensively studied in this organisms, which might provide insights to extracellular electron transfer to electrodes (Kim et al., 2008). *Geobacteraceae* species are not considered strict anaerobes as in the past, they have the ability to scavenge small amounts of dissolved oxygen, presumably as a method of maintaining low redox conditions required for growth (Logan et al., 2005, Lin et al., 2004). It is however suggested that *Geobacter sulfurreducens* is capable of producing higher power densities in the complete absence of oxygen or perhaps in the presence of another microorganism capable of scavenging the oxygen (Logan, 2009).

2.3 Microbial fuel cells

A microbial fuel cell (MFC) is fundamentally a fuel cell with regenerative, living microbial catalyst. An MFC harnesses the power of respiring microbes directly converting organic substrates to electrical energy. MFCs principally comprise an anode compartment, separated from the cathode compartment by a cation specific membrane. The microorganisms in the anode compartment oxidise the fuel, producing electrons at the anode which is transferred through the external circuit to the cathode and protons transferred through the membrane. Both the electrons and protons are consumed in the cathode compartment with the protons combining with oxygen to produce water. (Bond and Lovley, 2003, Aviles et al., 2017)

2.3.1 Historical perspective

Italian physician and physicist, Luigi Galvani discovered the connection between biology and electricity in the 18th century when he applied an electric current to a severed frog's leg, allowing it to twitch. And since an electrical action can induce a biological reaction, the opposite is possible in many cases, i.e. biological processes can be used to generate electricity. (Davis and Higson, 2007)

In 1911 Michael Cresse Potter, a professor of Botany at the University of Durham made one of the earliest developments in bioelectrochemisty, when he generated a potential difference

by placing a platinum electrode into *E. coli* yeast cultures. This discovery led him to construct a basic microbial fuel cell. In 1931, Cohen at Cambridge revived Potter's idea when he described how a batch of biological fuel cells produced more than 35 V. (Davis and Higson, 2007, Bullen et al., 2006)

The interest in microbial fuel cells expanded after the USA space program developed microbial fuel cells not only as a human waste disposal system for space flights, but also as a power generator, in the late 1950s and early 1960s. Biofuel cells utilising cell-free enzyme systems was used in 1960 with the primary objective of using it as a power supply for a permanently implantable artificial heart. (Bullen et al., 2006)

The first enzyme-based biofuel cell using glucose oxidase (GOx) as the anodic catalyst and glucose as the "fuel" was reported in 1964 (Kim et al., 2006).

2.3.2 Electron transfer in microbial fuel cells

2.3.2.1 Electron transfer

Electrons and protons are generated from the oxidation of organic fuel by microbes at the anode. The protons pass through the proton exchange membrane to the cathode, and the electrons pass through the anode to an external circuit to generate a current. The electrons released by the microbes as they respire may be collected. (Davis and Higson, 2007)

2.3.2.2 Direct electron transfer (DET)

Immobilisation of the microbes or enzymes at the electrode surface greatly facilitates the electron transfer rate (Davis and Higson, 2007). Close contact of the enzyme active sites to the surface of the electrode is critical for direct electron transfer. A critical distance of 20 Å between enzyme active site and the electrode surface is suggested for laccase-catalysed direct electro-reduction of oxygen. The critical distance for horseradish peroxidase is reported as 18 Å. (Kim et al., 2006) The rate of the overall reaction is determined by electron conduction and with a distance greater than the critical distance, the overall reaction is slowed. With shorter distances the electron conduction is efficient, making the enzymatic reaction kinetics the rate-determining step. (Kim et al., 2006)

In many cases the enzyme active site is hosted by a thick and nonconductive protein shell which limits DET by producing a chemically modifying conductive enzyme, by which this limitation can be overcome. A different method of overcoming this limitation, is by introducing a redox mediator to facilitate the transportation of electrons by shuttling. (Kim et al., 2006)

2.3.2.3 Mediator

Prior to 1999 most MFCs required a mediator chemical. Mediators are typically organic dyes or organometallic complexes, which are either in solution or immobilised at the electrode surface. (Minteer et al., 2007) These mediators are necessary for the transfer of electrons from the bacteria to the electrodes. The requirement for mediators is problematic as many of these mediators are toxic which means that in an open atmosphere, the harvesting of electrical energy from organic material cannot be done commercially. Examples of mediators include potassium ferricyanide, anthraquinone 2,6-disulfonic acid, cobalt sepulchrate, thionine, neutral red, methylene blue and azure A. These mediators are expensive and toxic. (Bond and Lovley, 2003, Osman et al., 2010)

In these types of systems an inorganic mediator replaces oxygen in the bacterial electron transport chain. The mediator crosses through the bacterial outer membrane and accepts electrons which would typically be accepted by oxygen or other solubles. As soon as the mediator has been “reduced”, it exits the cell saturated with electrons which is then transferred to the anode. Higher efficiency of microbial fuel cells have been observed when mediators were introduced, even though the mediators introduce an additional step in the redox reaction chains from fuel to electron generation. (Kim et al., 2006)

2.3.2.4 Mediator-less

If no exogenous mediators are added, the MFC system is considered mediator-less (Logan et al., 2006). Microorganisms capable of exocellular electron transfer (mediators not required) are defined as exoelectrogens, also known as electrochemically active bacteria, anode respiring bacteria and electricigens (Logan, 2009). These types of bacteria are able to respire directly into the electrode under certain conditions by using the anode as the electron acceptor as part of its standard metabolic process. The exoelectrogens sticks to the anode surface. The electrons are transferred involving direct contact through conductive pili and conductive biofilm which is travelled via excreted mediator enzymes. In today’s energy industry, this is the most favourable MFC system. (Logan et al., 2006)

2.3.2.5 Limitations

The electrochemical losses can be characterised as: (1) the electrical resistance of the electrolyte and electrodes, known as ohmic losses; (2) activation losses lowered by the microbial production of electron transfer; and, (3) a decrease of reactants on the electrode surface leading to mass losses. The relation between the growth of microbial community and electrochemical parameters is not yet known. (Alterman et al., 2006)

2.3.3 Different configurations

The power densities produced by isolates or mixed cultures are often more dependent on the architecture of the MFC; electrode spacing and solution conductivity of the fuel cell than the bacterium type. Power densities produced by bacteria in one study cannot directly be compared with another type of bacterium, or mixed cultures, unless the architecture and chemical solution of the MFC are identical. Comparison can only be determined through extensive testing of various strains and inocula in the device. (Logan, 2009)

The diversity of configurations and the material used for building MFCs is extensive. These systems are operated under a range of conditions, including variations in pH, electrode surface areas, device size, and temperature, retention time of cells, as well as aerobic or anaerobic atmospheres. (Logan et al., 2006)

2.3.3.1 Single chamber

An MFC is considered a single chamber configuration when it is operated in the absence of a proton exchange membrane (PEM) (Cheng et al., 2006). When employing a single chamber device, no energy input is required for aeration, as an air-cathode is used which is passively aerated, thereby allowing for simplicity and cost-effectiveness compared to the dual-chamber configuration (Chouler et al., 2016). Another advantage for the use of a single chamber air-cathode MFC is that the catholyte does not need recycling or chemical regeneration, and with smaller cell volume, higher volumetric power density is achieved. The Coulombic efficiency is much lower with a PEM-less MFC which is one of the challenges with a single chamber configuration. (Fan et al., 2007)

2.3.3.2 Dual chambers

A dual chamber MFC comprises two chambers, viz. an anode chamber and a cathode chamber, separated by a cation specific membrane. A common and inexpensive configuration design employed is where the dual chamber MFC is constructed in an "H" shape comprising two bottles connected by a tube containing the separator membrane. The separator in the H-configuration is clamped between the tubes connecting the two bottles. The H-configuration is not an optimum configuration as the power density produced is limited due to high internal resistance and electrode-based losses. This type of configuration is acceptable for basic parameter research such as examining new materials or types of microbial communities. The main pre-condition for using a dual chamber cell is that the two chambers must be kept separate. The chambers can be clamped together directly, separated by the membrane, increasing membrane surface and limiting the electrode-based losses, therefore increasing power density. The dual chamber configuration has thus far been adopted for miniature MFC designs. (Logan et al., 2006, Chouler et al., 2016)

One main reason for the use of a dual chamber configuration is to avoid the mixing of solutions of the electron acceptors and electron donors and therefore loss of electrons (Deval and Dikshit, 2013).

The early two-chamber MFC configuration using *Geobacter* strains obtained low power densities of between 7 mW/m^2 to 45 mW/m^2, this is known to be due to the high internal resistance of these systems (Logan, 2009).

2.3.3.3 Stacked

The voltages and currents produced by MFCs can be increased by connecting stacked MFCs in series or parallel. By connecting cells in series, the voltages over the stacked MFC system can be added, with one common current flowing through each MFC. By connecting the MFCs in parallel, the currents of the stacked MFCs can be added, while the voltage will be an average of the system. Using this configuration, a desired voltage or current can be obtained by combining the appropriate amount of connected MFCs in either series or parallel. The electricity production will be influenced by external conditions such as the electrical circuit. By stacking MFCs, the theoretical thermodynamic limitations can be overcome. (Alterman et al., 2006, Logan et al., 2006, Chouler et al., 2016)

2.3.4 **Design parameters**

The architecture of an MFC is of utmost importance when considering the performance (power density) of the MFC. The reactor should be considered the essence and heart of any electrochemical process. The factors affecting the performance include, but are not limited to, the microbial inoculum, the membrane type, the electrode material, size and spacing and the electrolyte as well as the internal and external resistance due to electronic influences. Among all these factors, the electrode material has the most significance. (Cheng et al., 2006, Ghasemi et al., 2013, Walsh and de León, 2018)

2.3.4.1 Electrode material

An anodic or cathodic reaction or electrode must not be considered alone, because cells are integrated devices necessitating use of both electrodes in contact with an electrolyte and an external circuit. Electrodes should ideally have high electroactive area, low electrical resistivity, must be chemically stable and resistant to oxidation. They should be able to operate at high current densities, must have adequate mechanical strength and elastic modulus and must have a long life cycle. The electrodes are usually made of cost-effective materials such as carbon cloth or paper, graphite rods, plates and granules. Even metals such as copper and silver have proved to be effective materials as anodes. Ceramics, polymeric and composites are becoming increasingly significant. (Arenas et al., 2017, Walsh et al., 2018)

The cathode chamber is the positive part if the cell consisting of a cathode subjected to an oxidising agent in the catholyte solution. The oxidising agent is reduced as the electrons travel through the circuit to the cathode. In order to improve the oxygen reduction reaction (ORR), more expensive metals such as platinum (Pt) may be used at the cathodes. The power output has shown to improve by 15.6 % by replacing a Pt-free cathode with a Pt cathode. Cobalt- and iron-based catalysts both produce similar power densities in MFC systems. (Chouler et al., 2016, Logan et al., 2005, Logan and Regan, 2006). The platinum (Pt)-group metals are the most widely studied and used electrocatalysts because they are proven to show optimum electrocatalytic behaviour (Watt-Smith et al., 2008a).

Utilisation of nanostructures, which provide large surface areas, and which enable increased microbial attachment, improves power density due to an increased biofilm loading. Nanoscale engineering of biocatalysts is the next stage advancement of microbial fuel cells. (Kim et al.,

2006) Porous, 3D electrodes can possess a high surface area and offer reasonable mass transfer rates. One disadvantage normally with such materials is the difficulty in making effective electrical connections. Porous electrodes should be able to operate free of blockages. (Walsh and de León, 2018, Arenas et al., 2017)

In MFCs that produce high power outputs, the anode is the limiting factor; therefor the anode and the anode chamber are extremely important components in any investigation. Additional factors that influence the power output is the microbial attachment to the anode, electron transfer and substrate oxidation, these parameters can be influenced by the anode. It is imperative to select the appropriate anode material or to modify the surface for increased conductivity. The microbial growth also needs to be optimised for optimal microbial attachment and electron transfer. (Ghasemi et al., 2013)

2.3.4.2 Size: The ratio of the electrode surface area to the chamber volume

The assumption is that the current and power generation will drop significantly with device size reduction. Reduced size results in reduced electrode surface area and cross-sectional area of membrane, which has a direct correlation to the power output. By increasing the true surface area of the electrode, but not the volume of chamber, thereby increasing ratio of the electrode surface area to the chamber volume, the current and power density per cross-sectional area and chamber volume increases. (Ringeisen et al., 2006) Typical characteristics of a miniature MFC is a large true surface area-to-volume ratio, and short electrode distance, which lead to reduced ohmic losses and improved mass transfer between biofilm, electrolyte and electrodes, and a consequent enhancement of power output (Chouler et al., 2016). An effective to increase the true surface area of the electrodes, is to use a material with a highly porous structure. The use of graphite felt or foam has proven to produce up to three times as much power than typical graphite rods. (Davis and Higson, 2007)

2.3.4.3 Electrolyte

The power density produced is directly proportional to the concentration of good electron acceptors. Ferricyanide is an electron acceptor proven to increase the power density by 1.5 to 1.8 times compared to H-design two-chambered reactor with a Nafion^{TM} PEM with dissolved oxygen and a Pt-catalyst cathode. Even though ferricyanide is an outstanding catholyte in terms of system performance, it must be chemically regenerated. Therefore it is not sustainable for practical use. In contrast systems using oxygen as electron acceptor in the catholyte can be

operated continuously, making the reaction self-sustaining. (Logan et al., 2006, Cheng et al., 2006) Power densities as high as 4.31 W/m^2 have been reported when using non-renewable ferricyanide at the cathode (Logan and Regan, 2006).

2.3.4.4 Retention time

MFCs can either be operated as a batch, where the system is run for a certain time-period without adding nutrients or media to the microbes in the cell, which might decrease the functionality of the cell or the microbes over time. To operate the MFC under continuous flow conditions, the microbes will continuously have fresh media and therefore increase power density production. The retention time has an influence on the performance. An apparent constant performance has been observed in a miniature-MFC with a single culture being consumed for up to 2 weeks. (Ringeisen et al., 2006)

2.3.4.5 Membrane

There are many types of separators one can use. These are usually a cation exchange membrane (CEM) also known as a proton exchange membrane (PEM) such as Nafion^{TM} or Ultrex, or a plain salt bridge. The choice of membrane is especially important in dual-chamber configurations, to ensure only protons pass between the chambers, but to restrain the substrate or electron acceptor in the cathode compartment from passing through the membrane. When using a salt bridge, the internal resistance is increased allowing for limiting power densities. (Logan et al., 2006) Proton exchange membranes such as the Nafion^{TM} have high proton conductivities, but unfortunately are permeable to oxygen. This is disadvantageous to an anoxic anode chamber with anaerobes, which can raise the redox potential of the half-cell respiration. Introducing an oxygen scavenger will alleviate this problem, such as cysteine which reacts with oxygen to form the disulphide dimer cystine. (Logan et al., 2005)

The maximum rate (W) of oxygen diffusion through a membrane of cross section A can be approximated as $W \approx -DAC_{eq}/\delta_m$ assuming an oxygen solubility in the membrane equal to oxygen saturation in water at equilibrium of C_{eq} = 2:6 x 10^{-7} mol/cm^3 and a diffusion constant of oxygen in the membrane, D = 4.4 x 10^{-6} cm^2/s (Logan et al., 2005) .

2.3.4.6 Pure vs mixed cultures

Substantially greater power densities have been achieved by utilising mixed cultures rather than pure cultures in the operation of MFCs (Cheng et al., 2006, Logan et al., 2005).

2.3.4.7 Inorganic growth substrates

There is a clear synergy when combining biofuel cells with material chemistry. Nanostructures have great potential in the stability and activation of enzymes due to the large surface area facilitating the attachment of microbes. The increased microbe loading will possibly improve the power density. (Kim et al., 2006)

2.3.5 Mass transfer

In microbial fuel cells there are three mass transfer processes subject to transfer limitations, listed as: (1) diffusion of the fuel/oxidant to the active sites of the biocatalyst; (2) proton transfer through the membrane; (3) diffusion or redox mediators between electrodes and biocatalysts for mediator systems or the electron transfer between the active sites of the biocatalysts to the electrodes (Kim et al., 2006).

High resistance with respect to mass transfer processes tends to build a concentration difference between the bulk phase and the reaction sites, thereby slowing the reaction leading to the polarisation of the electrodes. The mass transfer of fuel limits the performance of porous composite electrodes. Standard engineering methodologies may relieve the limitations; these include mechanical stirring, patterned electrode design, or the introduction of convective transport by forced flow. (Kim et al., 2006)

2.3.6 Thermodynamics and electromotive force

Only when the overall reaction in an MFC is thermodynamically favourable will electricity be generated. The Gibbs free energy expressed in units of Joules (J mol^{-1}) can be used to evaluate a reaction. The expression is given by Equation 2-1. It is a measure of the maximal work possible to be derived from the reaction. (Bard et al., 1985, Logan et al., 2006)

$$\Delta G_r = \Delta G_r^0 + RTln(\Pi) \qquad 2\text{-}1$$

ΔG_r is the Gibbs free energy for the specific condition, ΔG_r^0 is the Gibbs free energy for the standard conditions (normally defined as 298.15 K, 1 bar pressure and 1 M concentration for all species), R is the universal gas constant (8.31447 J/(mol K)), T (K) is the absolute temperature and Π is the reaction quotient which is the ratio of the activities or concentrations of the products of the reaction to the concentration of activity of the reactants, raised to the respective stoichiometric coefficients, and is dimensionless. The standard reaction Gibbs free

energy can be calculated from energies of formation of organic compounds in water, available from many sources. (Amend and Shock, 2001, Thauer et al., 1977, Logan et al., 2006, Perry and Green, 2008)

The overall cell electromotive force, (emf), ε_{emf}, is the potential difference between the cathode and anode. It would therefore be more appropriate to determine the reaction in MFC calculation in terms of ε_{emf} (V). This is related to the work, W (J) produced by the cell, given in Equation 2-2.

$$W = \varepsilon_{emf} Q = -\Delta G_r \qquad 2\text{-}2$$

Here $Q = nF$ is the charge transferred in the reaction, expressed in Coulomb (C), determined by the number of electrons exchanged in the reactions, n is the number of electrons per reaction mol and F is Faraday's constant (9.64853 x 10^4 C/mol). Combination of these equations results in Equation 2-3;

$$\varepsilon_{emf} = -\frac{\Delta G_r}{nF} \qquad 2\text{-}3$$

If all reactions are evaluated at standard conditions, Π = 1, then Equation 2-3 can be rewritten as Equations as Equation 2-4;

$$\varepsilon^0_{emf} = -\frac{\Delta G^0_r}{nF} \qquad 2\text{-}4$$

Here ε_{emf}^0 (V) is the standard cell electromotive force. The overall reaction in terms of the potentials can therefore be expressed as follows in Equation 2-5;

$$\varepsilon_{emf} = \varepsilon^0_{emf} + \frac{RT}{nF} ln(\Pi) \qquad 2\text{-}5$$

The calculated emf value will be positive for a favourable reaction and gives the upper limit for cell voltage; the actual potential obtained from the MFC will be lower due to various potential losses. (Logan et al., 2006)

2.3.6.1 Standard electrode potential

The reactions taking place in the MFC can be examined in terms of the half-cell reactions, or the separate reactions taking place at the anode and cathode. According to the IUPAC convention, standard potentials (at 298 K, 1 bar and 1 M) are reported as reduction potentials,

in other words the reaction is written as consuming electrons. The cell emf is calculated by Equation 2-6;

$$\varepsilon_{emf} = V_{Cat} - V_{An} \quad 2\text{-}6$$

Here ε_{emf} (V) is the overall cell emf, V_{cat} (V) is the potential of the cathode, and V_{An} (V) is the potential of the anode. The minus sign is a result of the definition of the anode potential as a reduction reaction, although an oxidation reaction is occurring. Equation 2-6 is only equal to Equation 2-3 and Equation 2-5 when the pH at the cathode and anode are equal. The power output is significantly dependent on the cathode conditions, and not only the anode and anode compartment. The power produced is dependent on the choice of cathode and should be taken into consideration when comparing power densities by different MFCs. (Logan et al., 2006)

2.3.6.2 Open circuit voltage (OCV)

The cell emf is a thermodynamic value that does not take internal losses into account. The open circuit voltage (OCV) is the cell voltage that can be measured in the absence of current after a certain amount of time. Theoretically, the OCV should approach the cell emf, but in industry, the OCV is significantly lower than the cell emf due to various potential losses. The main application of thermodynamic calculations is to identify the size and nature of energy losses in the MFC. (Logan et al., 2006)

2.3.7 Factors influencing cell voltage

MFCs have thermodynamic limitations because the maximum voltage or emf attainable from an MFC will never exceed the theoretical open circuit voltage of 1.14 V (determined by NADH (-0.32 V) and pure oxygen (+0.82 V)), even when neglecting the internal losses. The highest OCV thus far reported is 0.80 V. Closed circuit voltages remain below 0.62 V. (Alterman et al., 2006, Chouler et al., 2016, Logan et al., 2006)

The difference between the measured cell voltage (V) and the cell emf (ε) is referred to as overvoltage and is the sum of the overpotentials of the anode and the cathode, and the ohmic loss of the system, given by Equation 2-7;

$$V_{cell} = \varepsilon_{emf} - (\Sigma\eta_a + |\Sigma\eta_c| + IR_\Omega) \quad 2\text{-}7$$

Here $\Sigma\eta_a$ and $|\Sigma\eta_c|$ are the overpotentials of the anode and the cathode respectively, and IR_Ω is the sum of all the ohmic losses which is proportional to current generated (I) and ohmic resistance of the system (R_Ω). The electrode overpotentials for both the anode and cathode are current dependent and can be categorised as activation losses, microbial metabolic losses and mass transport or concentration losses. (Logan et al., 2006)

The cell voltage (V) in MFCs is a linear function of the current, and can be expressed by Equation 2-8;

$$V_{cell} = OCV - IR_{int} \quad 2\text{-}8$$

Here IR_{int} is the sum of all internal losses of the MFC, which are proportional to the generated current (I) and the internal resistance of the system (R_{int}). The performance of MFCs can be expressed in terms of overpotentials and ohmic losses, or in terms of OCV and internal losses. High R_{int} causes low energy conversion efficiency because as the power is generated inside the MFC it is consumed. (Logan et al., 2006)

2.3.7.1 Ohmic losses

Also known as ohmic polarisation include the ohmic resistance (R_Ω); the resistance to the flow of electrons through the electrodes and interconnections, and the resistance to the flow of ions through the membrane and the anodic and cathodic electrolytes. Methods to employ in order to minimise ohmic losses include (i) reduction of the inter-electrode space, (ii) the use of low resistivity membranes, (iii) increaseing solution conductivity. (Logan et al., 2006)

2.3.7.2 Activation losses

These losses, also known as activation polarisation, occur during the transfer of electrons from or to a compound reacting at the electrode surface, and are due to the activation energy required for a reduction/oxidation reaction. This compound can be present at the microorganism surface, as a mediator in the solution, or as the final electron acceptor reacting at the cathode. At low currents, activation losses often show a strong increase, and steadily increase with an increased current density. By increasing the electrode surface area and operating temperature, by improving the electrode catalysis, and an enriched biofilm is established on the electrode that can lower the activation losses in MFCs. (Logan et al., 2006)

2.3.7.3 Microbial metabolic losses

For metabolic energy to be generated, microorganisms should transport electrons from a substrate (the electron donor, for example acetate or fumarate) at a low potential through the electron transport chain to the final electron acceptor (for example oxygen or nitrate) at a higher potential. In MFCs the final electron acceptor is usually the anode and its potential determines the energy gain for the microorganism. The higher the difference between the redox potential of the electron donor (substrate) and the anode potential, the higher the possible metabolic energy gain for the microorganism; however, the maximum possible MFC voltage is lowered. When the MFC circuit is opened, the anode potential becomes more negative and approaches the thermodynamic limit for the oxidation of the substrate under conditions of the medium. When the circuit is closed, or connected to a load or external resistor, the anode potential increases, or becomes less negative. This is due to the respiratory enzymes and electron carriers that are oxidised. The more negative the anode potential, the greater power output of the MFC and the lower the energy consumed by the microorganism. This is where a trade-off should be considered when attempting to lower the microbial metabolic losses. Keeping the anode potential as low as possible (i.e. negative), the MFC voltage can be maximized; however, if the potential of the anode becomes too low, electron transport will be inhibited and fermentation of the electron donor (substrate) may provide greater energy for the microorganism. (Logan, 2009, Logan et al., 2006)

2.3.7.4 Concentration losses

This phenomenon is also known as concentration polarisation. Current production is limited due to the rate of mass transport of a species to or from the electrode. Concentration losses occur mainly at high current densities due to limited mass transport of chemical species by diffusion to the electrode surface. The concentration losses at the anode are caused by either a limited supply of reduced species toward the electrode or a limited discharge of oxidised species from the electrode surface. The ratio between the reduced and oxidised species at the electrode is therefore increased. This can cause an increase in the anode potential. The opposite will occur at the cathode, causing a decrease in the cathode potential. In systems with poor mixing, diffusional gradients may arise in bulk liquids, where mass transport limitations can limit electron donor (substrate) flux to the biofilm. This is a different type of concentration loss. (Logan et al., 2006)

2.3.8 **Measurements**

MFC systems may require specialized electrochemical instrumentation. In most cases cell voltages and electrode potentials are adequately measured with commonly available voltage meters or multimeters, and data acquisition systems connected in parallel with a circuit. Cell voltages can be determined directly from the voltage difference between the anode and cathode. Using Ohm's law, in Equation 2-9, the current, I (A) can be calculated using the measured voltage, V_{cell} (V) and the external load or resistance R_{ext} (Ω). (Chouler et al., 2016, Logan et al., 2006)

$$I = \frac{V_{cell}}{R_{ext}} \qquad 2\text{-}9$$

2.3.8.1 Electrode potential

The potential of an electrode, anode or cathode, can only be determined by measuring the voltage against an electrode with a known potential, which is a reference electrode. A reference electrode is composed of several phases of constant composition and therefore has a constant potential. The standard hydrogen electrode or normal hydrogen electrode (NHE) consists of a platinum electrode in a hydrogen saturated acidic solution (all components at unit activity (1 M)), has a potential of 0 V. The NHE is not a practical reference electrode to use in an experimental setup and therefore other reference electrodes are often used. The silver-silver chloride (Ag/AgCl) reference electrode is the most popular reference electrode due to its simplicity, stability and nontoxicity. The Ag/AgCl reference electrode develops a potential of +0.197 V against the NHE in a saturated potassium chloride solution at 25 °C. Electrode potentials are strongly dependent on the pH of the systems, and it is therefore important to report the pH of the electrolytes, preferably reported against the NHE expressed in V or V vs NHE (or Ag/AgCl). (Logan et al., 2006, Minteer et al., 2007)

2.3.8.2 Power

Principally the overall performance of MFCs is evaluated through power output and Coulombic efficiency, which is the actual amount of conversion of substrate (electron donor) to electricity (Alterman et al., 2006). Equation 2-10 is used for calculating power output, P (W);

$$P = IV_{cell} \qquad 2\text{-}10$$

The MFC is normally connected to a circuit containing a fixed external resistor (R_{ext}) over which the voltage of the cell is measured across, and the current can be calculated from Ohm's law in Equation 2-9, giving Equation 2-11;

$$P = \frac{V_{cell}^2}{R_{ext}} \qquad 2\text{-}11$$

Power can also be calculated using Joule's law, Equation 2-12;

$$P = \frac{I^2}{R_{ext}} \qquad 2\text{-}12$$

The maximum power is calculated from the polarisation curve. The internal resistance (R_{int}) of the device is determined by fitting the ohmic region of each polarisation cell potential curve ($R_{int} = \Delta V/\Delta I$). By recording polarisation curves, the onset of concentration losses can be determined. (Logan et al., 2006, Chouler et al., 2016, Alterman et al., 2006)

2.3.8.3 Polarisation curves

A polarisation curve represents the voltage as a function of the current. If a potentiostat is available, polarisation curves can easily be recorded for the anode, cathode or for the entire reactor. If a potentiostat is not available, one can use a variable resistor box to set variable external loads. Using Ohm's law, periodically decreasing the load measuring the voltage at the current. The polarisation curve should be recorded from high to low external resistance and vice versa. When using an external resistance, only when pseudo-steady-state conditions have been established should the current and potential values be taken. (Logan et al., 2006)

A polarisation curve generally has three dominant regions, the first where the activation losses are dominant, the second where the ohmic losses are dominant, and the third where the concentration losses or mass transport effects are dominant. The first region starts with the open circuit, OCV at zero current, where there is a steep initial decrease in voltage. In the second region the voltage drop is linear with current, in the third region, at higher currents the voltage falls rapidly. When the polarisation curve is linear, the slope is equal to the internal resistance (Equation 2-8). With a non-linear polarisation curve, a current-dependent internal resistance, R_{int}, cannot be defined and the system should rather be expressed with an ohmic resistance R_{Ω} and the electrode over potentials ($\Sigma\eta_a$ and $|\Sigma\eta_c|$) (Equation 2-7) which can be determined with the current interrupt method. (Logan et al., 2006)

2.3.8.4 Power density

To compare various MFC systems, power is often normalised to a certain characteristic of the reactor. The power density is usually calculated on basis of either the total or the macro surface area of the anode, because the anode is where the biological reaction takes place. In some cases, the area of the cathode can be used to determine the power density. Normalisation to reactor volume is also performed frequently. The choice of parameter for normalisation depends on the application. Equation 2-13 and Equation 2-14 gives the power densities;

$$P_{An} = \frac{V_{cell}^2}{A_{An} R_{ext}} \quad 2\text{-}13$$

$$P_v = \frac{V_{cell}^2}{v R_{ext}} \quad 2\text{-}14$$

Here P_{An} is the power density (W/m^2), P_v is the volumetric power (W/m^3), A_{An} is the surface area of the anode (m^2) and v is the total reactor volume (m^3). A comparison based on total reactor volume is not always useful when comparing different configuration MFCs (Dual- and single chambered reactors). Comparison of different MFCs is very difficult. (Chouler et al., 2016, Logan et al., 2006)

2.3.8.5 Power curves

A power curve describes the power or power density as a function of current or current density and is calculated from the polarisation curve. From the open circuit, where no current flows there is no power produced. From the zero point the power output increases with an increase in current to a maximum power point (MPP), and after this point the power starts to decrease due to ohmic losses which increases and electrode overpotentials to the point of short circuit conditions, where zero power is produced. The MPP is predominantly defined by the ohmic resistance in most MFCs, partially due to low ionic conductivity of the electron donor (substrate) solutions, but usually to a low degree of optimisation in the fuel cell design. (Logan et al., 2006)

2.3.8.6 Coulombic efficiency

The Coulombic efficiency, ϵ_C, describes the efficiency with which Coulombs or charge is transferred in the MFC system from the substrate or electron donor to the anode (actual Coulombs transferred/maximum possible Coulombs). The total Coulombs obtained can be

calculated by integrating current over time. The Coulombic efficiency, ϵ_{Cb}, in a batch-fed MFC system over a time-period, t_b, can be calculated using Equation 2-15;

$$\epsilon_{Cb} = \frac{M \int_0^{t_b} I \, dt}{Fbv_{An}\Delta COD} \quad 2\text{-}15$$

Here M is the molecular weight of oxygen (M = 32), F is Faraday's constant, b is the number of electrons exchanged per mole of oxygen, v_{An} is the volume of the liquid in the anode compartment, and ΔCOD is the change in chemical oxygen demand (COD) over time t_b. For continuous flow, based on steady condition current generation, the Coulombic efficiency can be calculated by Equation 2-16;

$$\epsilon_{Cb} = \frac{MI}{Fbq\Delta COD} \quad 2\text{-}16$$

Here q is the volumetric influent flow rate and ΔCOD the difference of the COD in the influent and effluent. (Logan et al., 2006)

One of the factors that may reduce the Coulombic efficiency includes the utilisation of alternative electron acceptors by the microorganisms, but providing that the anode remains attractive enough for the microorganism with its potential, the alternative electron acceptors will mostly not be used. Microorganisms unable to use the electrode as electron acceptor will probably use the substrate for fermentation or methanogenesis. Other factors that may reduce Coulombic efficiency is microbial growth and competitive processes. (Logan et al., 2006)

2.3.8.7 Growth yield

Due to the diversion of electrons into biomass, cell growth will reduce Coulombic efficiency. The observed cell yield, Y, is used to measure the utilisation of substrate for growth, and is calculated by Equation 2-17;

$$Y = \frac{X}{\Delta COD} \quad 2\text{-}17$$

Here X is the biomass (g COD) produced over time. (Logan et al., 2006)

2.3.8.8 Energy efficiency

One of the most important evaluations of performance of an MFC is the energy recovery. The overall energetic efficiency ϵ_E, is the ratio of power produced by the cell over a time interval,

t, and the heat of combustion of the organic substrate added in that time frame, as given by Equation 2-18;

$$\epsilon_E = \frac{\int_0^t V_{cell} I \, dt}{\Delta H m_{added}} \qquad 2\text{-}18$$

Here ΔH is the heat of combustion (J mol^{-1}) and m_{added} is the amount (mol) of substrate added. (Logan et al., 2006)

2.3.9 Applications

MFCs can be considered as general devices for power generation; however, recent studies have been focused on their unique applications. These special applications are discussed below. (Kim et al., 2006)

2.3.9.1 Biomedical applications

MFCs are associated with the use in self-powered and low-energy consuming micro- or nanoscale biomedical devices due to MFCs being able to operate in physiological conditions and having miniature dimensions. The list of the biomedical applications for biofuel cells is comprehensive. The biofuel cells can be used to provide a long term or even permanent power supply, since the used fuel can be withdrawn without the limit of blood flow. This power supply can be used to power devices such as pacemakers, small valves for bladder control, or glucose sensors for diabetics. It can be used as implantable devices, sensors, drug delivery and micro-chips. Biofuel cells have successfully been implanted and operated in a grape. (Bullen et al., 2006, Kim et al., 2006, Ringeisen et al., 2006, Mano et al., 2003)

2.3.9.2 Wastewater bioremediation

Wastewater is characterised based on the amount of dissolved oxygen. This value is known as the biochemical oxygen demand (BOD) and correlates with the amount of organic solute in waste water solution. Microbes in MFCs have the ability to oxidise and reduce a broad range of these organic contaminates by using the dissolved oxygen present in the waste water. MFCs are being used to treat process water while generating renewable resources like clean water and clean energy which can be used to power the process. (Aviles et al., 2017, Ghasemi et al., 2013)

2.3.9.3 Methane production

Electromethanogenesis is a process in which the anaerobic treatment process is enhanced by improving biogas production. The EcoVolt Reactor is a flagship product from Cambrian Innovation where the anode is "coated" with biological substrates to convert the organic contaminants in the wastewater into electrons. The electrons and carbon dioxide are converted to methane gas by the biologically "coated" cathode. (Aviles et al., 2017)

2.3.9.4 Space applications

Not only have they used biofuel cells as a power generating system by utilising human waste as fuel during space flights, the Naval Research Laboratory (NRL) have are now working on a prototype rover powered by the exoelectrogen bacteria *Geobacter sulfurreducens* known for breaking down metals. Dr Gregory P. Scott is working on a hybrid MFC and battery system to power a small, approximately 1 kg, hopping rover, in which the MFC will be responsible for powering the low load devices such as the electronics, sensors and control systems. The MFC will also be used to recharge the battery responsible for the heavy loads. (Barret, 2000)

2.3.9.5 Desalination

Microbial electrochemical technologies can be used for water desalination. The addition of an anion exchange membrane (AEM) and a cation exchange membrane (CEM), with salt water in the middle, water desalination and electricity production can be attained in a microbial desalination cell (MDC). The energy efficiency for desalination can be increased by using stacks of membranes. A reverse electrodialysis (RED) stack is a stack of paired AEM and CEM membranes with water containing high or low salt concentrations in alternating channels, which produces an electrical potential. More power is generated when an RED stack is inserted between the anode and an air cathode in a microbial reverse electrodialysis fuel cell (MRFC) than a normal MFC. More hydrogen gas is produced in a microbial reverse electrodialysis electrolysis cell (MREC) without the need for an electrical power source, which is required for an MEC. Other types of desalination systems exist with conservative MFC modifications. (Logan et al., 2015)

2.3.9.6 Hydrogen production

It is possible to generate hydrogen at the cathode of the MFC, by "supporting" the potential generated by the microorganism at the anode with a small potential via an external power source of approximately more than 0.25 V. These reactors are known as bioelectrochemically

assisted microbial reactors (BEAMRs) or biocatalysed electrolysis systems. These systems are not true fuel cells because they are operated to produce hydrogen rather than electricity. Modifying the conservative MFC, by adding a secondary chamber for capturing the hydrogen gas, it is possible to develop many new systems for hydrogen production. (Logan et al., 2006) Hydrogen production from acetate have yielded 2.9 moles of hydrogen per moles of acetate, approaching the theoretical maximum of 4 mol/mol for an energy input equivalent of 0.5 moles of hydrogen. This represents a net energy gain by a factor of 5.8 in terms of electricity requirement for hydrogen production by the BEAMR process versus the required net energy loss for water electrolysis, which means that biohydrogen net energy requirement is sustainable by the organic matter degraded by microorganisms. (Logan and Regan, 2006)

2.3.9.7 Electronics

Microbial fuel cells have the possibility to be used as a portable power cell, or a portable power supply for numerous electronic devices, such as mobile telephones. The benefits include that it does not require any precious metals, so it can be readily recycled or disposed of, it has instant recharge times, with lifetimes in the order of a month between replacements. (Bullen et al., 2006, Kim et al., 2006)

2.3.10 **Comparative performance data**

Comparison of various MFCs is extremely difficult due to the various factors influencing the power outcomes. Most studies expressed power output as mA/m^2 and mW/m^2 of electrode surface, as derived from descriptions of conventional catalytic fuel cells. Expressing power output as mW/m^2 might be sufficient for chemical fuel cells, but MFCs are different due to the living catalysts utilised, i.e. microbes in the MFCs, since these catalysts have specific requirements and occupy a certain volume in the reactor, thus decreasing free space and pore size. Most studies refer to the combination of parameters such as reactor volume, PEM, catholyte, and anode surface, but comparison remains problematic due to the large number of factors that influence the power output.

It is also worth noting that the normalisation of the power output is difficult since some studies only use the anode compartment volume and others use the total volume when referring to mW/m^3 (Rabaey and Verstraete, 2005). The power densities obtained from MFCs from the literature are summarised in Table 2-1.

Table 2-1: Comparison of the construction and performance of some recent MFCs.

Power output	Microbial source	Electrode type	Reference
0.35 W/m^3 *	*Geobacter sulfurreducens*	Plain graphite	(Rabaey and Verstraete, 2005, Bond and Lovley, 2003)
0.08 W/m^3 *	*Shewanella putrefaciens*	Woven graphite	(Rabaey and Verstraete, 2005, Kim et al., 2002)
0.25 W/m^3 * 1.7 W/m^3 * 0.96 W/m^3 *	*Rhodoferax ferrireducens*	Plain graphite Woven graphite Graphite foam	(Rabaey and Verstraete, 2005, Chaudhuri and Lovley, 2003)
8.8 W/m^3 *	*Pseudomonas aeruginosa*	Plain graphite	(Rabaey et al., 2005a, Rabaey and Verstraete, 2005)
48 W/m^3 *	Wastewater (mixed culture)	Granular graphite matrix	(Davis and Higson, 2007, Rabaey et al., 2005b)
7 – 13 W/m^3 *	Domestic wastewater	Carbon fibre brush	(Logan et al., 2015)

* Normalised to anodic compartment volume

3. Materials and experimental setup

3.1 Materials used

3.1.1 Microorganism

Geobacteraceae sulfurreducens strain PCA (ATCC® 51573™) was acquired from the German Collection of Microorganisms and Cell cultures (DSMZ). The product sheet for the microorganism is given in Appendix B. This microorganism was chosen because it is the most extensively studied electricigen because it produces high current densities and is capable of producing highly conductive nanowires. Further reasoning behind the choice is that the complete genome sequence and genetic system are available. (Logan, 2009, Kim et al., 2008) *Geobacter sulfurreducens* is capable of producing higher power densities in the complete absence of oxygen. For this reason the microbial fuel cell will be running anaerobically. (Logan, 2009)

3.1.2 Growth media

All chemicals for the growth media were sourced from Sigma-Aldrich, South Africa. The growth media is made up of three separate solutions, namely the Geobacter medium (also known as the acetate-fumarate (NBAF) medium), the trace element solution and the vitamin solution.

3.1.2.1 Geobacter (NBAF) medium:

Ammonium chloride (NH_4Cl),	1.50 g
Disodium phosphate (Na_2HPO_4),	0.60 g
Potassium chloride (KCl),	0.10 g
Sodium acetate (Na-acetate),	0.82 g
Sodium bicarbonate ($NaHCO_3$),	2.50 g
Disodium fumarate (Na_2-fumarate),	8.00 g
Trace element solution;	10.00 mL
Vitamin solution;	10.00 mL
Distilled water;	980.00 mL

3.1.2.2 Trace element solution

Nitrilotriacetic acid,	1.50 g
Magnesium sulphate heptahydrate ($MgSO_4 \cdot 7H_2O$),	3.00 g
Manganese sulphate monohydrate ($MnSO_4 \cdot H_2O$),	0.50 g

Sodium chloride (NaCl),	1.00 g
Iron (II) sulphate heptahydrate ($FeSO_4 \cdot 7H_2O$),	0.10 g
Cobalt (II) sulphate heptahydrate ($CoSO_4 \cdot 7H_2O$),	0.18 g
Calcium chloride dihydrate ($CaCl_2 \cdot 2H_2O$),	0.10 g
Zinc sulphate heptahydrate ($ZnSO_2 \cdot 7H_2O$),	0.18 g
Copper (II) sulphate pentahydrate ($CuSO_4 \cdot 5H_2O$),	0.01 g
Aluminium potassium sulphate dodecahydrate ($KAl(SO_4)_2 \cdot 12H_2O$),	0.02 g
Boric acid (H_3BO_3)	0.01 g
Nickel (II) chloride hexahydrate ($NiCl_2 \cdot 6H_2O$),	0.01 g
Sodium selenite pentahydrate ($Na_2SeO_3 \cdot 5H_2O$),	0.03 g
Sodium tungstate dihydrate ($Na_2WO_4 \cdot 2H_2O$)	0.30 g
Distilled water	1000 mL
3.1.2.3 Vitamin solution	
Biotin,	2.00 mg
Folic acid,	2.00 mg
Pyridoxine hydrochloric acid (pyridoxine-HCl),	10.00 mg
Thiamine hydrochloric acid dihydrate (thiamine-$HCl \cdot 2H_2O$),	5.00 mg
Riboflavin,	5.00 mg
Nicotinic acid,	5.00 mg
D-Ca-pantothenate,	5.00 mg
Vitamin B_{12},	0.10 mg
p-Aminobenzoic acid,	5.00 mg
Lipoic acid,	5.00 mg
Distilled water,	1000.00 mL

3.1.3 **Carbon particles as growth substrates**

The carbon growth substrate was chosen with the following two parameters in mind: 1) large surface area to improve microbial growth; and, 2) conductive surface area to improve electricity conduction in the MFC. Two types were investigated individually and as a mixture, with their effect on the microbial growth and power production monitored. The two types of carbon chosen are an amorphous and a natural crystalline carbon.

3.1.3.1 Amorphous carbon: granular activated carbon (GAC)

Fine granular activated carbon (GAC) was supplied by Activated Carbon Innovations Filtatech, South Africa. According to Weck Laboratories, Inc. the product received from Activated Carbon Innovations Filatech, South Africa complies with the certificate of analysis summarised in Table 3-1. For full certificate of analysis, see Appendix C.

Table 3-1: Certificate of analysis for granular activated carbon (GAC).

Analyte	Result	Units
Apparent Density	0.389	g/cm
Ash content	1.55	% by Weight
Ball-Pan Hardness Number	98	Units
Iodine, Triple Point	879	mg I_2 / g GAC
Moisture @ ASTM D2867	8.63	% by Weight
Water Solubles	0.86	%
Size:	12 x 30	Mesh
	1.7 x 0.6	mm

3.1.3.2 Natural crystalline carbon: high purity natural graphite flakes

High purity natural graphite flakes (RFL 99.9) supplied by Graphit Kropfmühl AG, Germany were used. The certificate of analysis 3.1 EN 10204:2004 is summarised in Table 3-2, for full certificate of analysis, see Appendix C.

Table 3-2: Certificate of analysis for natural crystalline graphite.

Analyte		Result
Carbon content		99.9 %
Ash		0.1 %
Particle size (µm)	315	24.1 %
	200	54.3 %
	160	15.7 %
	100	4.0 %
	71	0.6 %
	-71	1.3 %

3.1.4 MFC construction material

All material used to build the MFC, which includes the polycarbonate plates, the M5 counter sunk machine screws, the 8 mm thick copper electrodes and copper wire as well as the Viton rubber gaskets were sourced from a local plastics supplier. The Nafion$^{TM.}$ 117 Perfluorinated proton exchange membrane were supplied by Sigma-Aldrich, South Africa. The components used to build the external circuit was supplied by Micro Robotics, South Africa and RS Components, South Africa.

3.1.5 Instrumentation and software

A PicoScope 2000 Series (2405A, Pico Technology, Ltd.) was used with a National Instruments USB-DAQ-6008 data acquisition system and National Instruments LabVIEW 2017^{TM} software.

SolidWorks 2017 was used to draw all illustrations (see Figure 3-1, Figure 3-2, Figure 3-3 and Figure 3-5) and mechanical drawings (see Appendix A) of the MFC. Schematic of the electrical circuit was drawn with Microsoft Visio (see Figure 3-4). Mathworks Matlab 2016 software was used to generate all graphs.

For the characterisation analyses, the following lab and instrumentation were used. The growth samples were sent to the Central Analytical Facilities CAF of Stellenbosch University who conducted the DNA sequencing. A Turbidity Meter Model: TU-2016 LTLUTRON was utilised to test the turbidity. A Nova 1000e Brunauer-Emmet-Teller instrument was used to determine the surface area of the samples. An ultrahigh resolution field emission scanning electron microscope (HR FE-SEM Zeiss Ultra Plus 55) was used to investigate the morphology of the carbon particles before and after growth.

3.2 Cultivation

The trace element solution was prepared separately and autoclaved for sterilisation at 121 °C for 40 min. Prior to any use, the solution was left to cool to room temperature to prevent unwanted reactions amongst components and was stored at room temperature. The vitamin solution was also prepared separately; its components cannot be autoclaved due to temperature sensitivity. This solution was filter-sterilised using a 0.2 µm filter, and as the solution is light sensitive, the bottle was covered with aluminium foil and stored at 4 °C. A Na-fumarate

solution in distilled water was prepared separately as well and filter-sterilised using a 0.2 μm filter and stored at room temperature.

The Geobacter (NBAF) media were prepared by dissolving all ingredients (except the fumarate and vitamin solution). Diluted HCl was added to the mixture until the pH of the mixture reached a value of 6.8. The growth media was transferred into the 10 mL Hungate anaerobic culture tubes filled with the respective carbon growth substrates (Sigma-Aldrich South Africa).

The carbon growth substrates were added to the Hungate tubes before the growth medium was added. 0.5 g of the two carbon types were added to their respective Hungate tubes and a mixture of the carbon in a ratio of 1:1 (0.25 g of each) were added to an additional tube, and then one empty tube as a reference or as a control sample. The tubes were then autoclaved at 121 °C for 40 min.

Once the Hungate tubes were cooled to room temperature, the vitamin and fumarate solutions were added, and the *Geobacter sulfurreducens* was then inoculated all anaerobically into the Hungate tubes containing the Geobacter (NBAF) media and carbon substrates in a glovebox under nitrogen atmosphere at atmospheric temperature (approximately at 30 °C). The growth cultures were incubated at 32 °C for 3 weeks without agitation.

3.3 MFC configuration

3.3.1 MFC design

It was decided to construct and investigate a batch operated dual chamber MFC, despite their characteristically high internal resistance. They allow for maintenance of anaerobic conditions in the anode chamber, which are ideal conditions for the *Geobacter sulfurreducens* specie which produces higher power densities in the complete absence of oxygen (Logan, 2009). Another reason for the dual chamber MFC is to avoid the mixing of the solutions of the electron acceptors and electron donors and therefore avoiding the loss of electrons (Deval and Dikshit, 2013).

The body of the cell was constructed with 12-mm-thick polycarbonate plates fastened with M5 counter sunk machine screws. Both electrodes were 8 mm thick copper electrodes. The macro-surface area of each electrode was 90 mm^2. The electrodes were soldered to an external circuit

using copper wire. Each chamber was constructed with 9 mL working volume. The chambers were separated with a Nafion$^{TM.}$ 117 Perfluorinated proton exchange membrane (Sigma-Aldrich, South Africa). To ensure the MFC was impermeable, it was tightly sealed with 3 mm Viton rubber gaskets. Figure 3-1 gives an illustration of the design of the MFC in full assembly design. The mechanical design of the MFC can be found in Appendix A, with its exact dimensions and material specifications. Figure 3-2 gives a sectioned view of the MFC design and Figure 3-3 gives an exploded view of the design. The two compartments are identical; therefore, one compartment is exploded separately to enable a better view of the construction.

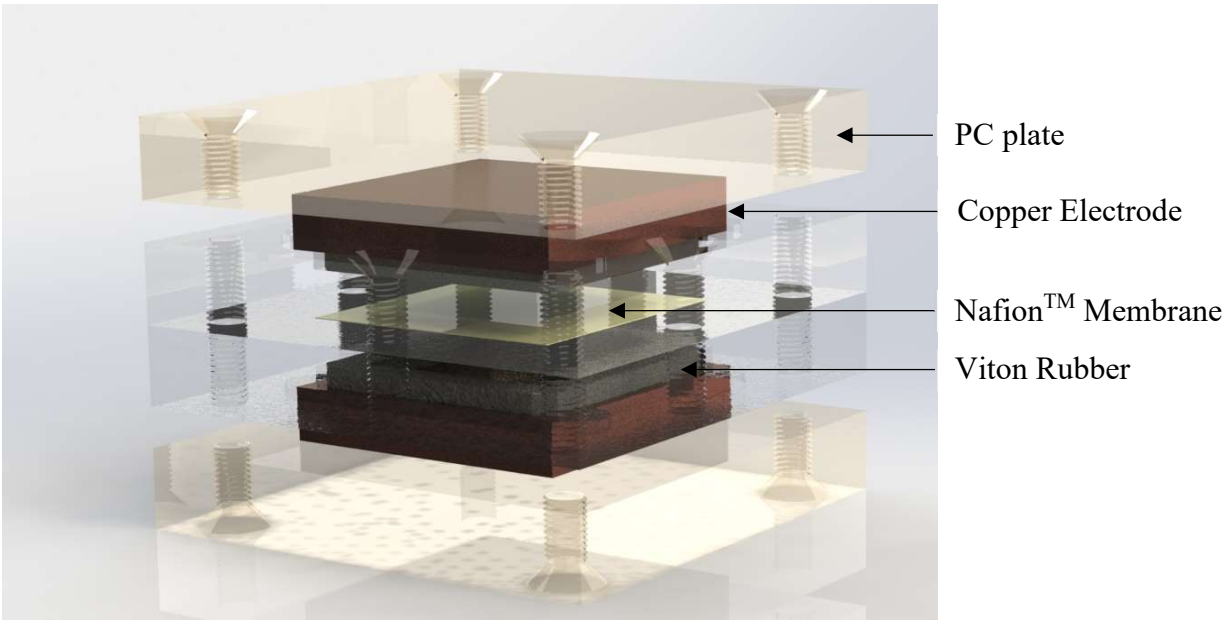

Figure 3-1: Full assembly illustration of MFC design employed for experiments (drawn with SolidWorks software 2017).

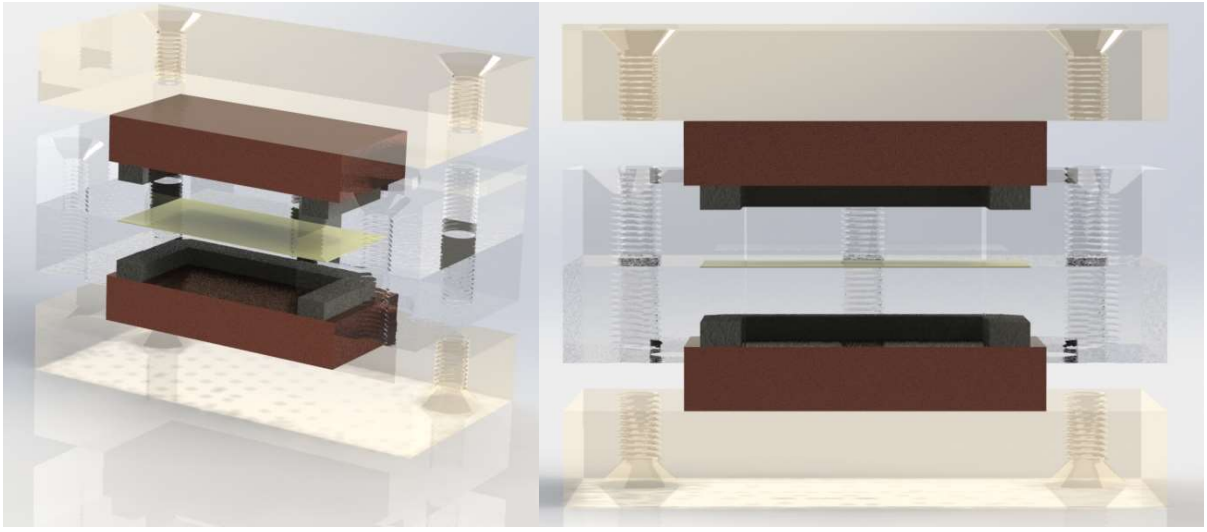

Figure 3-2: A sectioned view and a front view of the MFC enabling a perfect view of the anodic (bottom) compartment, where the G. sulfurreducens and carbon substrates reside (drawn with SolidWorks software 2017).

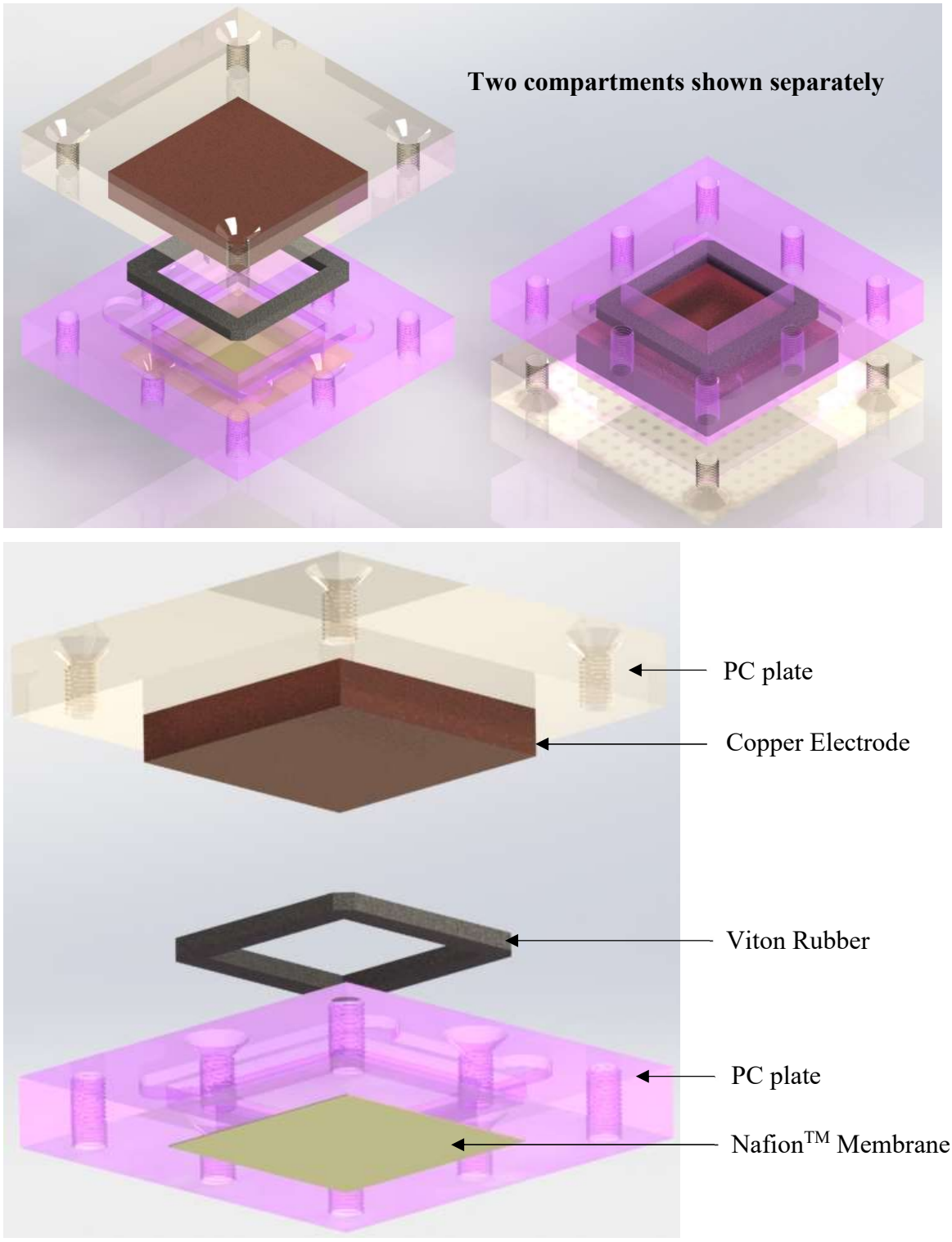

Figure 3-3: Exploded view of the MFC design. Top images illustrate the complete MFC; since the two compartments are identical the bottom image is an exploded view of one of the compartments of the cell (drawn with SolidWorks software 2017).

3.3.2 Electrolyte

For metabolic energy to be generated, microorganisms consume the electron donors which are transferred from the anolyte (electrolyte in anodic compartment) producing electrons and protons. The microorganism should transport the electrons from the electron donor through the electron transport chain to the anode which are passed through the external circuit and the proton is transported through the proton membrane. The electron acceptors receive the electrons from the cathode. This electron transfer from the anodic chamber to the cathodic chamber produces the electricity current. Both electrolytes, anolyte and catholyte (electrolyte in cathodic chamber) are important since they contain the electron donor and electron acceptor which influences the power density. (Ucar et al., 2017, Alterman et al., 2006, Bullen et al., 2006).

The catholyte was chosen to be the growth medium, i.e. all ingredients dissolved in distilled water in the absence of the Na-fumarate and the vitamin solutions, autoclaved for sterilisation and cooled. The fumarate was omitted since it was the electron donor and by avoiding the mixing of electron donor and electron acceptor in one chamber allows for the avoidance of loss of electrons (Deval and Dikshit, 2013). The vitamin solution was excluded since it contains expensive ingredients and since there were no microbes in the cathodic chamber that requires special vitamins and minerals, the vitamin solution was not required. This electrolyte was aerated before being added to the cathodic chamber since oxygen was the electron accepter. Oxygen is the most common electron acceptor used in the cathodic chamber due to its high oxidation potential and after reduction oxygen yields clean water (Ucar et al., 2017).

The anolyte was the contents of the Hungate tubes which was transferred under anoxic conditions. The contents of the Hungate tubes were the growth media, the *G. sulfurreducens* species after various growth periods and the carbon particles acting as the growth substrate. In this solution the electron donor was fumarate.

3.3.3 Electrical system and electrochemical monitoring

Three MFCs were built to be connected into the same circuit to run three tests in parallel to enable comparison. The anode and cathode both were connected to switches to disconnect the single MFC from the circuit completely when not measured. The cell potential (V) was continuously monitored using a PicoScope while using a National Instruments USB-DAQ-

6008 data acquisition system to switch between the MFCs and external resistors. LabVIEW 2017^{TM} software was used to log the data continuously. The PicoScope was connected in parallel to the MFCs. The external resistance, R, was varied between 250 Ω, 500 Ω, 1 kΩ, 2.5 kΩ and 5 kΩ. The schematic of the external circuit is given by Figure 3-4. The components used to build the external circuit was supplied by Micro Robotics South Africa and RS Components SA. All switches are relays which are activated via a DAQ, but from here on out will be referred to as switches.

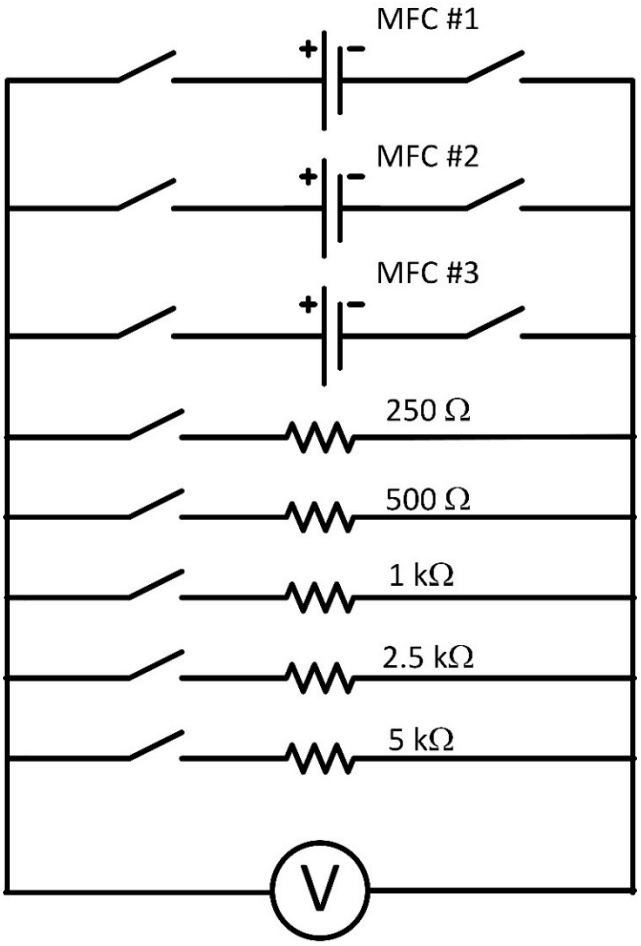

Figure 3-4: External electrical circuit including three MFC cells running and sampling simultaneously, connected to 5 resisters connected to a PicoScope measuring cell potential (drawn with Microsoft Visio).

The three MFCs were filled with the growth media of choice under anoxic conditions using the glovebox under nitrogen atmosphere. For most of the runs MFC #1 was filled with pure *G. sulfurreducens* (no carbon substrate was added), MFC #2 was filled with *G. sulfurreducens* with the growth substrate graphite, and MFC #3 was filled with *G. sulfurreducens* with the growth substrate GAC. Figure 3-5 gives and illustration of the 3 different MFCs that are

described above. The following sequence was followed for each consecutive MFC. For the measuring of MFC #1, both anode and cathode switches were closed for MFC #1, but open for both MFC #2 and #3. Then the software worked as follows for a single measurement:

The switch was closed for the desired resistor, starting at the lowest, 250 Ω, 10 s were allowed for the signal to stabilise, then a measurement, or "sample", was taken. The program waited 2.5 s before taking another sample at the same resistor (250 Ω), this was repeated 5 times to take an average measurement for MFC #1 at 250 Ω. This averaged measurement was then recorded.

The switch for 250 Ω was then opened and the switch for the next resistor, 500 Ω was closed. The process mentioned above was repeated, i.e. there was a 10 s waiting period after closing the switch to the 500 Ω resistor, to enable stabilisation of the signal before a sample was taken. After waiting 2.5 s another sample was taken (up to a total of 5 samples at the same resistor). An average value of the 5 sample measurements was then recorded, before opening the switch.

This sequence was repeated for the remaining 1 kΩ, 2.5 kΩ and 5 kΩ resistors, including the MFC #1 in an open circuit position, i.e. not connected to any resistor or load. After all resistors, and the open circuit voltage was measured for MFC #1, MFC #1 was completely disconnected from the circuit by opening the switches at both the anode and cathode.

This entire procedure was repeated for MFC #2, and MFC #3 respectively. After all three MFCs were measured sequentially, all switches were opened with a 10 min waiting period before repeating the entire procedure from MFC #1, 250 Ω until MFC #3, V_{OC}. This was repeated for approximately 170 h.

The runs were performed for pure *G. sulfurreducens* (no carbon substrate), *G. sulfurreducens* with graphite, and *G. sulfurreducens* with GAC, all at various growth periods. The first run was done for a growth period of 1 month, the second for a growth period of 3 months, and the third for a growth period of 4 months. Then the three MFCs were all filled with *G. sulfurreducens* in a GAC to graphite mixture (1:1) as a growth substrate all at a growth period of 4 months.

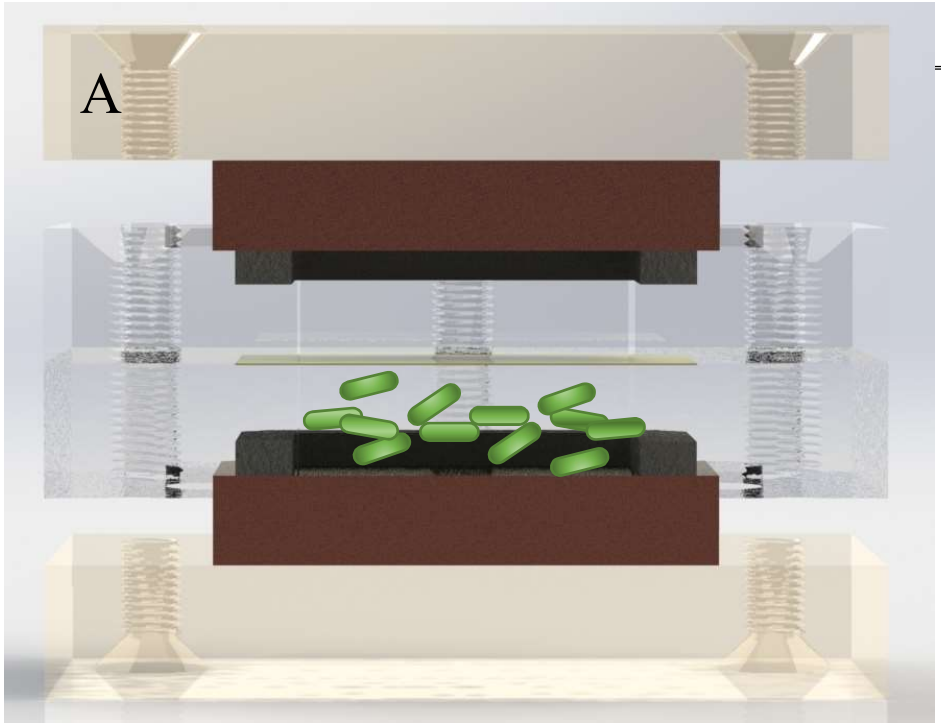

Figure 3-5: All MFCs connected in parallel per experiment;

A: Pure G. sulfurreducens;

B: Pure G. sulfurreducens with GAC particles;

C: Pure G. sulfurreducens with graphite particles

(drawn with SolidWorks Software 2017).

Key:

GAC:

Graphite:

G. sulfurreducens:

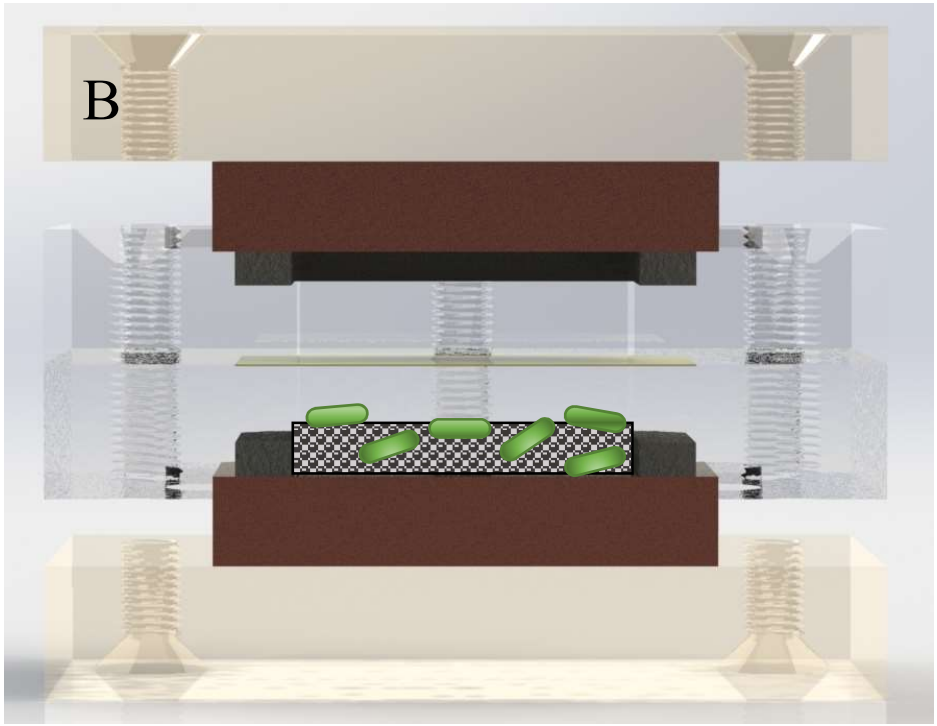

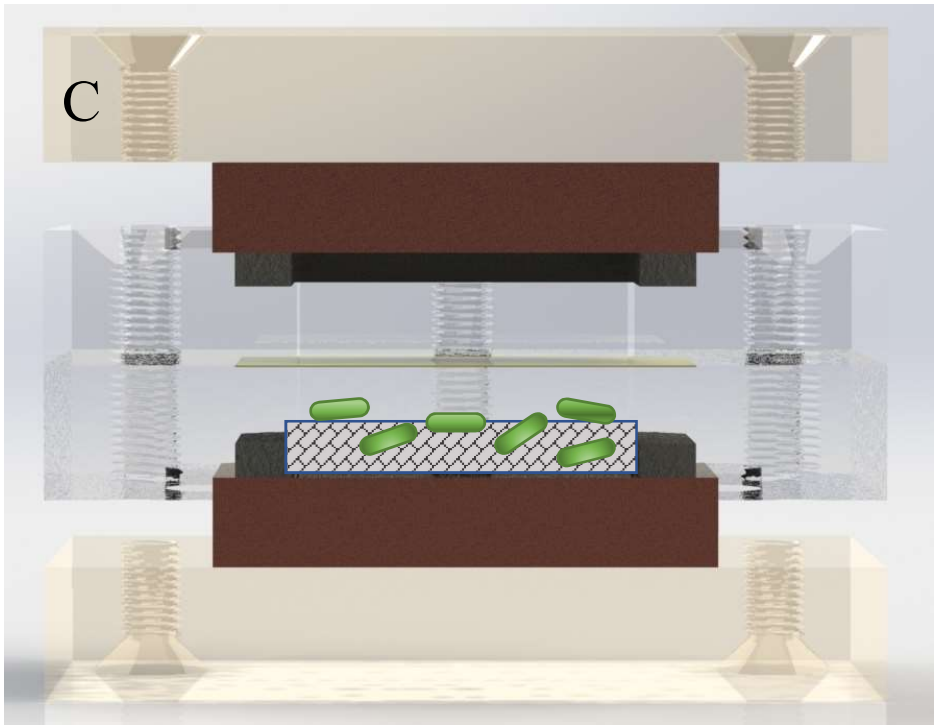

3.3.4 Electrical parameters and measurements

As explained in Section 3.3.3, the cell potential was measured at various external resistances. Using Ohm's law, in Equation 2-9, the current, I (mA) was calculated using the measured voltage, V_{cell} (mV) and the external load or resistance R_{ext} (Ω). (Chouler et al., 2016, Logan et al., 2006)

$$I = \frac{V_{cell}}{R_{ext}} \qquad 2\text{-}9$$

Principally the overall performance of MFCs is mainly evaluated through power output and Coulombic efficiency, which is the actual amount of conversion of substrate (electron donor) to electricity. The conversion of the substrate was not measured; therefore, the performance of the cells was quantified by power output. Equation 2-10 was used for calculating power output, P (W):

$$P = IV_{cell} \qquad 2\text{-}10$$

Combining Ohm's law, Equation 2-9, with Equation 2-10, the power output of the MFCs was determined using Equation 2-11, only taking into consideration the measured voltage, V_{cell} (mV) and the external load or resistance, R_{ext} (Ω):

$$P = \frac{V_{cell}^2}{R_{ext}} \qquad 2\text{-}11$$

To compare the various MFC systems, power was normalised to the total reactor volume (m^3). The normalised power output is referred to as power density, the power density was determined using Equation 2-14:

$$P_v = \frac{V_{cell}^2}{vR_{ext}} \qquad 2\text{-}14$$

Here P_v is the power density (W/m^3) and v is the total reactor volume with a value of 18 mL using units of m^3. (Chouler et al., 2016, Logan et al., 2006, Alterman et al., 2006).

The energy, E (J) generated by the system can be determined by integrating the power, P (W) generated over a time-period, using Equation 3-1.

$$E = \int_0^t P(t) \qquad 3\text{-}1$$

The definite integral of an integrable function can be approximated to within a desired degree of accuracy by a Riemann sum, which states that the Riemann sum can be interpreted as a sum

of areas of approximating rectangles. With an arbitrary function, *f(x)* with $a \leq x \leq b$, and dividing the interval [*a,b*] into *n* subintervals of equal width $\Delta x = (b - a) / n$. There will be x_n^* sample points. The definite integral, or Riemann sum, can be described by Equation *3-2*. (Stewart, 2011)

$$\int_a^b f(x)dx = \lim_{n \to \infty} \sum_{i=1}^{n} f(x_i^*)\Delta x \qquad 3\text{-}2$$

Equation 3-3 represents the formula in terms of the variables specific for the system in question, power density (P_v) and energy (E), which was employed for all calculations.

$$E_v = \sum_{i=0}^{n} \left[\left(\frac{P_v(t_i) + P_v(t_{i+1})}{2} \right) \cdot \left(\frac{b-a}{n} \right) \right] \qquad 3\text{-}3$$

The power density, P_v (mW/m^3) generated over time (t) for all the various external loads have a consistent consecutive sampling time of 0.1681 h i.e. 10.086 min. This sampling time is equal to the width of each rectangle in the Riemann sum, $\left(\frac{b-a}{n}\right)$, where *b* represents the ending time, *a,* the starting time and *n,* the number of samples taken. By substituting the constants for this specific calculation Equation 3-3 can be re-written as Equation 3-4.

$$E_v = \sum_{i=0}^{n} \left[\left(\frac{P_v(t_i) + P_v(t_{i+1})}{2} \right) \cdot (0.1681) \right] \qquad 3\text{-}4$$

The above formula was used to determine the total energy density (MJ/m^3) generated by the cell under a specific load.

3.4 Characterisation

3.4.1 PCR amplification and DNA sequencing of 16S rRNA gene fragments

The complete genome sequence and genetic system are available for *Geobacter sulfurreducens*, and since it is known that power densities produced from a pure culture are generally lower than that produced from a rich and diverse source of bacteria. In order to justify the results obtained it should be specified from which microorganism power was generated. (Kim et al., 2008, Logan, 2009)

DNA was extracted from the biofilm in the growth media before being transferred into the MFC anode chamber. The growth media were vigorously homogenised by vortex stirrer for 10 s. 1000 µL of sample containing DNA was pipetted into a 1.5 mL tube and frozen at -80 °C for approximately 10 min. The samples were allowed to thaw at room temperature and again

homogenised for 10 s. The freeze-thawing process was repeated a total of three times. The purpose of this process is to break the cell wall apart and/or for membrane to release the genetic material. The samples were syringe-filtered with a 0.1 µm filter with ultra-pure filtered water into 1.5 mL tubes.

For PCR preparation, the above-mentioned samples were diluted three sequential times using 30 µL of the sample in 270 µL of ultra-pure filtered water (3 DNA samples with different dilution). The PCR preparation took place in a UV-sterilised fume hood. PCR amplification was performed at final volume of 25 µL. One microliter of each DNA sample was added to the PCR master mixture, which consisted of the following (µL): ultra-pure filter water, 97.6; buffer 10x, 15; dNTP (2mM), 15; E9F, 7.5; U1510R, 7.5; BSA (20 ng/µL), 1.5 and *Taq*, 0.3. PCR amplification was done on all 3 different dilution samples together with a control sample as a reference, at a 1500 kb base sequence.

To purify the DNA samples, NucleoSpin® Gel and PCR Clean-up column were utilised. The following protocol for PCR clean-up, as well as DNA concentration and removal of salts and enzymes from enzymatic reactions were followed. To adjust the DNA binding condition, buffer NTI and the sample was mixed with a volume-ratio of 2:1. To enable binding of the DNA, a NucleoSpin® Gel and PCR Clean-up column was placed into a 2 mL collection tube and loaded with 700 µL of the DNA samples and centrifuged at 11000 x *g* for 30 s. The flow-through was discarded. To wash the silica membrane, 700 µL of buffer NT3 was added to the NucleoSpin® Gel and PCR Clean-up column and again centrifuged at 11000 x *g* for 30 s. The flow-through was again discarded. In order to dry the silica membrane, the sample was centrifuged again at 11000 x *g* for 1 min to ensure that all of the buffer NT3 was removed. To elute the DNA, the NucleoSpin® Gel and PCR Clean-up column was placed into a new 1.5 mL micro-centrifuge tube and 30 µL of buffer NE was added. The mixture was incubated at room temperature for 1 min and then centrifuged one last time at 11000 x *g* for 1 min. The column can now be discarded, whereas the tube now contains the DNA. The samples were sent for sequencing at the Central Analytical Facilities CAF of Stellenbosch University.

The samples were also assessed for nucleic acid purity. Proteins and nucleic acids have absorbance maxima at 280 and 260 nm, respectively. The purity in both nucleic acid and protein extraction have been historically measured by the ratio of the absorbance at these

wavelengths. A ratio of the 260/280 absorbance values of approximately 1.8 is generally accepted as "pure" for DNA whereas a ratio of 260/280 approximately 2.0 is generally accepted as "pure" for RNA. One would normally look for a value of 260/280 between 1.8 and 2.0 to consider the sample as "pure" (Matlock, 2015)

Absorbance at 230 nm is recognised as being the result of various contaminants; consequently, the ratio of the wavelength A_{260}/A_{230} is frequently calculated. For "pure" nucleic acid the 260/230 ratio values are often higher than the respective 260/280 ratio values. The expected range for 260/230 ratio values are commonly between 2.0 and 2.2 (Matlock, 2015).

3.4.2 **Turbidity**

Optical density (OD) or turbidity liquid solution is the cloudiness due to particles, and in this case biomass which is generally invisible to the naked eye. Turbidity is measured by a nephelometer with a detector connected on the side on the light beam. The higher the number of particles, or biomass in the solution, the higher the amount of scattering of light that will take place and more light will reach the detector. From a calibrated nephelometer the units of turbidity are called Nephelometric Turbidity Units (NTU). The output is dependent on a number of factors, including the shape, colour and reflectivity of the particles in the solution, whether the particles settle out etc.

A Turbidity Meter Model: TU-2016 LT_{LUTRON} was used to test the turbidity of the growth media containing pure *G. sulfurreducens*. The turbidity of the growth media with the carbon growth substrates could not be tested due to the carbon particles in the mixture. The colour of the carbon particles influences the measurement, both carbon substrates settled out quite quickly, but small particles were observed floating which would lead to an inaccurate measurement. The graphite particles have a high reflectivity which would also influence the measurement. Therefore, only the control samples containing only *G. sulfurreducens* was measured to correlate with the growth curves discussed below in Section 3.4.3.

3.4.3 **Dry cell mass/growth curves**

To determine the effect of the added carbon substrates on the microbial growth of *G. sulfurreducens*, the growth curves of the various inoculants were determined for the initial 3 weeks. In order to determine the growth curve, the biomass needed to be quantified after

initial inoculation for a period of 3 week. This was challenging due to the carbon substrates in the mixture. It was decided to measure the dry mass of the mixture – the carbon as well as the biomass from the *G. sulfurreducens* – and then ultimately subtracting the initial carbon mass measured and noted for each sample, resulting in the dry cell mass of the microorganism.

To collect all microbial cells from the suspended culture from all the various samples (pure *G. sulfurreducens*, with GAC and with graphite), each sample was subjected to centrifugation at 4000 rpm for 15 min, so that the microbes and carbon substrates (where applicable) could sediment in a pellet at the bottom of the centrifugation tube. The supernatant was discarded and the wet precipitate, or pellet was frozen at -40 °C overnight. The frozen pellets were then freeze-dried, and the mass of the freeze-dried pellets were determined. The mass of the carbon substrate per sample was subtracted from the final mass yielding the dry biomass. This was done over a course of 3 weeks to estimate a growth curve for *G. sulfurreducens*, and to compare the growth of pure bacteria to that grown on the two different carbon growth substrates. This is an indication of how well the bacteria grows on the added growth substrate, for instance aiding growth or possibly inhibiting growth.

3.4.4 **Brunauer-Emmet-Teller (BET) surface area analysis**

The theory of multimolecular adsorption proposed by Brunauer, Emmett and Teller (BET) explains qualitatively many common features of gas adsorption isotherms and gives a quantitative measure of the surface area of the adsorbent. The BET model states that the molecules in the one layer can act as a possible adsorption site for the molecules in the following layer. This is the most popular technique to use for the determination of the surface area over a wide range of porous materials. (Brunauer et al., 1938, McMillan and Teller, 1951, Watt-Smith et al., 2008b)

The surface area of the carbon particles was measured on a Nova 1000e BET instrument by means of the 5-point BET method. Approximately 0.5 g of freeze dried samples were outgassed using nitrogen. Nitrogen (at 77 K) is the most widely used adsorptive for surface area determination (Watt-Smith et al., 2008b). The analysis adsorptive was therefore nitrogen and the analysis bath temperature 77 K. An equilibration interval of 10 s was used.

3.4.5 **Field emission scanning electron microscope (FE-SEM)**

The principle of electron microscopy is the same as with light microscopy, but it uses very energetic electrons as a source instead of visible light. This shortens the wavelength enabling the observation of vary small features. The wavelength is proportional to the applied high voltage. By applying the Rayleigh criterion, using Planck's constant and by following the derivative by Alyamani and Lemine (2012), one can determine the exact wavelength for a set accelerated voltage. The extremely small wavelengths make it possible to see atomic structures using accelerated electrons. (Alyamani and Lemine, 2012)

An ultrahigh resolution field emission scanning electron microscope (HR FE-SEM Zeiss Ultra Plus 55) was used to investigate the morphology of the carbon particles used as growth substrates, with an InLens detector at an acceleration voltage of 3 kV to ensure maximum resolution of surface detail. The freeze-dried samples as prepared in section 3.4.3 were prepared with electrically conductive coatings and investigated to compare the growth of microbial cells on the crystalline and amorphous carbon.

4. Results

4.1 PCR amplification and DNA Sequencing of 16S rRNA gene Fragments

Database searches for the related 16S rRNA genes sequences attained by CAF of Stellenbosch University were conducted using the BLAST program and the GenBank nucleotide sequence database. The BLAST result for sample A (Accession number: NC_002939.5) yielded a complete genome for the *Geobacter sulfurreducens* PCA chromosome with a length of 3814128. The result yielded 100 % query cover with 100 % identification (1083 bits – 586/586) with 0 % gaps (0/586). The sequence for the complete genome *Geobacter sulfurreducens* PCA chromosome with sequence ID: NC_002939.5 is given in Figure 4-1.

```
Query  1       TCCTTCGGGGTGGTGAAAGTGGCGCACGGGTGAGTAACGCGTGGATAATCTGCCCGAGGA  60
               ||||||||||||||||||||||||||||||||||||||||||||||||||||||||||||
Sbjct  684763  TCCTTCGGGGTGGTGAAAGTGGCGCACGGGTGAGTAACGCGTGGATAATCTGCCCGAGGA  684822

Query  61      TTTGGGATAACATCTCGAAAGGGGTGCTAATACCGAATAAGCCCACGGGGTCTACGGATC  120
               ||||||||||||||||||||||||||||||||||||||||||||||||||||||||||||
Sbjct  684823  TTTGGGATAACATCTCGAAAGGGGTGCTAATACCGAATAAGCCCACGGGGTCTACGGATC  684882

Query  121     TTGCGGGAAAAgggggggACTTTCGGGCCTCCTGTCTTCGGATGAGTCCGCGTACCATTA  180
               ||||||||||||||||||||||||||||||||||||||||||||||||||||||||||||
Sbjct  684883  TTGCGGGAAAAGGGGGGGACTTTCGGGCCTCCTGTCTTCGGATGAGTCCGCGTACCATTA  684942

Query  181     GCTAGTTGGTAGGGTAATGGCCTACCAAGGCGACGATGGTTAGCTGGTCTGAGAGGATGA  240
               ||||||||||||||||||||||||||||||||||||||||||||||||||||||||||||
Sbjct  684943  GCTAGTTGGTAGGGTAATGGCCTACCAAGGCGACGATGGTTAGCTGGTCTGAGAGGATGA  685002

Query  241     TCAGCCACACTGGAACTGAGACACGGTCCAGACTCCTACGGGAGGCAGCAGTGGGGAATT  300
               ||||||||||||||||||||||||||||||||||||||||||||||||||||||||||||
Sbjct  685003  TCAGCCACACTGGAACTGAGACACGGTCCAGACTCCTACGGGAGGCAGCAGTGGGGAATT  685062

Query  301     TTGCGCAATGGGGGAAACCCTGACGCAGCAACGCCGCGTGGGTGATGAAGGCCTTCGGGT  360
               ||||||||||||||||||||||||||||||||||||||||||||||||||||||||||||
Sbjct  685063  TTGCGCAATGGGGGAAACCCTGACGCAGCAACGCCGCGTGGGTGATGAAGGCCTTCGGGT  685122

Query  361     CGTAAAGCCCTGTCGGGAGGGAAGAAATGATTGAGAGCTAATACCTCTTGGTCTTGACGG  420
               ||||||||||||||||||||||||||||||||||||||||||||||||||||||||||||
Sbjct  685123  CGTAAAGCCCTGTCGGGAGGGAAGAAATGATTGAGAGCTAATACCTCTTGGTCTTGACGG  685182

Query  421     TACCTCCGAAGGAAGCACCGGCTAACTCCGTGCCAGCAGCCGCGGTAATACGGAGGGTGC  480
               ||||||||||||||||||||||||||||||||||||||||||||||||||||||||||||
Sbjct  685183  TACCTCCGAAGGAAGCACCGGCTAACTCCGTGCCAGCAGCCGCGGTAATACGGAGGGTGC  685242

Query  481     AAGCGTTGTTCGGAATTATTGGGCGTAAAGCGCGTGTAGGCGGTCTTTTAAGTCTGATGT  540
               ||||||||||||||||||||||||||||||||||||||||||||||||||||||||||||
Sbjct  685243  AAGCGTTGTTCGGAATTATTGGGCGTAAAGCGCGTGTAGGCGGTCTTTTAAGTCTGATGT  685302

Query  541     GAAAGCCCCGGGCTCAACCTGGGAAGTGCATTGGAAACTGGGAGAC  586
               ||||||||||||||||||||||||||||||||||||||||||||||
Sbjct  685303  GAAAGCCCCGGGCTCAACCTGGGAAGTGCATTGGAAACTGGGAGAC  685348
```

Figure 4-1: DNA sequence of Geobacter sulfurreducens PCA chromosome, complete genome.

The BLAST result for sample B (Accession number: CP010430.1) yielded the *Geobacter sulfurreducens* strain AM-1 genome with a length of 4566144. The result yielded 100 % query cover with 100 % identification (987 bits – 534/534) with 0 % gaps (0/534). The sequence for *Geobacter sulfurreducens* strain AM-1 genome with sequence ID: CP010430.1 is given in Figure 4-2.

```
Query  1        GTGGCGCACGGGTGAGTAACGCGTGGATAATCTGCCCGAGGATTTGGGATAACATCTCGA  60
                ||||||||||||||||||||||||||||||||||||||||||||||||||||||||||||
Sbjct  2780488  GTGGCGCACGGGTGAGTAACGCGTGGATAATCTGCCCGAGGATTTGGGATAACATCTCGA  2780547

Query  61       AAGGGGTGCTAATACCGAATAAGCCCACGGGGTCTACGGATCTTGCGGGAAAAgggggg  120
                ||||||||||||||||||||||||||||||||||||||||||||||||||||||||||||
Sbjct  2780548  AAGGGGTGCTAATACCGAATAAGCCCACGGGGTCTACGGATCTTGCGGGAAAAGGGGGGG  2780607

Query  121      ACTTTCGGGCCTCCTGTCTTCGGATGAGTCCGCGTACCATTAGCTAGTTGGTAGGGTAAT  180
                ||||||||||||||||||||||||||||||||||||||||||||||||||||||||||||
Sbjct  2780608  ACTTTCGGGCCTCCTGTCTTCGGATGAGTCCGCGTACCATTAGCTAGTTGGTAGGGTAAT  2780667

Query  181      GGCCTACCAAGGCGACGATGGTTAGCTGGTCTGAGAGGATGATCAGCCACACTGGAACTG  240
                ||||||||||||||||||||||||||||||||||||||||||||||||||||||||||||
Sbjct  2780668  GGCCTACCAAGGCGACGATGGTTAGCTGGTCTGAGAGGATGATCAGCCACACTGGAACTG  2780727

Query  241      AGACACGGTCCAGACTCCTACGGGAGGCAGCAGTGGGGAATTTTGCGCAATGGGGGAAAC  300
                ||||||||||||||||||||||||||||||||||||||||||||||||||||||||||||
Sbjct  2780728  AGACACGGTCCAGACTCCTACGGGAGGCAGCAGTGGGGAATTTTGCGCAATGGGGGAAAC  2780787

Query  301      CCTGACGCAGCAACGCCGCGTGGGTGATGAAGGCCTTCGGGTCGTAAAGCCCTGTCGGGA  360
                ||||||||||||||||||||||||||||||||||||||||||||||||||||||||||||
Sbjct  2780788  CCTGACGCAGCAACGCCGCGTGGGTGATGAAGGCCTTCGGGTCGTAAAGCCCTGTCGGGA  2780847

Query  361      GGGAAGAAATGATTGAGAGCTAATACCTCTTGGTCTTGACGGTACCTCCGAAGGAAGCAC  420
                ||||||||||||||||||||||||||||||||||||||||||||||||||||||||||||
Sbjct  2780848  GGGAAGAAATGATTGAGAGCTAATACCTCTTGGTCTTGACGGTACCTCCGAAGGAAGCAC  2780907

Query  421      CGGCTAACTCCGTGCCAGCAGCCGCGGTAATACGGAGGGTGCAAGCGTTGTTCGGAATTA  480
                ||||||||||||||||||||||||||||||||||||||||||||||||||||||||||||
Sbjct  2780908  CGGCTAACTCCGTGCCAGCAGCCGCGGTAATACGGAGGGTGCAAGCGTTGTTCGGAATTA  2780967

Query  481      TTGGGCGTAAAGCGCGTGTAGGCGGTCTTTTAAGTCTGATGTGAAAGCCCCGGG  534
                ||||||||||||||||||||||||||||||||||||||||||||||||||||||
Sbjct  2780968  TTGGGCGTAAAGCGCGTGTAGGCGGTCTTTTAAGTCTGATGTGAAAGCCCCGGG  2781021
```

Figure 4-2:DNA sequence of Geobacter sulfurreducens strain AM-1 genome.

The results of the absorbance measurements for the assessment of the nucleic acid purity of samples A and B are summarised in Table 4-1 and Table 4-2 respectively.

Table 4-1: Absorbance measurements for sample A.

Concentration	11.2 ng/µL
A_{260} (10 mm path)	0.223
A_{280} (10 mm path)	0.117
A_{260}/A_{280}	1.90
A_{260}/A_{230}	1.21
Baseline correction	340 nm

Table 4-2: Absorbance measurements for sample B.

Concentration	14.4 ng/µL
A_{260} (10 mm path)	0.287
A_{280} (10 mm path)	0.153
A_{260}/A_{280}	1.88
A_{260}/A_{230}	1.34
Baseline correction	340 nm

The A_{260}/A_{280} ratio values for both samples are between the acceptable range of between 1.8 and 2.0 to constitute a "pure" sample. Although the A_{260}/A_{230} values of both samples are below the desired range of 2.0 and 2.2 to constitute as "pure" nucleic acid of both samples, this could possible be due to a problem with the DNA extraction procedure such as residual organic contaminants after the extraction procedure.

The diluted samples with a control sample were analysed with PCR, the sequence ladder was considered a base of 1500 kb using Pure strain 16s Bio-Rad GelDoc XR. The sequence ladder is illustrated in Figure 4-3.

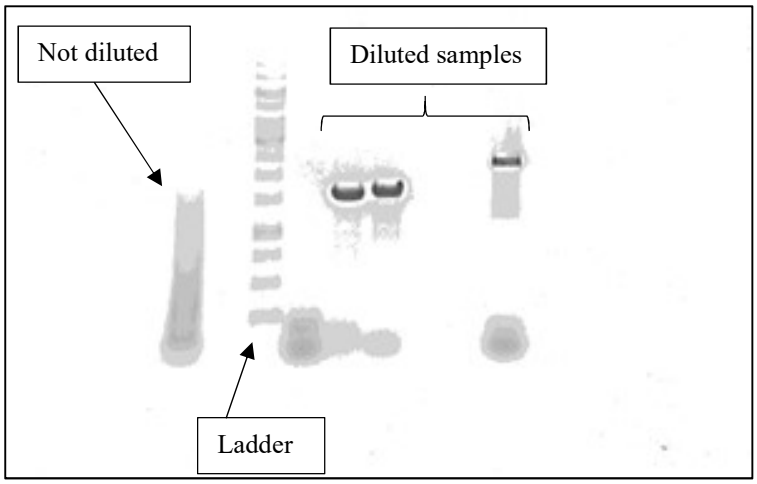

Figure 4-3: Sequence ladder at 1500 kb for G. sulfurreducens.

4.2 Growth of *Geobacter sulfurreducens*

The growth curves were prepared for the first 3 weeks after inoculation. These curves were prepared for pure *Geobacter sulfurreducens*, for *G. sulfurreducens* grown on graphite and GAC particles and are illustrated by Figure 4-4. Figure 4-5 illustrates the turbidity progression of *Geobacter sulfurreducens* over the initial 3 weeks growth period for the same samples used for the growth curves. This test is done to allow for an additional growth profile for the "control"

sample. This was only done for the pure *Geobacter sulfurreducens* growth media, due to interference of the carbon particles with the turbidity measurements that made comparison impossible.

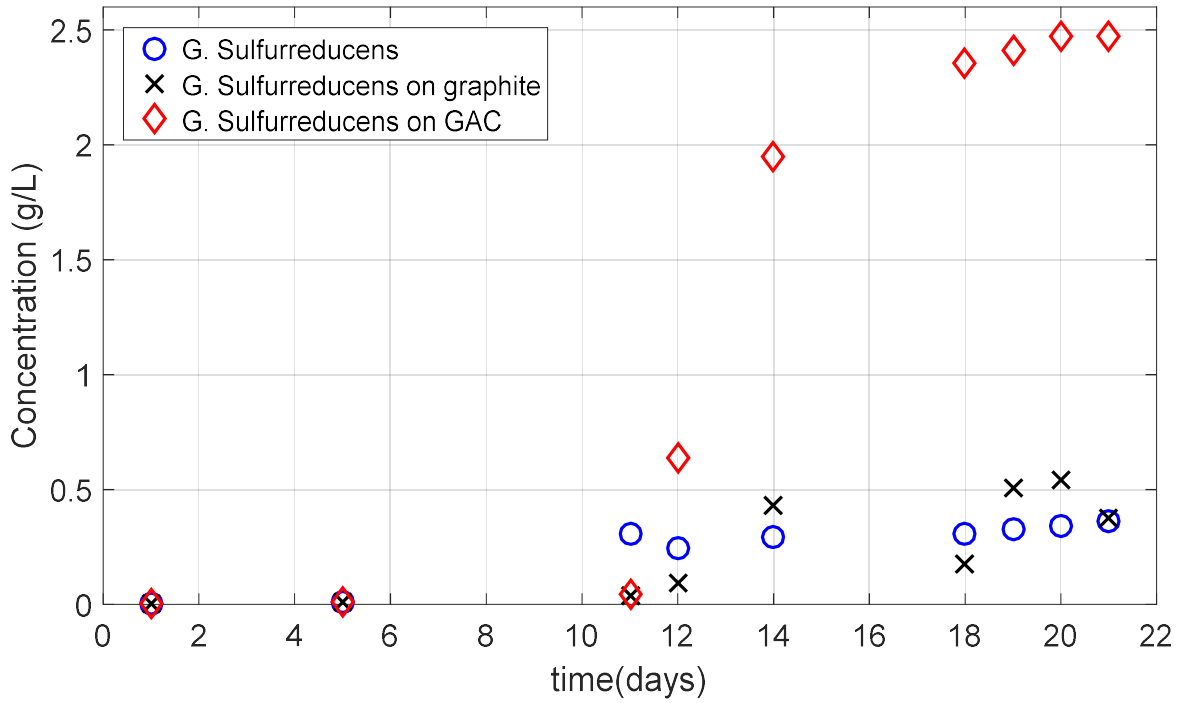

Figure 4-4: Growth curve for pure G. sulfurreducens and with added carbon growth substrates added over a period of 3 weeks.

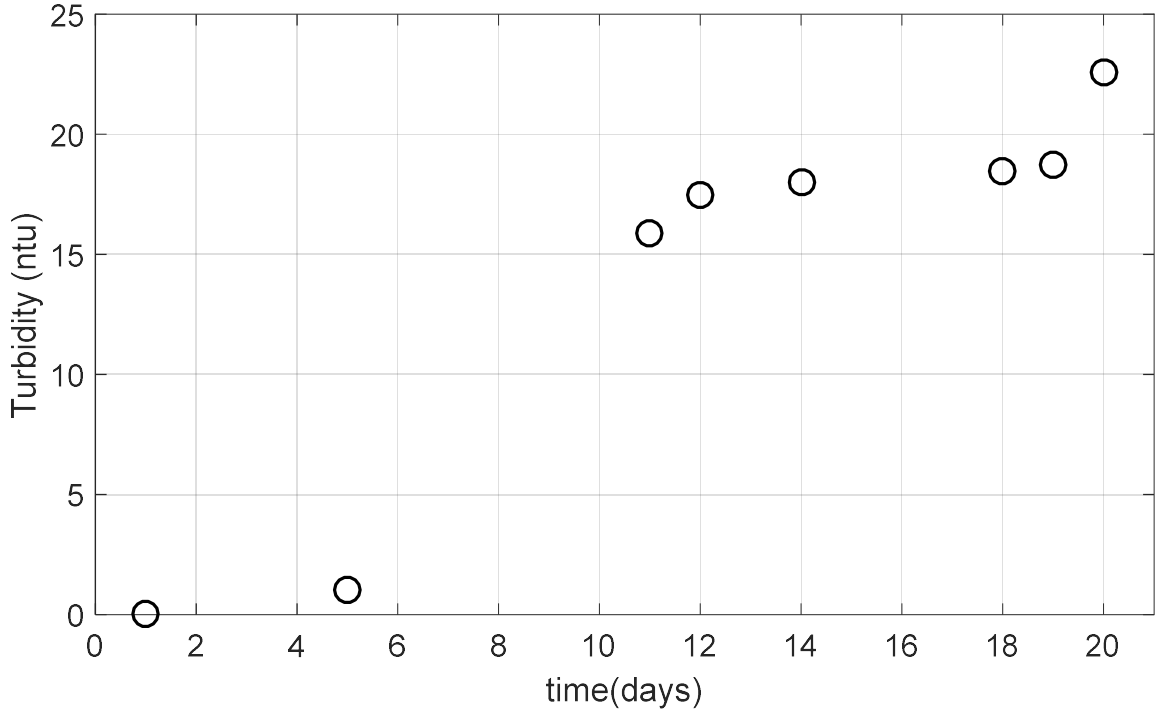

Figure 4-5: Turbidity progression of Geobacter sulfurreducens growth media over a period of 3 weeks.

4.3 Brunauer-Emmet-Teller (BET) surface area analysis

The BET analysis results for the carbon substrates as received and after growth are summarised in Table 4-3.

Table 4-3: BET analysis for carbon growth substrates, pure and after microbial growth.

Sample	Sample mass (g)	BET surface area (m^2/g)	Langmuir surface area (m^2/g)	Correlation coefficient	Single point surface area at P/Po (m^2/g)
GAC	0.50	601 ± 9	745 ± 4	0.999	0.2237:582.1
After 2 weeks	0.52	500 ± 9	623 ± 4	0.999	0.2230:486.3
After 3 weeks	0.48	562 ± 9	696 ± 4	0.999	0.2214:545.0
Graphite	0.50	0.13 ± 0.70	0.16 ± 0.88	0.100	0.2249: -0.0782
After 2 weeks	0.51	0.10 ± 0.02	0.12 ± 0.02	0.967	0.2247:0.1144
After 3 weeks	0.50	0.44 ± 0.01	0.62 ± 0.01	1.00	0.2017:0.4306

The molecular cross-section area for all samples were found to be 0.1620 nm^2.

Graphite and GAC were used as substrates for the growth of *Geobacter sulfurreducens*. The BET analysis illustrates the surface area of the clean GAC and graphite without bacterial growth.

4.4 Field emission scanning electron microscope (FE-SEM)

An ultrahigh resolution field emission scanning electron microscope (HR FE-SEM Zeiss Ultra Plus 55) was used to investigate the morphology of the carbon particles used as growth substrates to explain the differences in the growth

Granular activated carbon (GAC) is known for its large surface area and rough edges and flat or smooth plane, whereas graphite is known for its layered structure, with a smooth and glass-like basal plane due to the strong covalent bonds. With graphite the edges may be rough, depending on the type of graphite flakes. (Van Heerden, 2015) For this study both carbon substrates were used as received, refer to Appendix C, Table 3-1 and Table 3-2 for the certificates of analyses, i.e. no purification was implemented to allow for as much “roughness” and impurities as possible for bacterial attachment.

The large and rough surface area of neat granular activated carbon, GAC is illustrated by Figure 4-6 and Figure 4-7. The crystalline structure of graphite is displayed in Figure 4-8 and Figure 4-9.

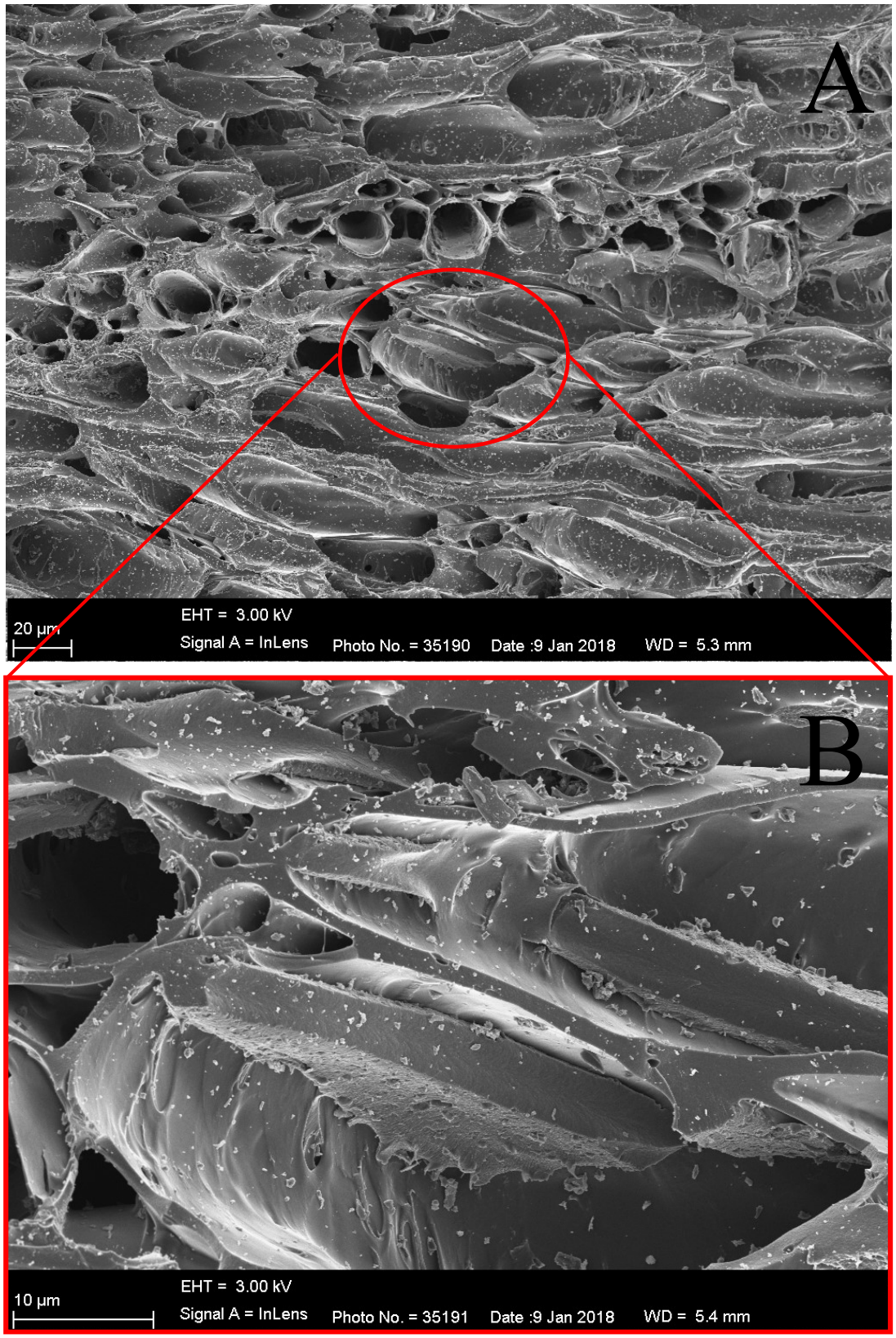

Figure 4-6: Pure granular activated carbon (GAC) flakes, untreated.

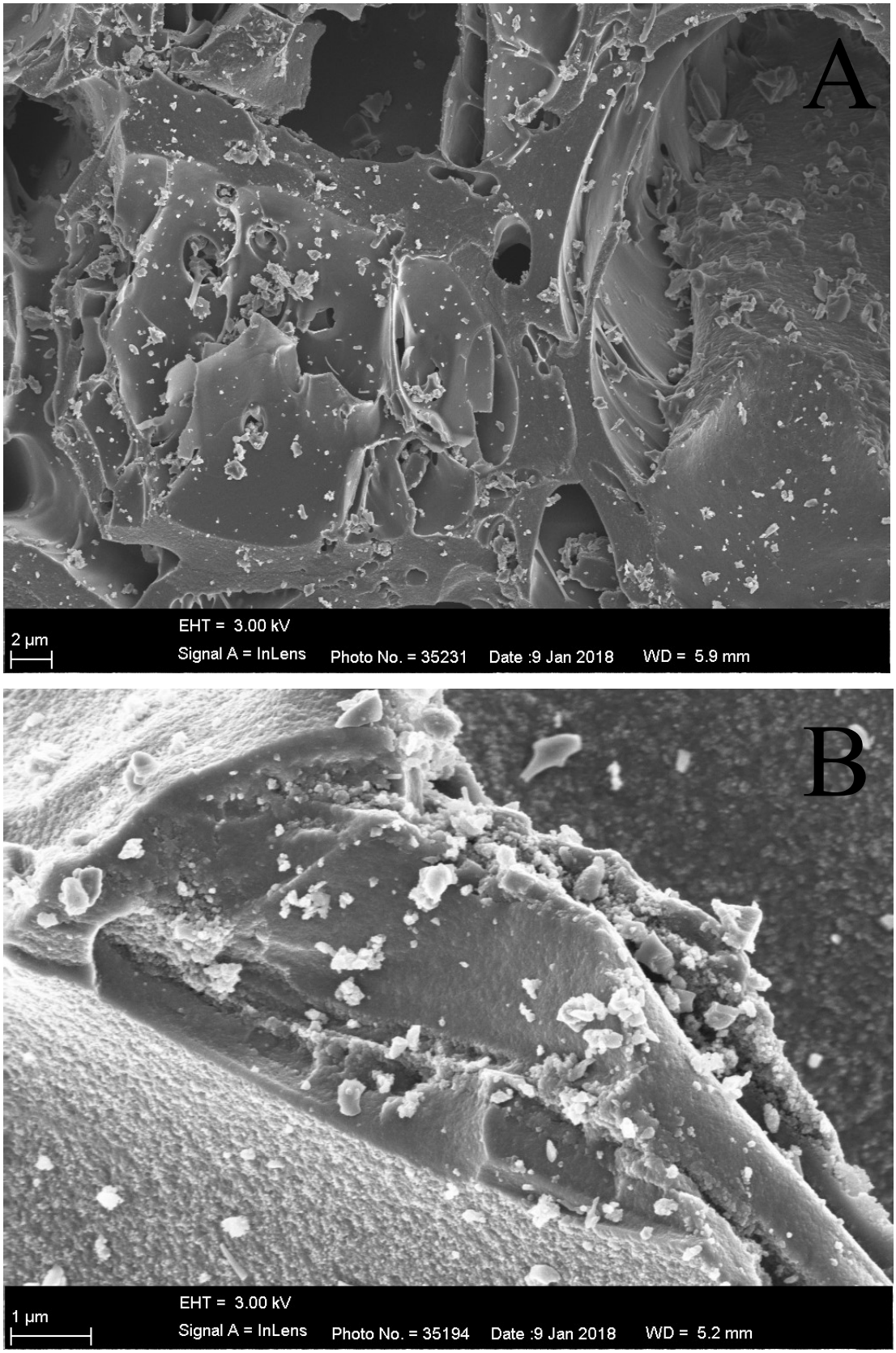

Figure 4-7: Pure granular activated carbon (GAC) flakes, untreated.

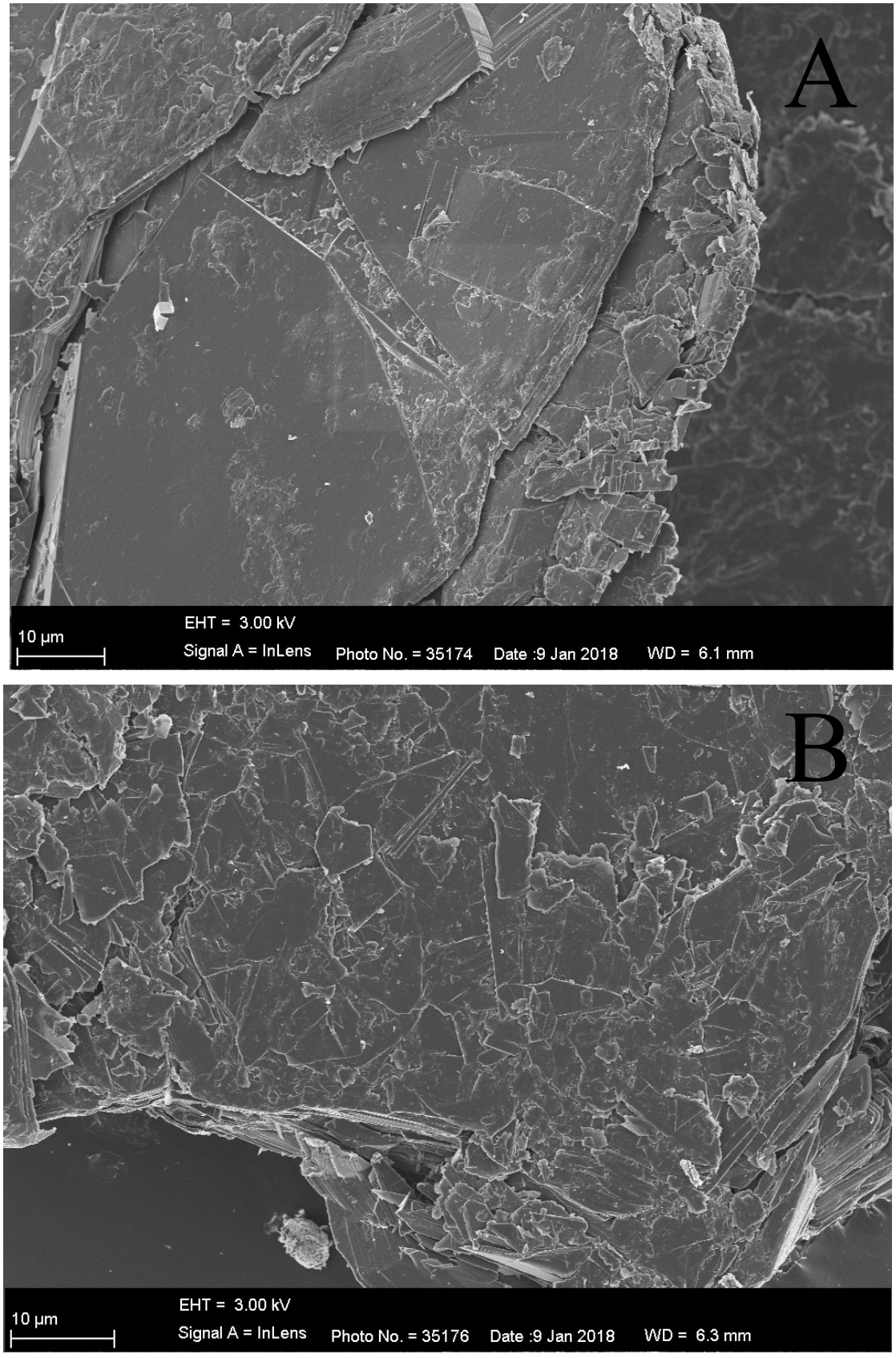

Figure 4-8: Pure natural graphite flakes, untreated.

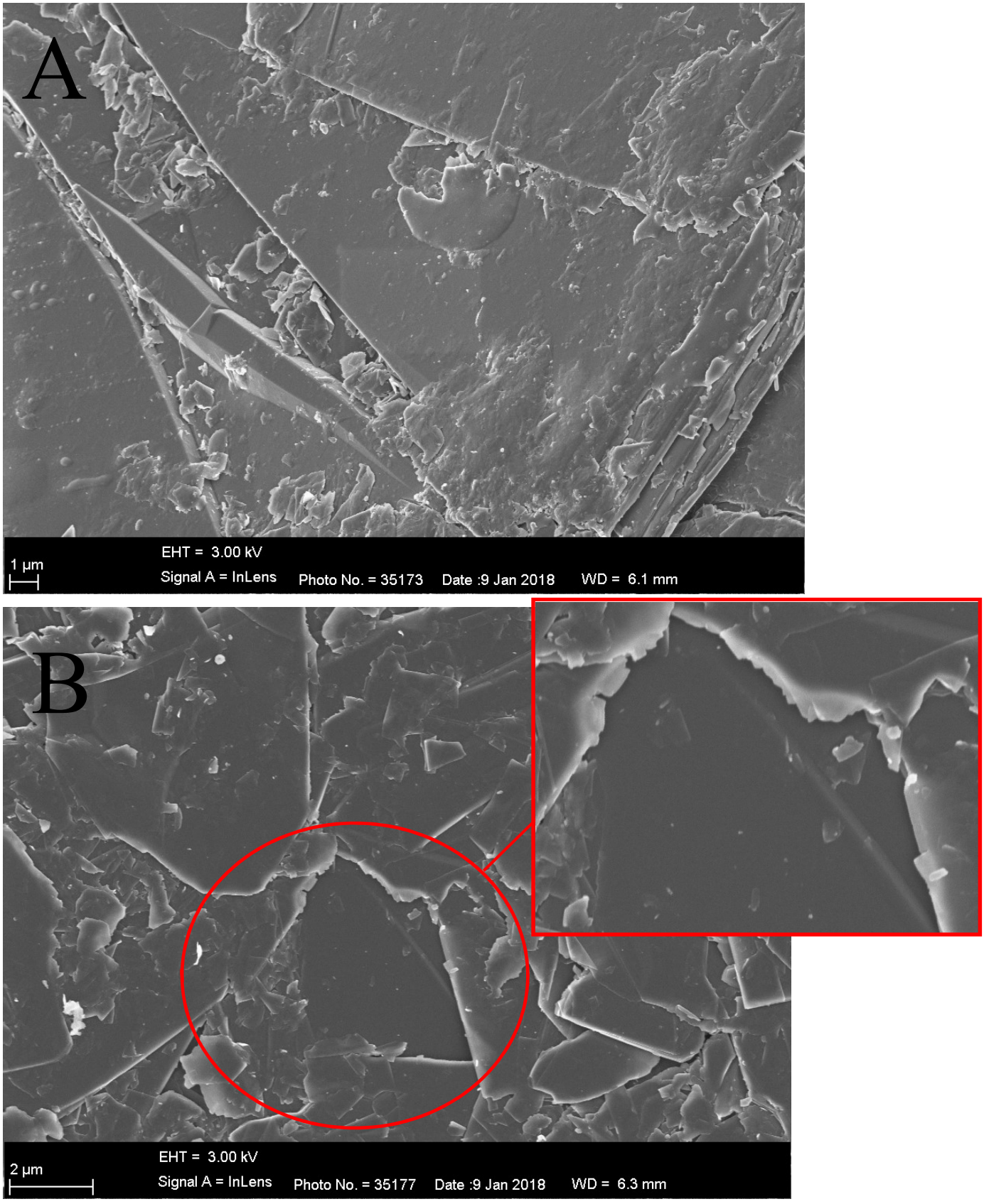

Figure 4-9: Pure natural graphite flakes, untreated – magnified.

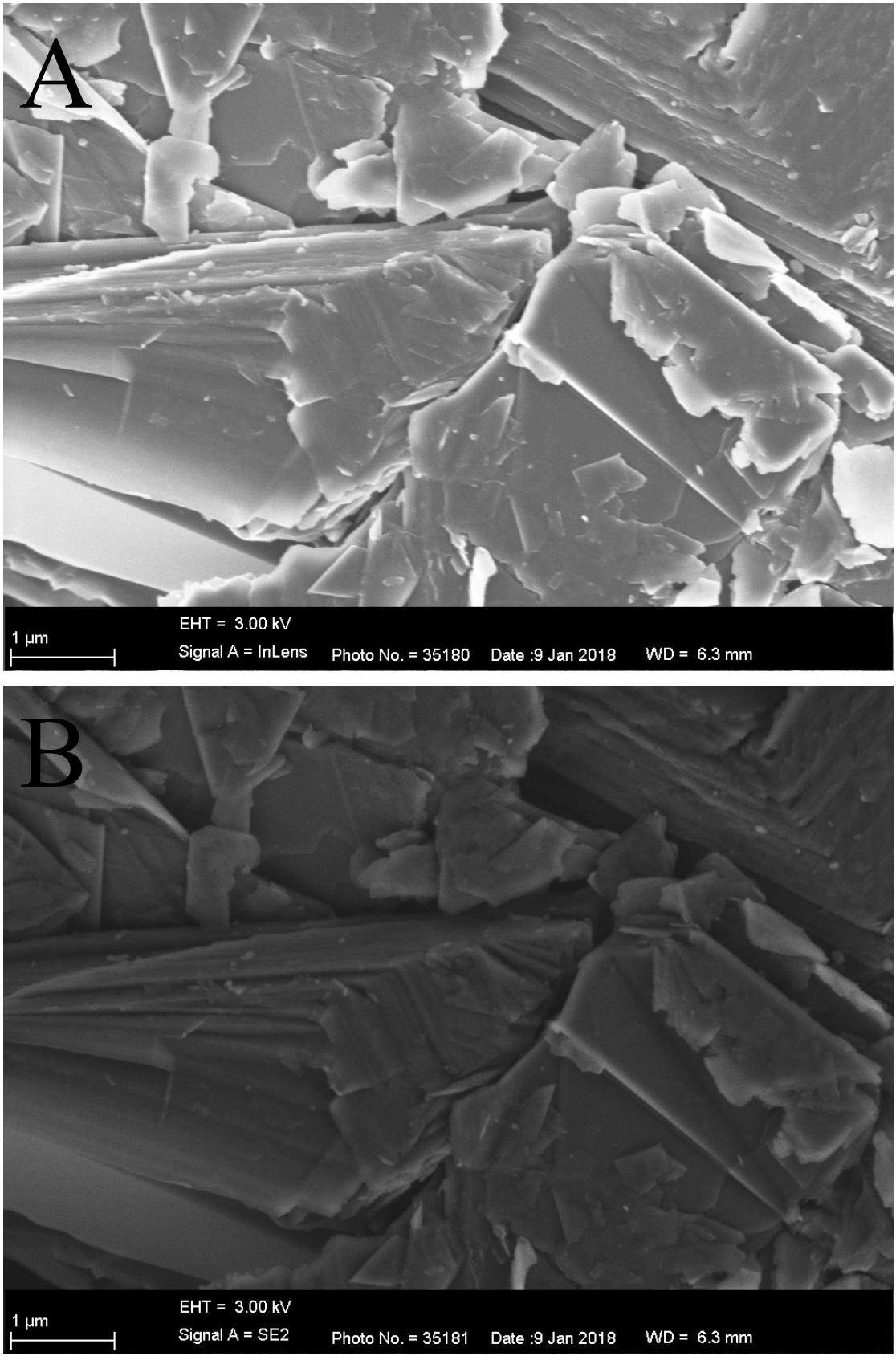

Figure 4-10: Pure natural graphite flakes – magnification of layers.

The difference in morphology of the two different carbon substrates – amorphous (GAC) and crystalline (graphite) – is clearly displayed in Figure 4-6 to Figure 4-10. The smooth basal plane and rough edges are displayed in graphite. The morphology of GAC is the exact opposite to that of graphite, since the uneven surface of GAC is evident and with numerous pores which constitute result in its large surface area. Both graphite and GAC contain impurities which is evident from the images; this is due to the material being untreated and with no purification being implemented.

The progress in growth on the two different carbon substrates were qualitatively analysed using FE-SEM and compared. The qualitative data collected from this technique will be used in conjunction with the growth curves and the BET data to discuss the growth effect of the carbon substrates.

After 2 weeks from the initial inoculation the samples were analysed and then also after 3 weeks after inoculation. These images were compared. Figure 4-11 to Figure 4-14 represent the microbial growth on GAC particles after 2 weeks after inoculation. Figure 4-11 illustrates the biofilm formed. From the investigation of the 2 week growth period samples, most of the microbial cells started to cover the smooth surface of the GAC particles, (evident from Figure 4-12 to Figure 4-14) before agglomerating on the ridges, which make attachment ideal, producing the thick biofilm observed in Figure 4-11.

Figure 4-15 to Figure 4-19 represent the growth progression on graphite particles – or rather the lack thereof after 2 weeks of growth after inoculation. An extensive search was conducted for the graphite particles, due to the struggle encountered in observing microbial growth. In all these images no microbial growth is observed, except for the possible single microbial cell captured in Figure 4-18A. Figure 4-18 is an excellent illustration of the layered structure and glass-like finish of graphite.

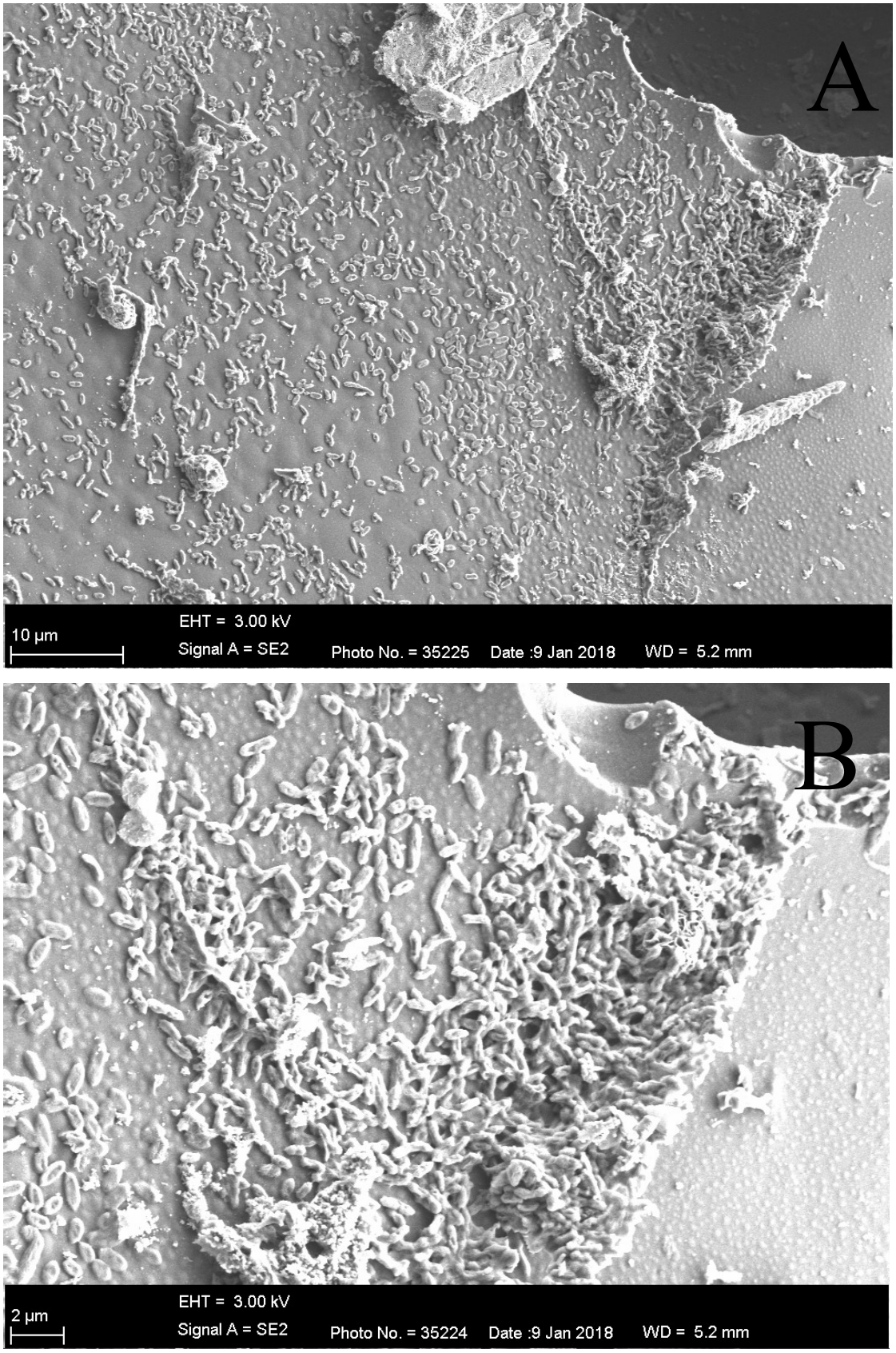

Figure 4-11: The growth substrate, GAC after a growth period of 2 – magnification of biofilm.

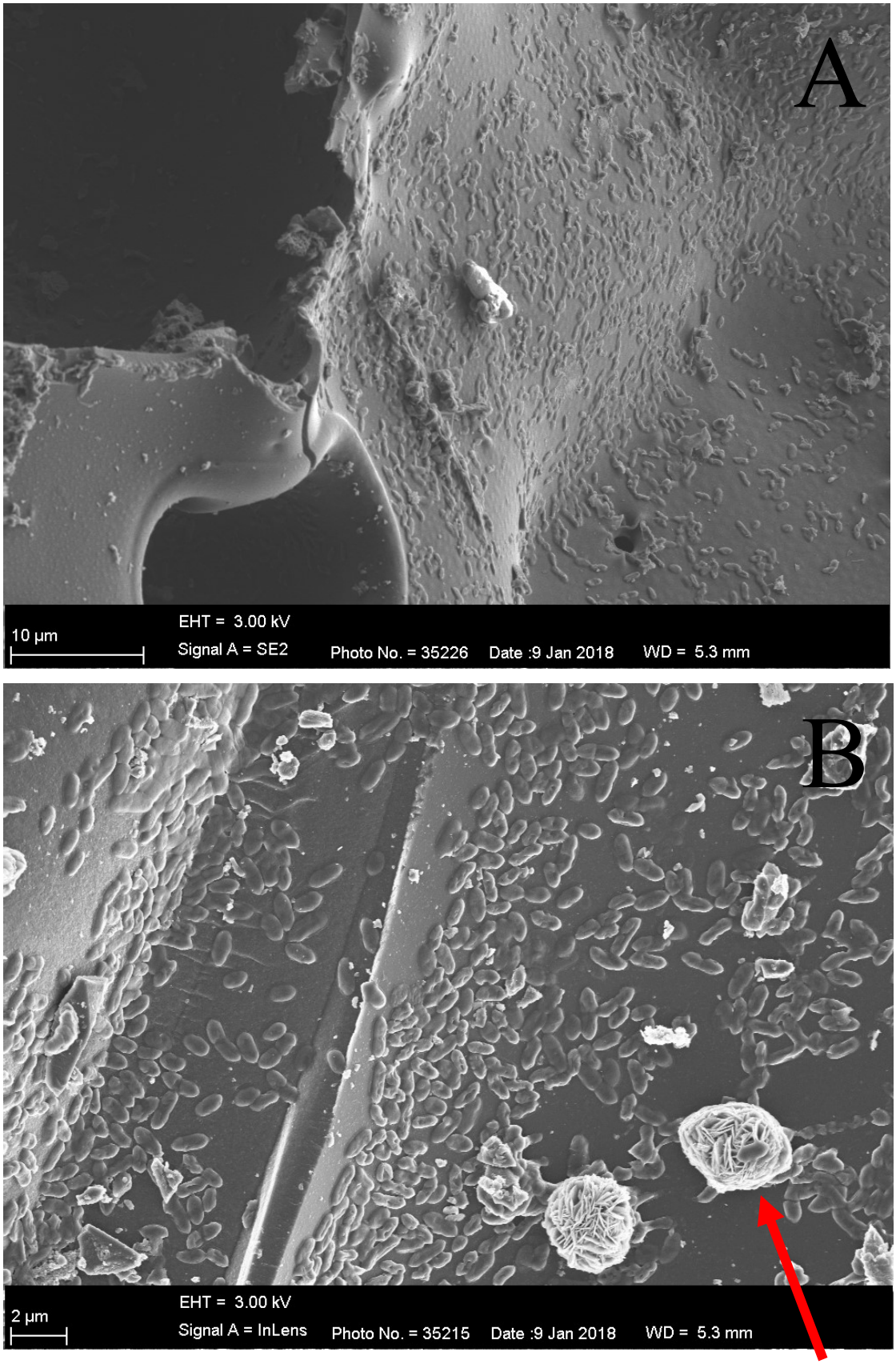

Figure 4-12: Microbial growth on GAC surface after 2 weeks of growth (arrow indicate crystal formed from freeze-drying process).

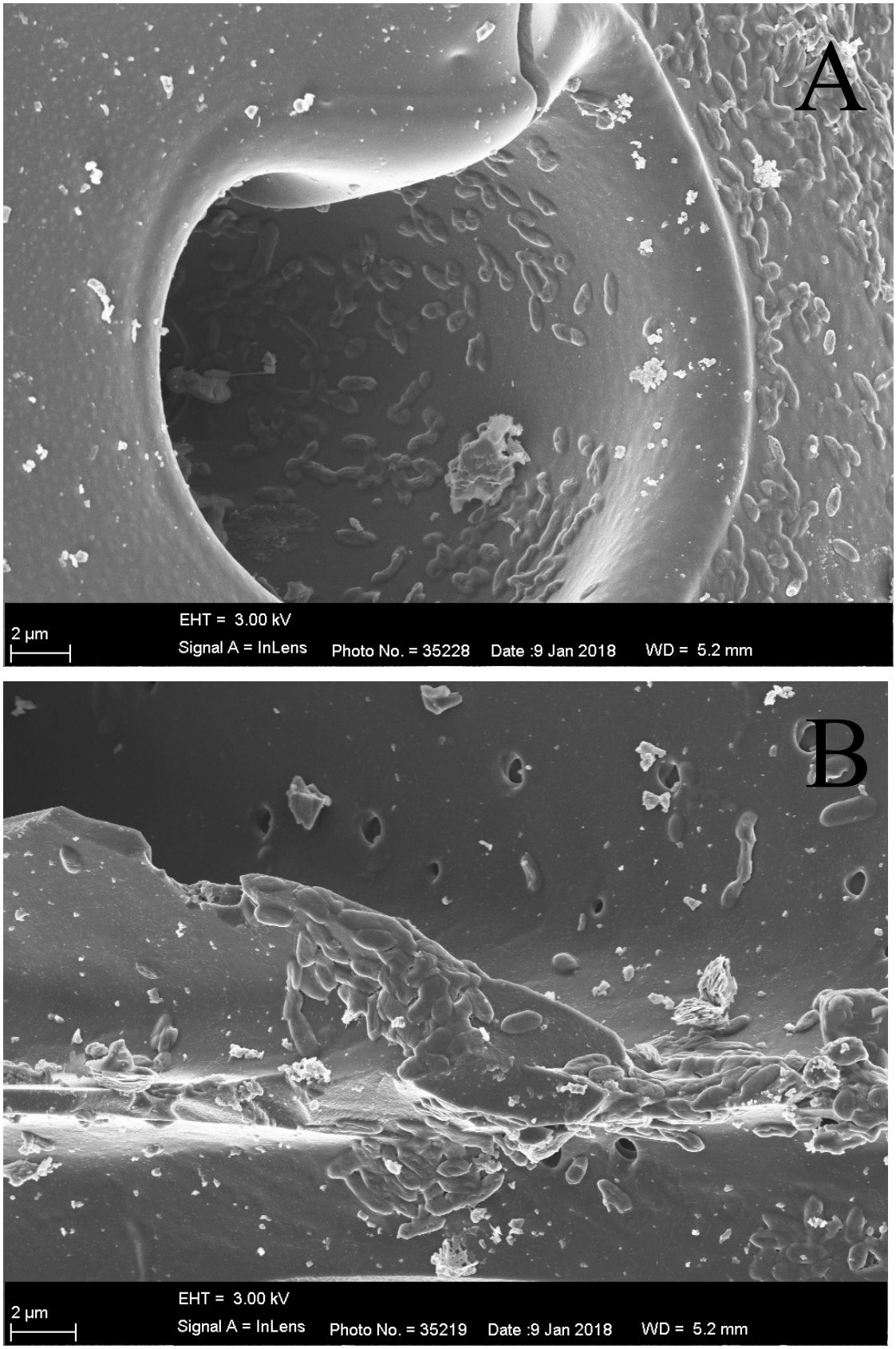

Figure 4-13: Microbial growth visible in the pores and edges of the GAC particles after 2 weeks of growth.

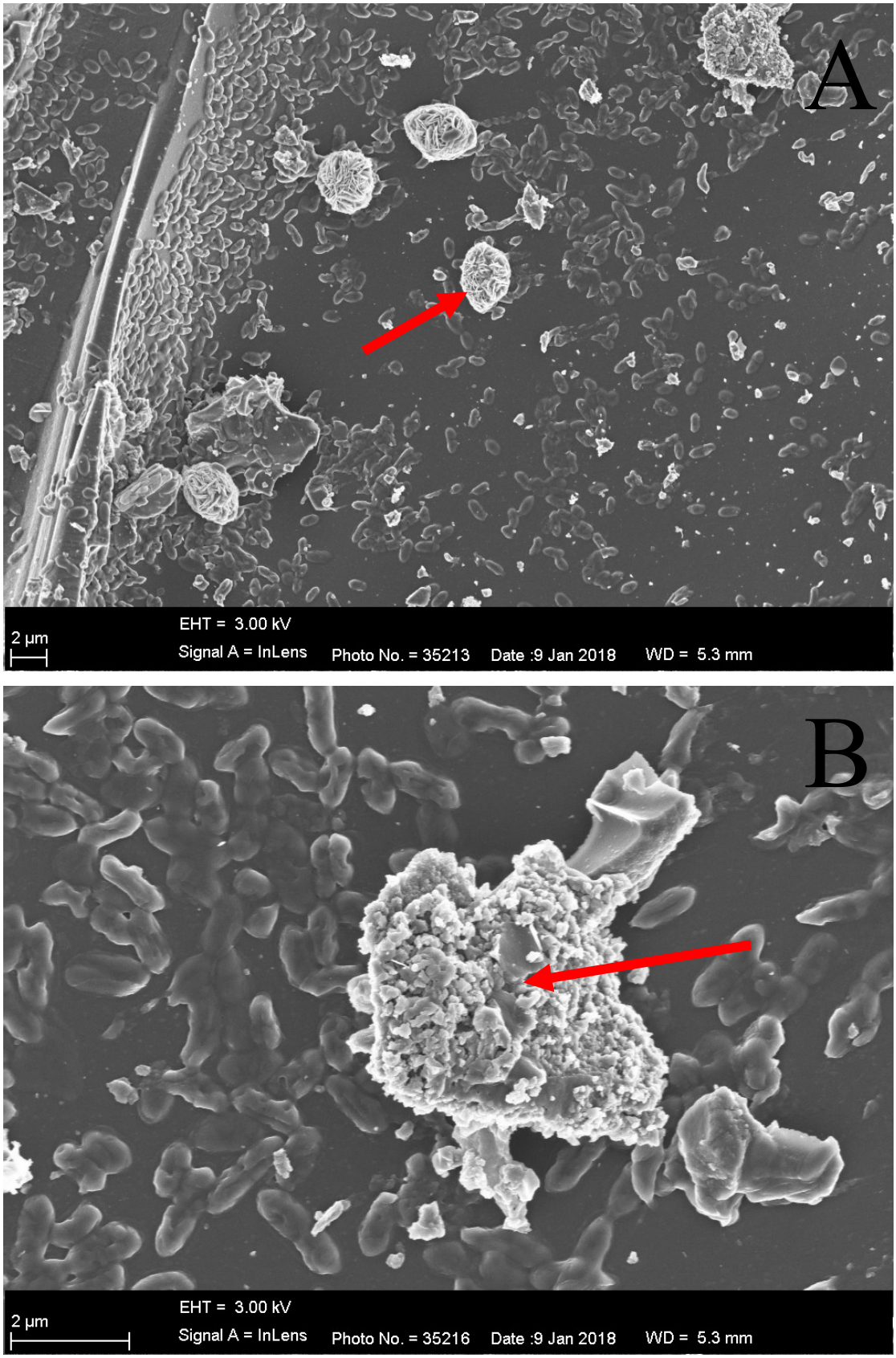

Figure 4-14: Microbial growth visible on the surface of the GAC particles after 2 weeks of growth – arrows indicate crystals formed from freeze drying process.

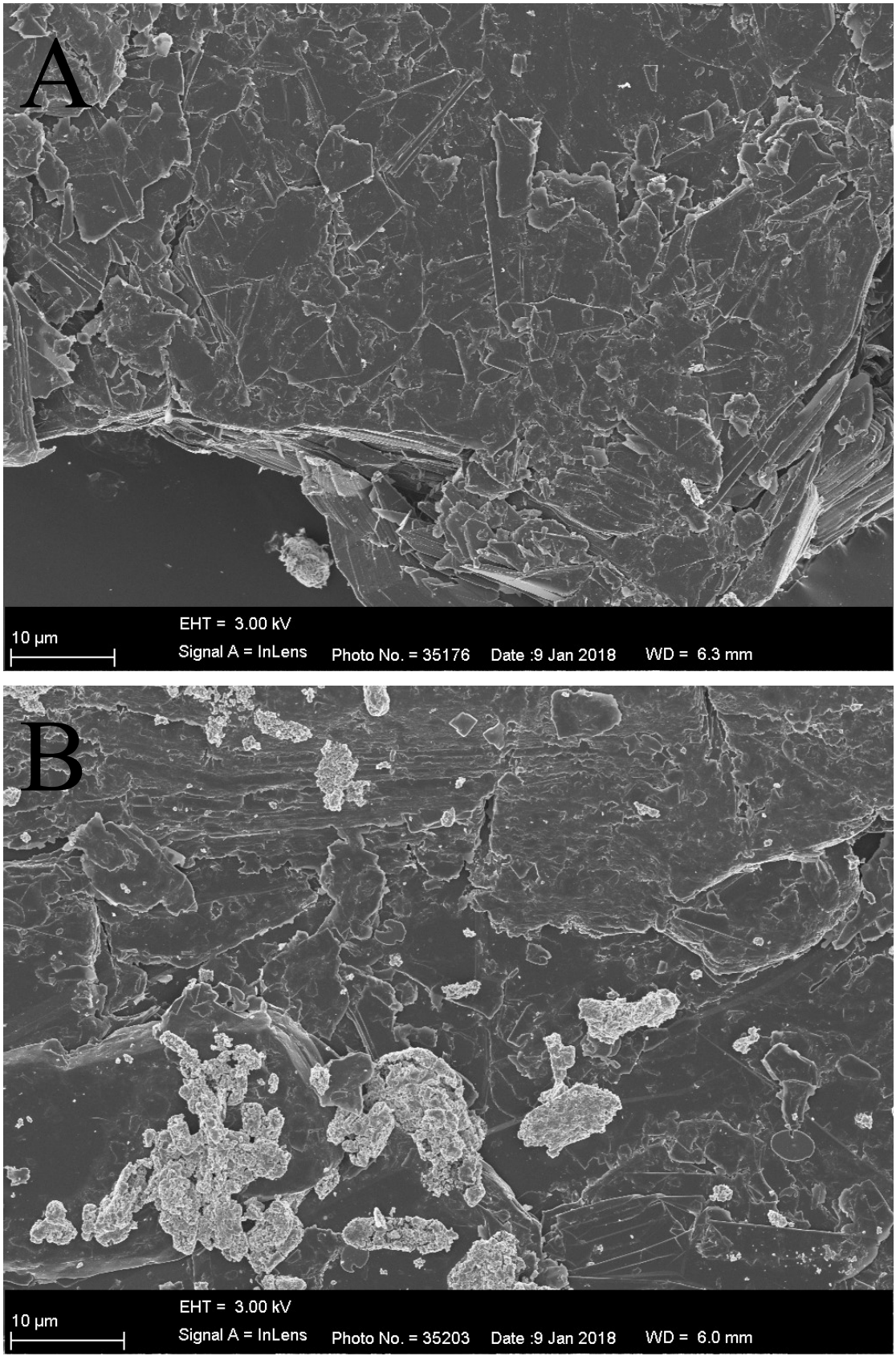

Figure 4-15: Graphite particles after 2 weeks of microbial growth.

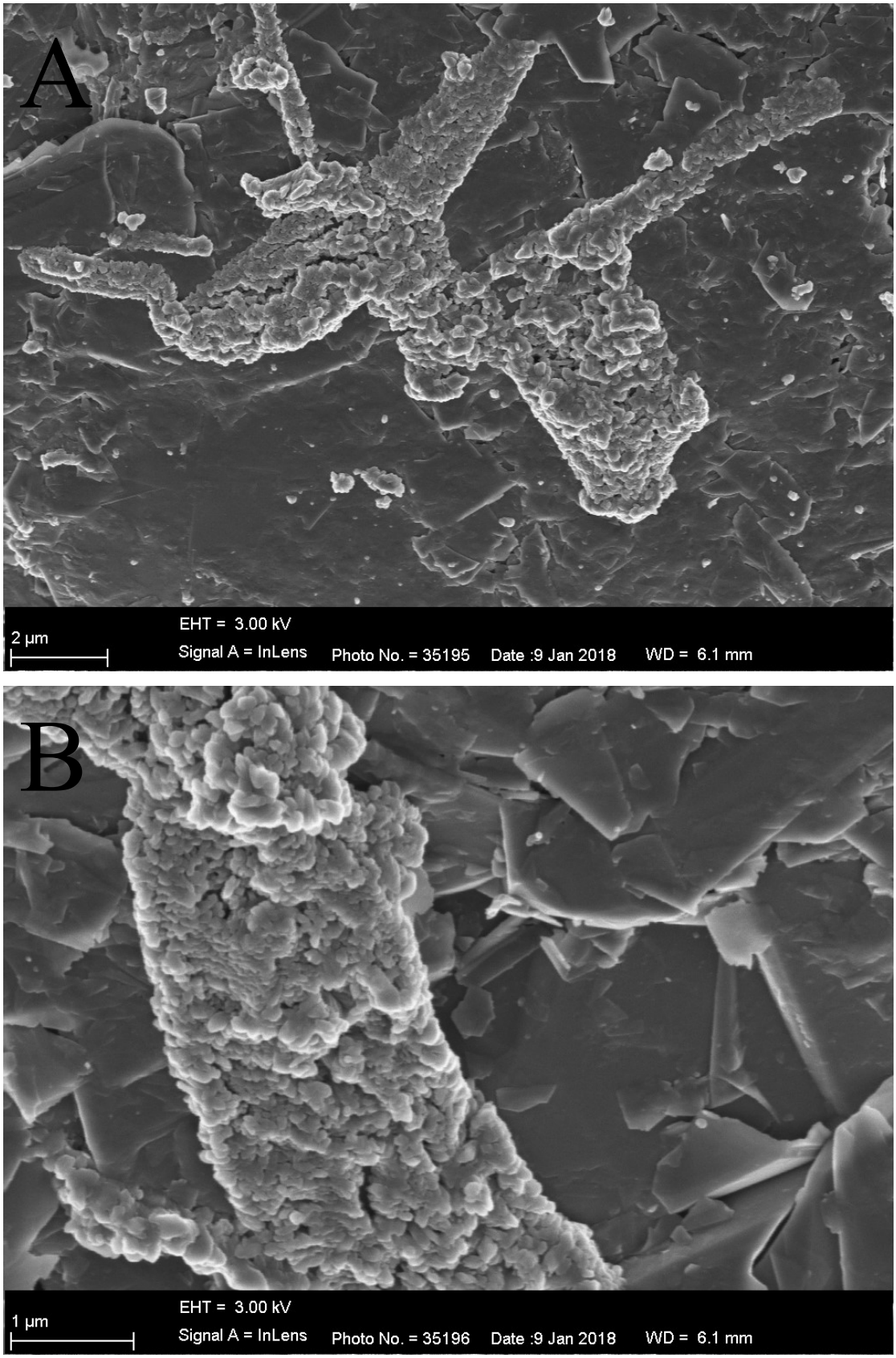

Figure 4-16: Magnification of graphite particles after 2 weeks of microbial growth – include magnification of crystals formed due to freeze-drying process.

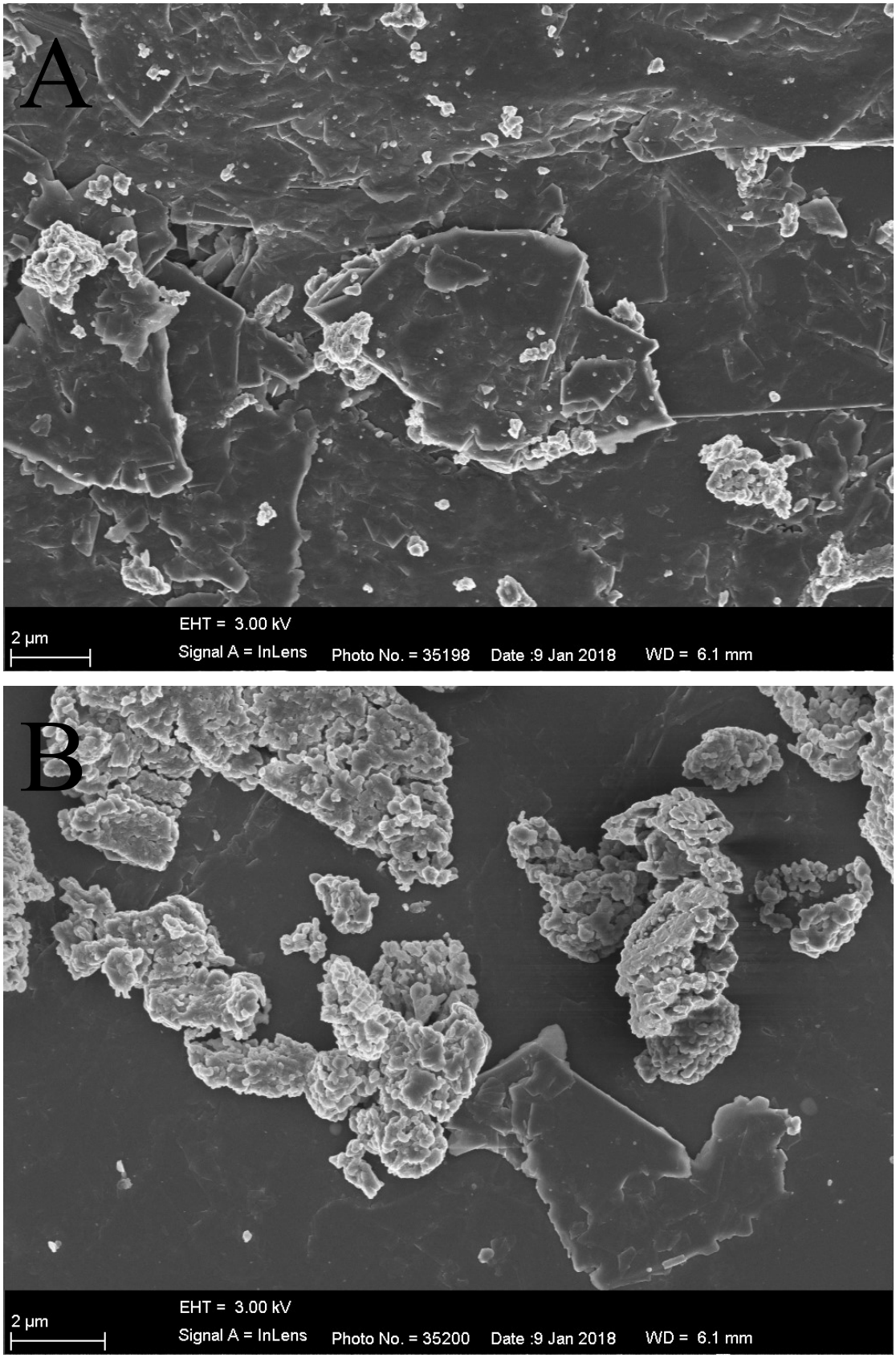

Figure 4-17: Magnification of basal plane of graphite particles after 2 weeks of microbial growth – no microbes visible, only crystals.

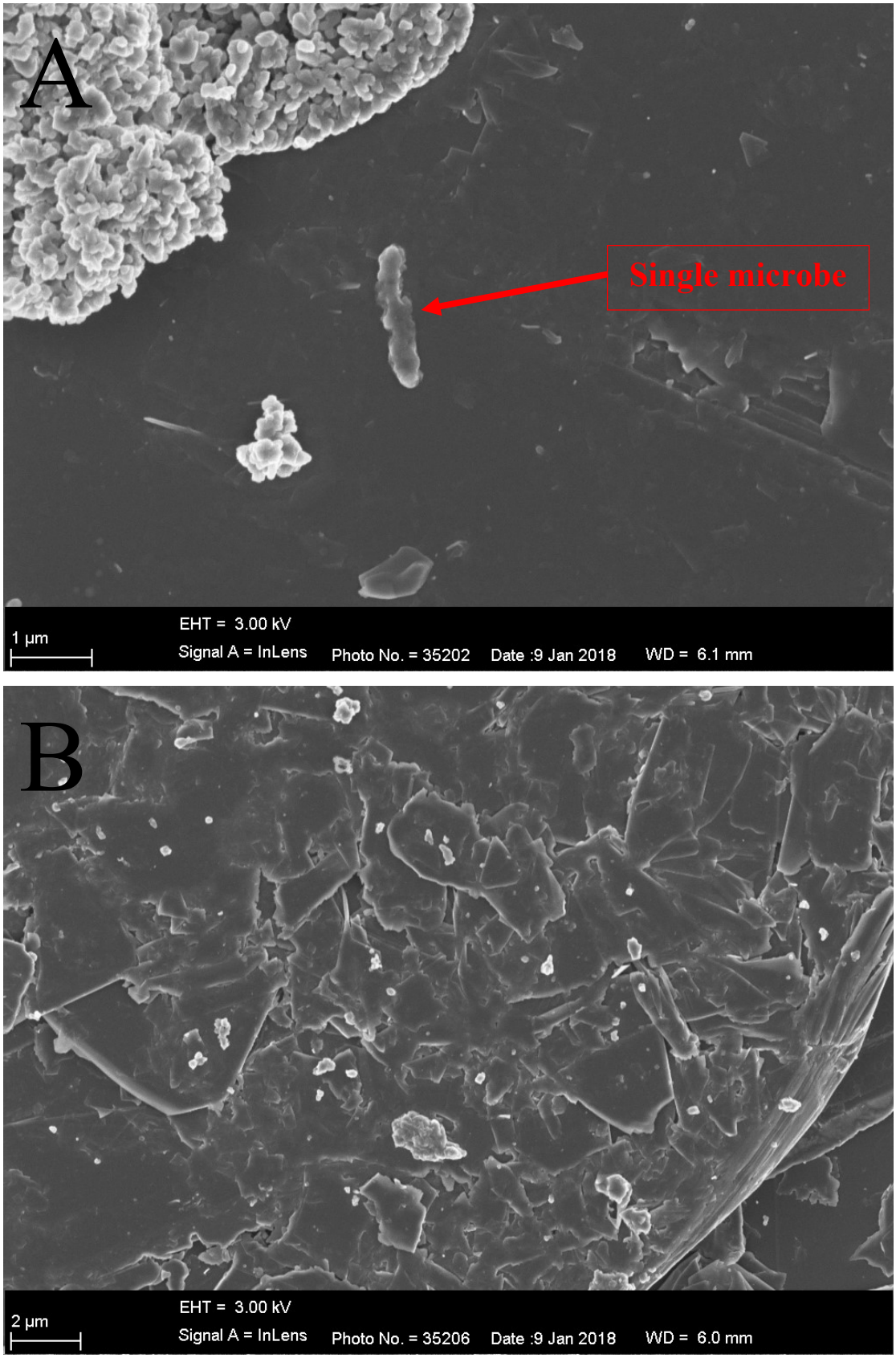

Figure 4-18: Magnification of basal plane of graphite after 2 weeks of growth. A: evidence of a single microbial cell. B: Damaged basal plane, no evidence of growth.

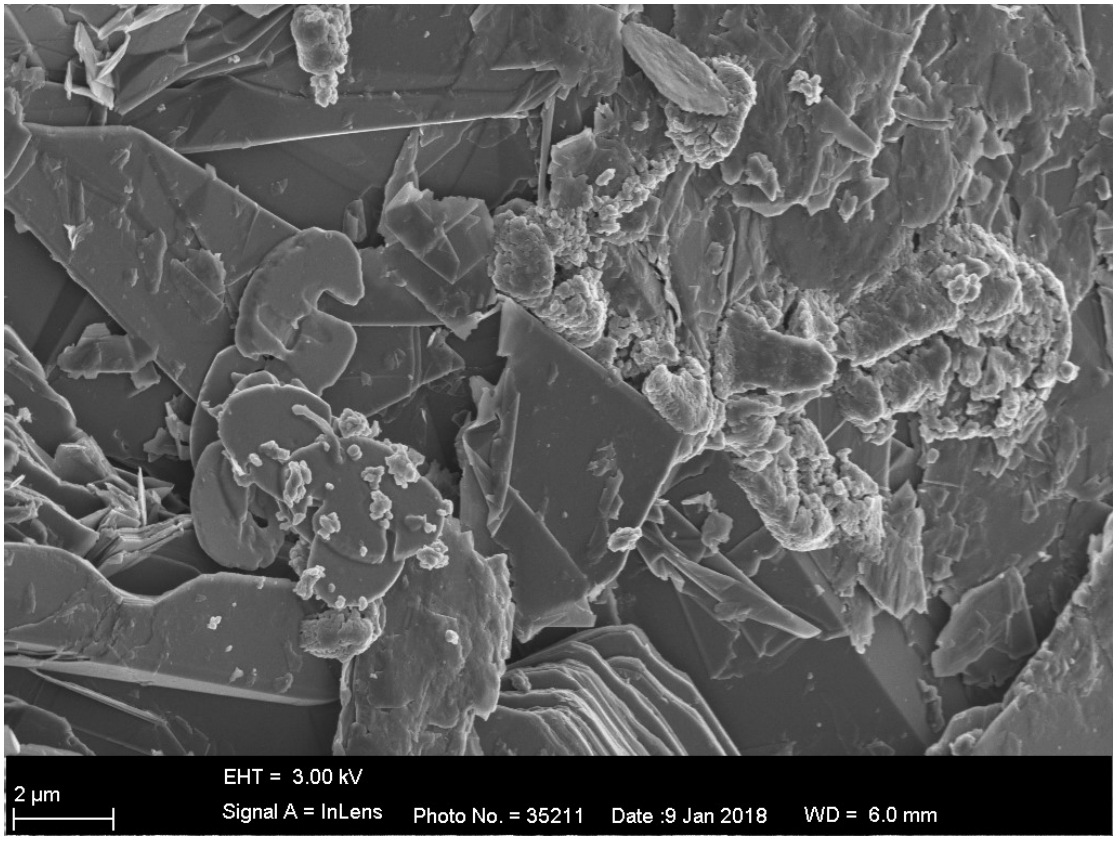

Figure 4-19: Graphite particles after 2 weeks of microbial growth. Layered structure and smooth basal plane excellently illustrated.

The microbial growth on the two different carbon growth substrates were compared after a period of 3 weeks subsequent to inoculation. Figure 4-20 and Figure 4-21 represent the growth progression of microbial cells on GAC particles after 3 weeks. Figure 4-20 illustrates the growth from an expanded view whereas Figure 4-21 magnifies the cells showing the irregular packing.

An extensive search on the SEM for microbial growth on all the graphite samples with a growth period of 3 weeks was conducted in search of any microbial growth. Figure 4-22 and Figure 4-23 was chosen as the repesentative of batch. These figures illustrate the graphite growth substrate after a growth period of 3 weeks, the lack of growth will be discussed in the Discussion section. Figure 4-23A shows the possibility of a single microbe (depicted by the red arrow); this might be evidence that growth is extremely poor, but will be discussed in the Discussion section together with additional results. Figure 4-23B illustrates the characteristics of graphite due to the layered structure present in the image as well as the smooth basal plane – depicted by the blue arrow.

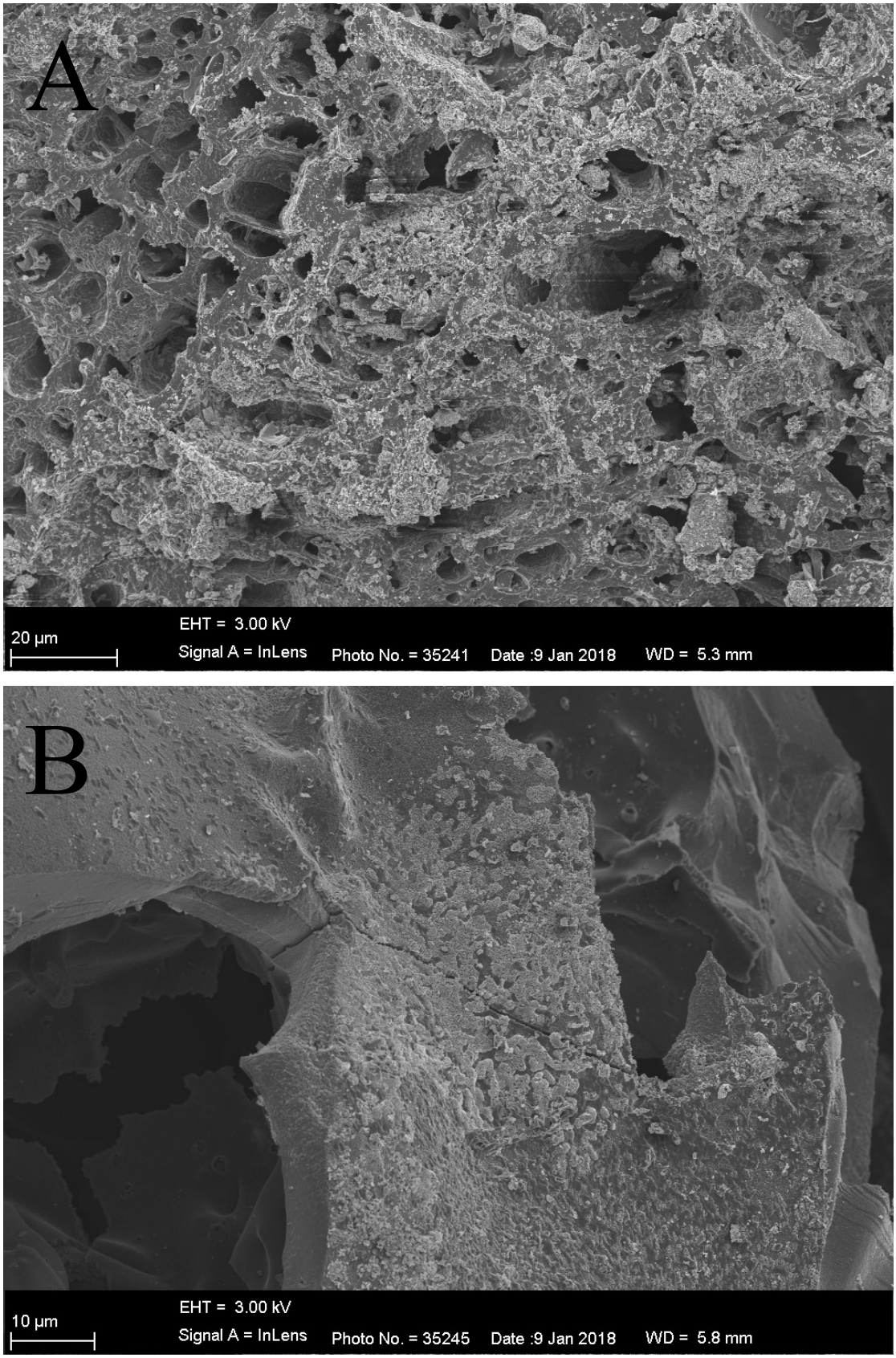

Figure 4-20: Microbial growth on GAC particles after 3 weeks of growth – A: on GAC edge and B: on flat plane.

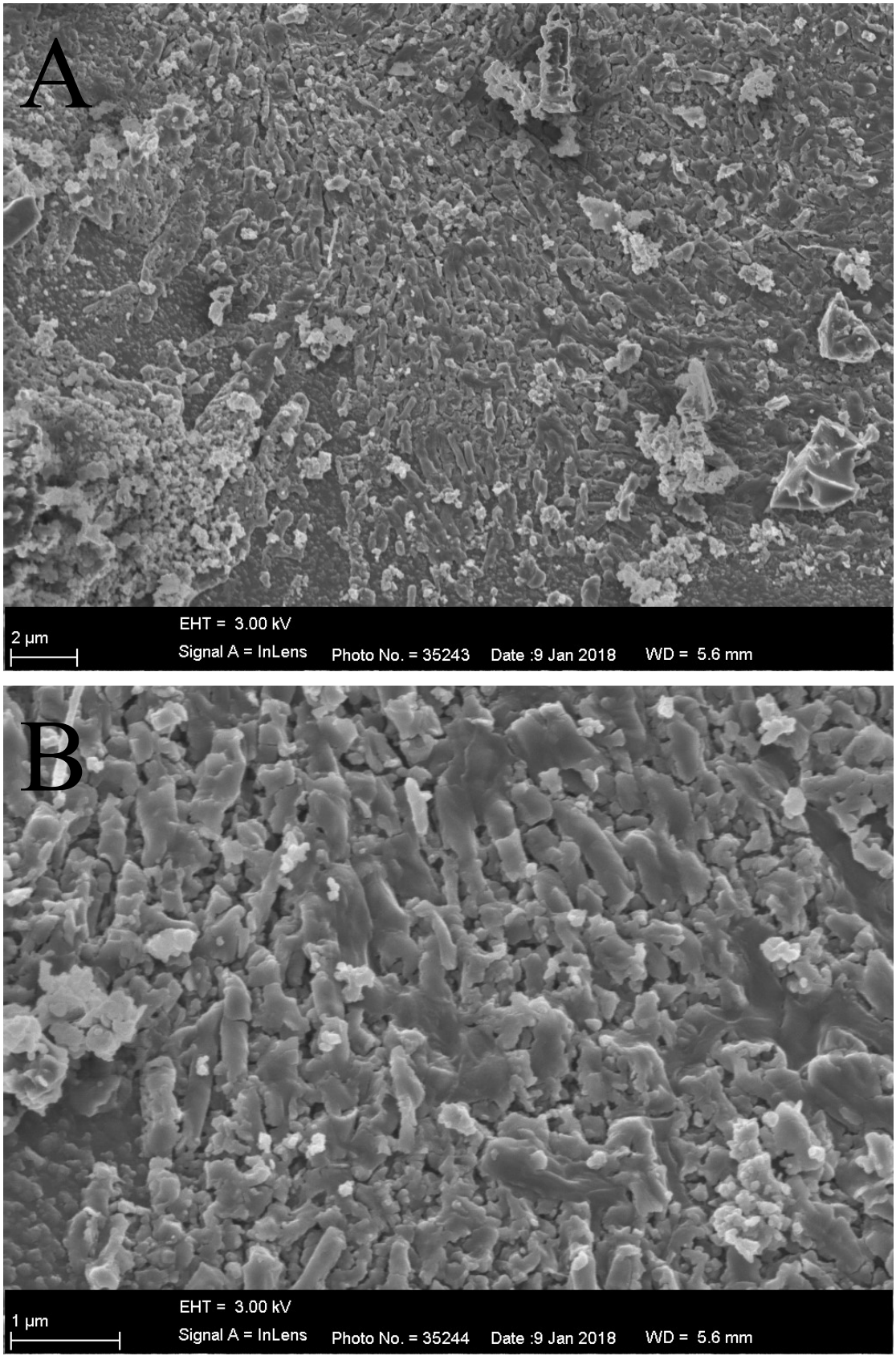

Figure 4-21: Magnification of microbial growth on GAC particles after 3 weeks of growth.

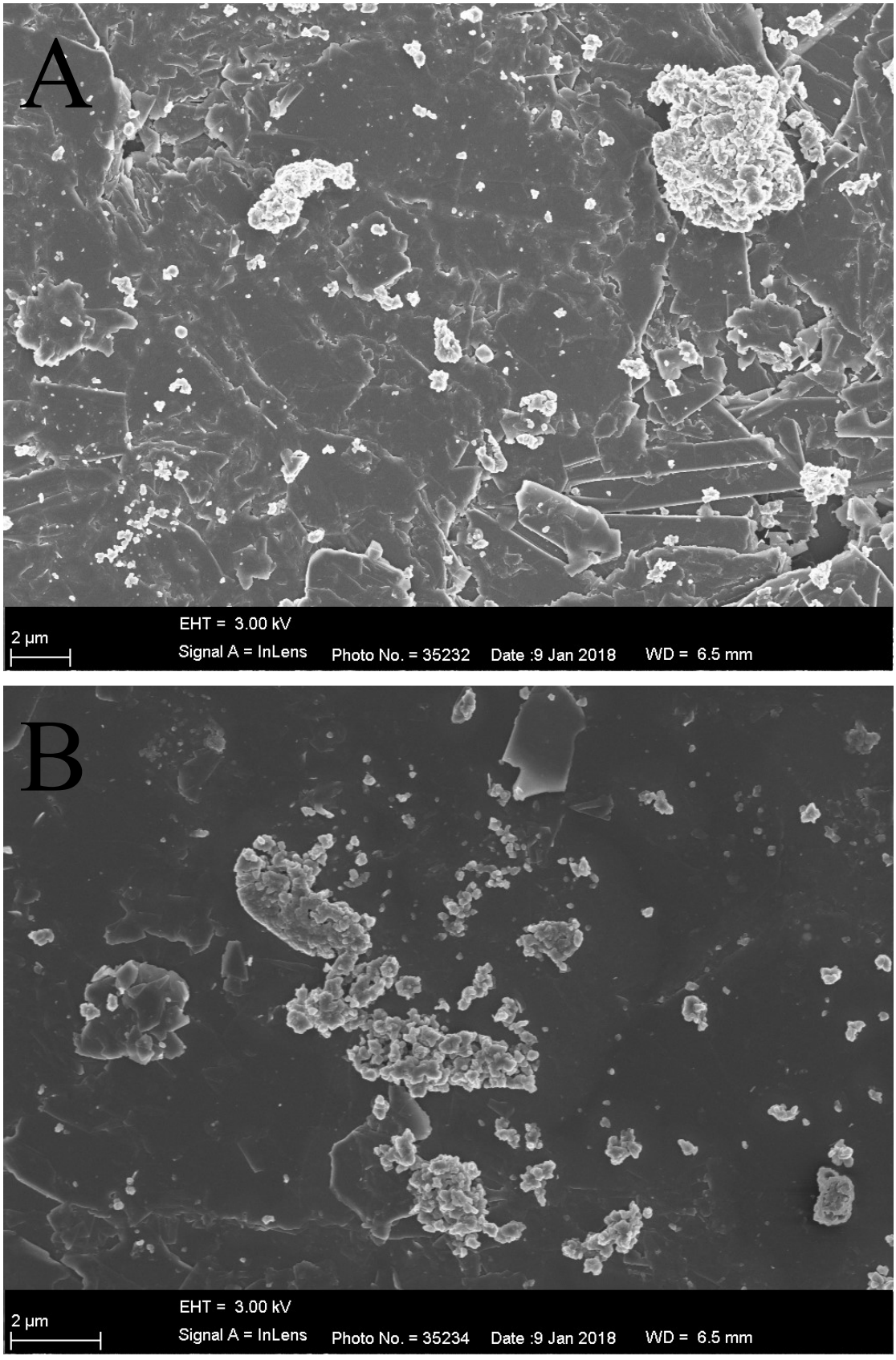

Figure 4-22: Graphite growth substrate after a growth period of 3 weeks.

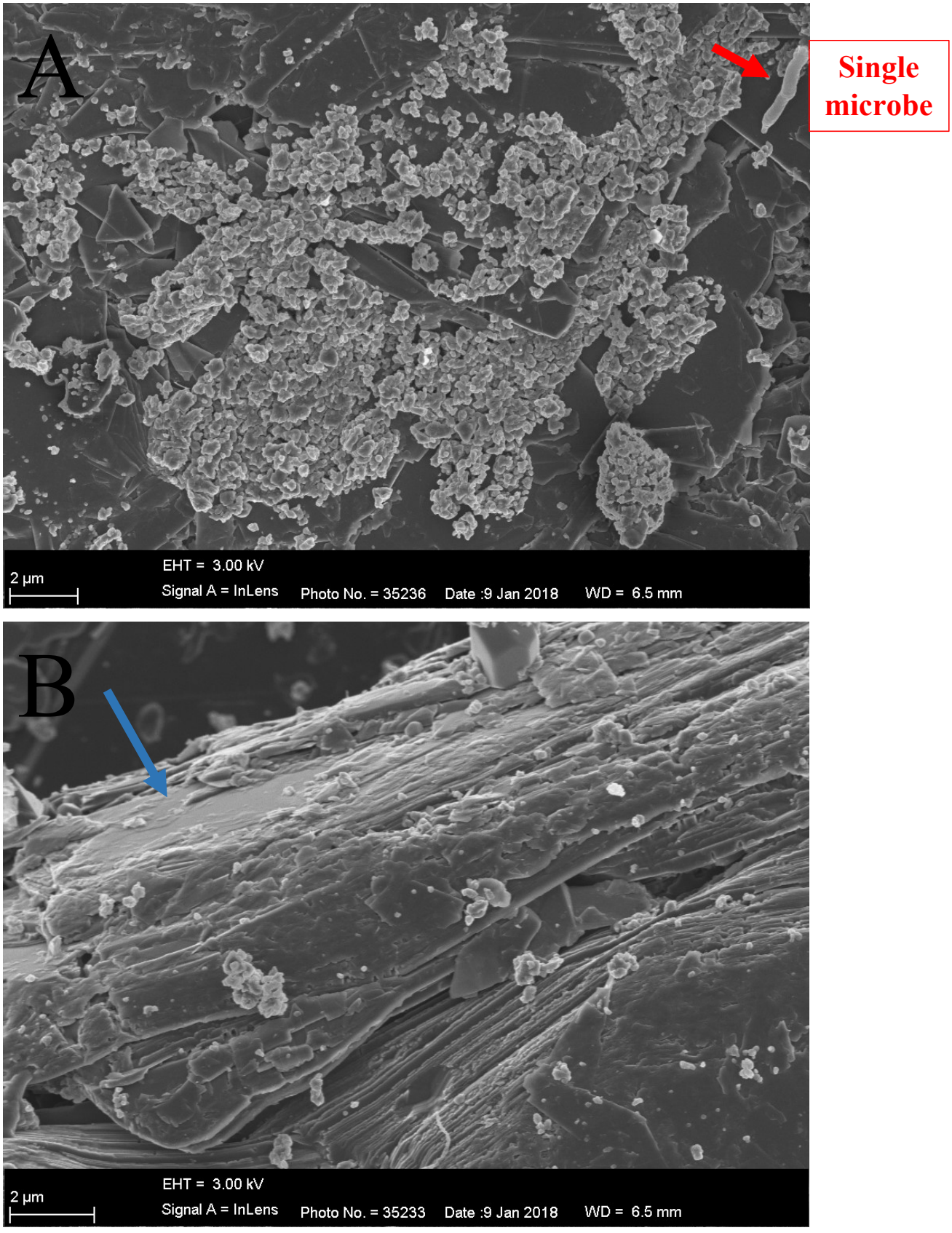

Figure 4-23: Graphite growth substrate after a growth period of 3 weeks. A: illustrating crystals and possible single microbe (depicted by red arrow). B: illustrating the layered structure typical for graphite, with smooth basal plane (blue arrow).

4.5 Bioelectricity generation

The cell potential of the microbial fuel cells was measured at various resistances as depicted by Figure 3-1. To determine the residual cell potential generated by the MFC due to its configuration, the cell potential of the MFC filled in the absence of microbial cells – *Geobacter sulfurreducens* – was measured. This cell is referred to as the blank cell. This was done to determine what the effect of the configuration, i.e. type of electrodes and electrolyte and the reaction between said parameters have on the bioelectrogenesis. Figure 4-24A represents the cell potential measured for the blank cell. Using Equation 2-14, the data is converted to power density, represented by Figure 4-24B. A steady cell potential of approximately 40 mV can be observed, and a power density of approximately 300 mW/m^3.

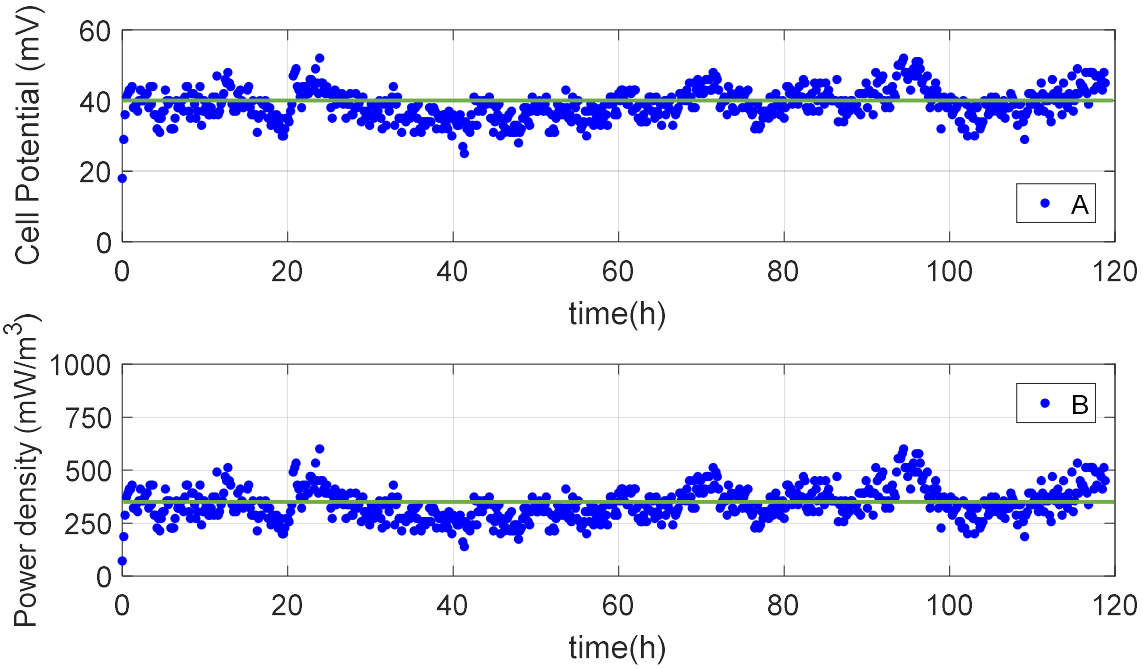

Figure 4-24: Cell potential measured (A); Power density generated (B) by blank cell. Green line illustrates the average value (—).

The MFC filled with electrolyte (i.e. NBAF growth media) and pure microbial cells – *Geobacter sulfurreducens* – is used as the control MFC and the bioelectrogenesis by *Geobacter sulfurreducens* grown on the two different carbon growth substrates are compared to the control MFC. At specific growth periods, one can compare the performance of the various MFCs – i.e. investigate the effect of the addition of a growth substrate. The different MFC configurations investigated are depicted in Figure 3-5 – the mixture of the carbon substrates was also investigated (not illustrated in Figure 3-5).

Figure 4-25 illustrates the cell potential measured and Figure 4-26 the power density generated by these MFCs after a growth period of 1 month – the power density is determined by converting the cell potential from Figure 4-25 using Equation 2-14. Only one external resistance is chosen to compare since the trend, again, remains the same. All power density curves represented are under an external load of 250 Ω.

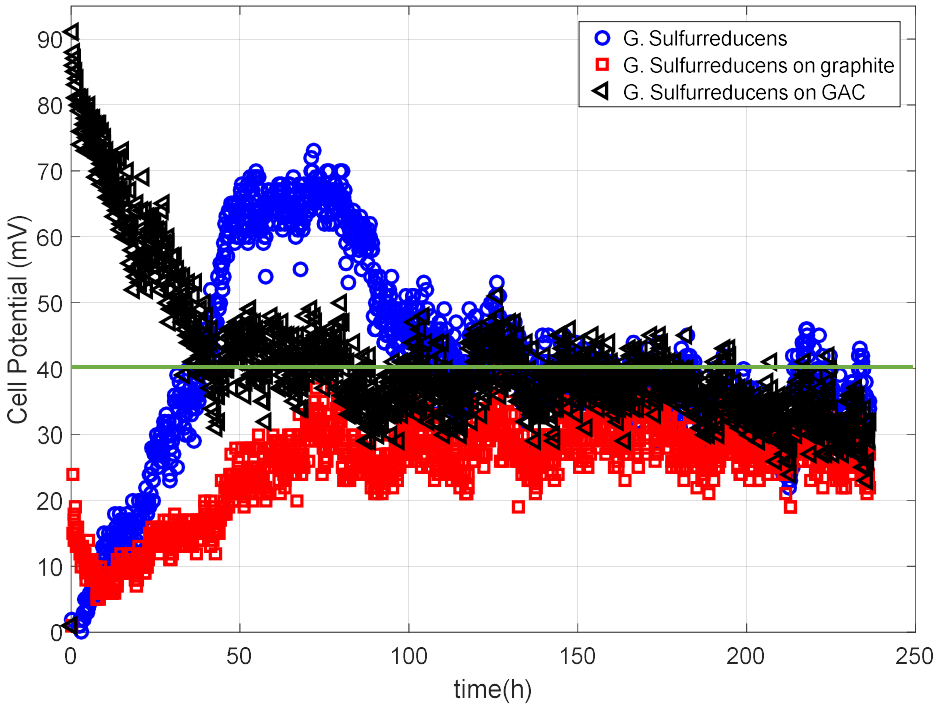

Figure 4-25: Cell potential (mV) after 1 month growth period. Blank cell average (—).

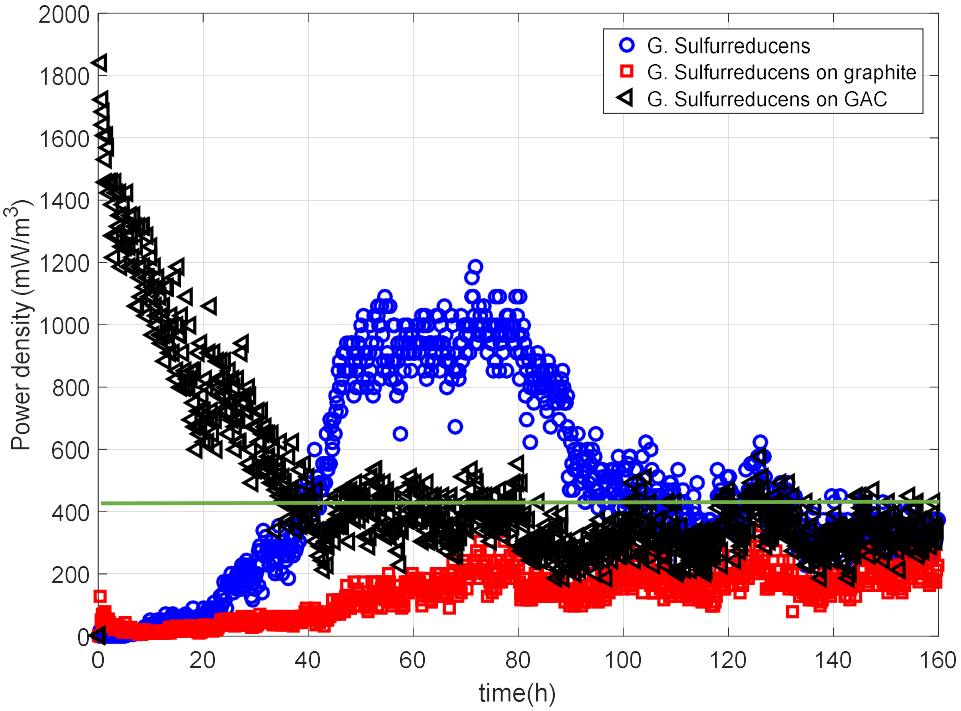

Figure 4-26: Power density (mW/m^3) generated after a growth period of 1 month. Blank cell average (—).

Due to the profiles of the cell potential and power density curves being the same, the results will only be given as power density, enabling the direct comparison of power generation. Figure 4-27 represents the power density generated by all MFC configurations after a 3 month growth period.

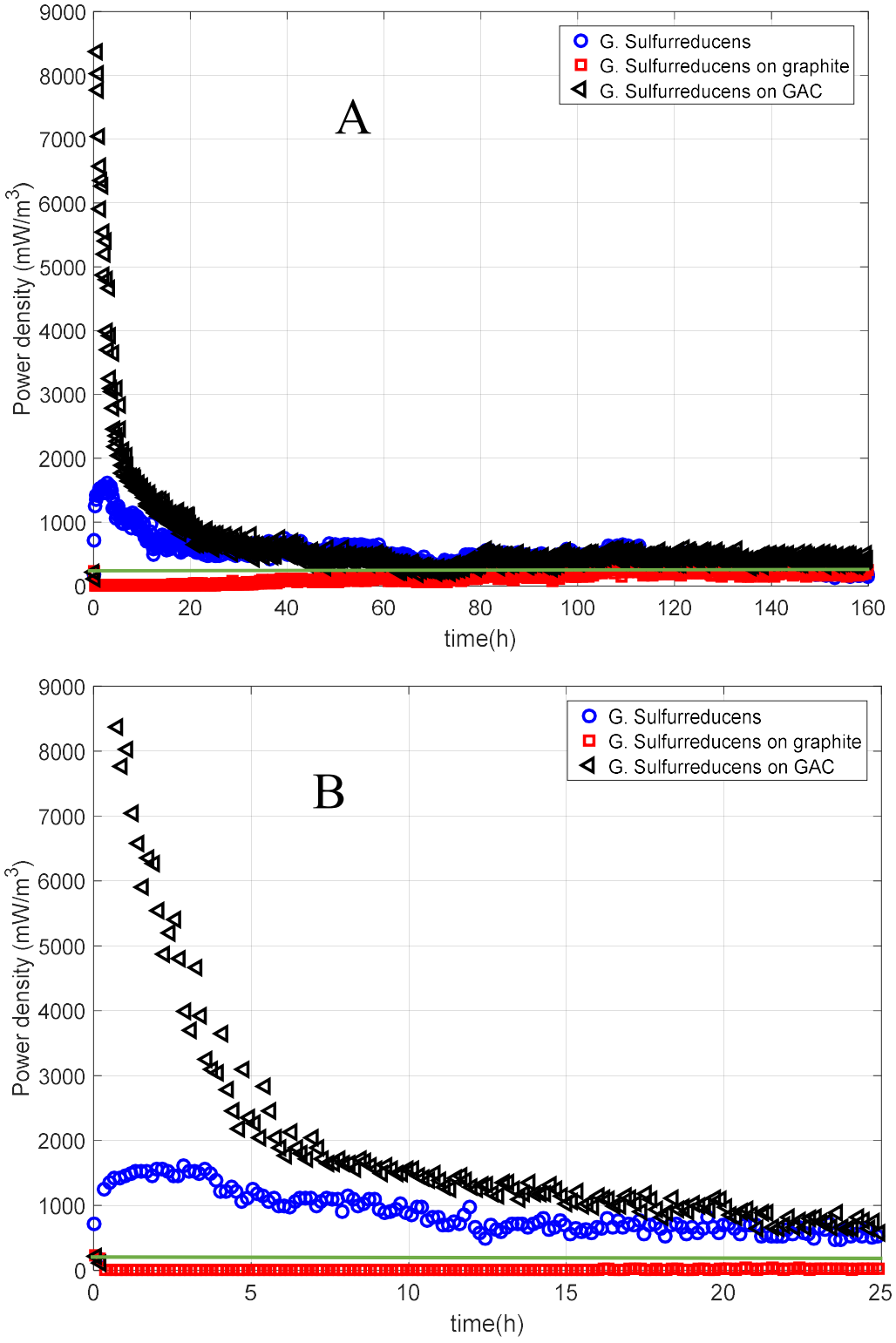

Figure 4-27: Power density (mW/m^3) generated after a 3 month growth period. A: Full experimental run; B: Zoom-in to illustrate initial 25 h. Blank cell average (—).

Figure 4-28 illustrates power density generated after a 4 months growth period.

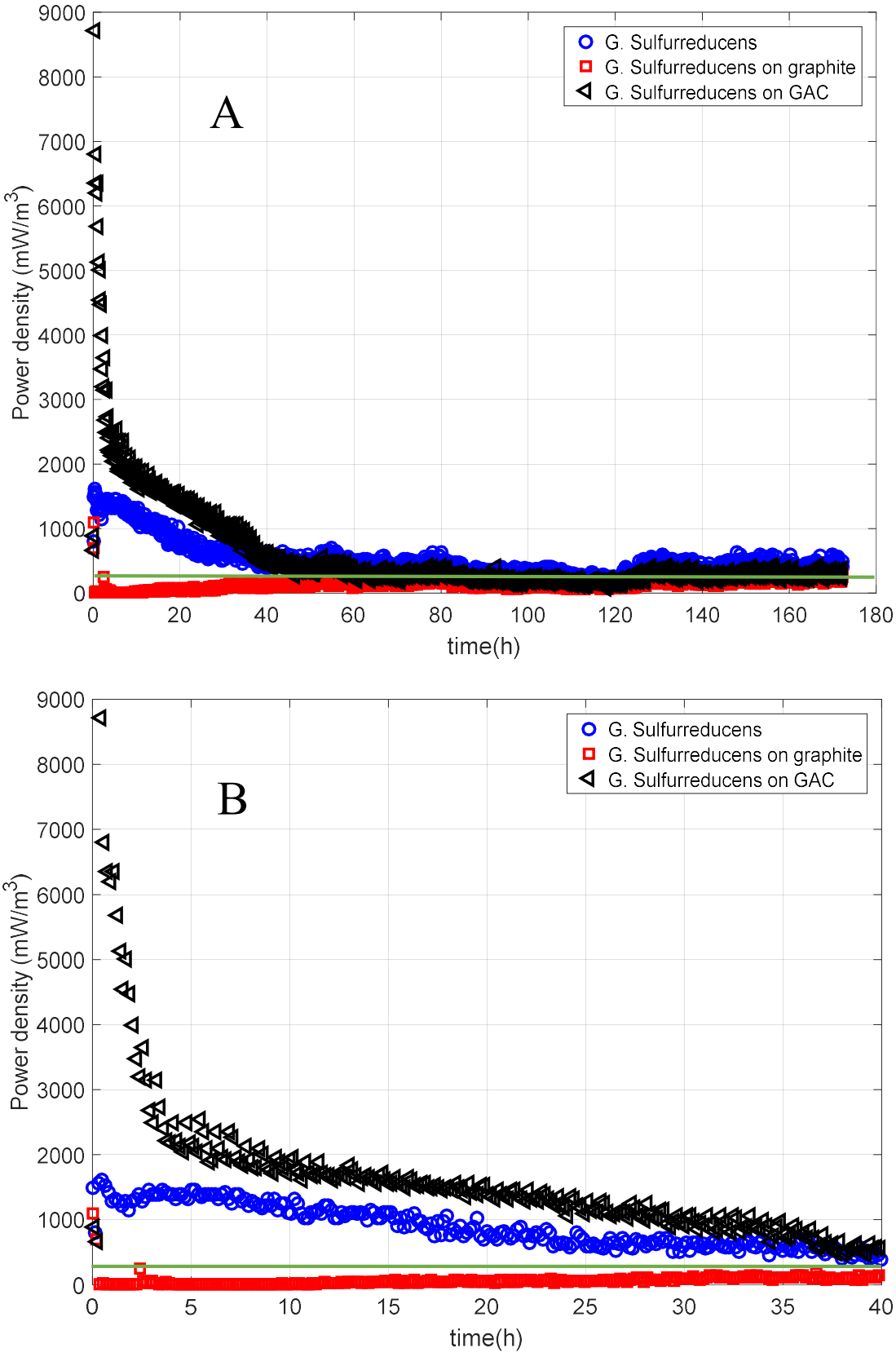

Figure 4-28: Power density (mW/m^3) generated after a 4 months growth period. A: Full experimental run; B: Zoom-in to illustrate initial 40 h. Blank cell average (—).

The microbial cells were also grown on a 1:1 mixture of the two carbon substrates. Figure 4-29 illustrates the effect of the carbon mixture substrate on power density. Figure 4-30 combines all MFCs with a growth period of 4 months.

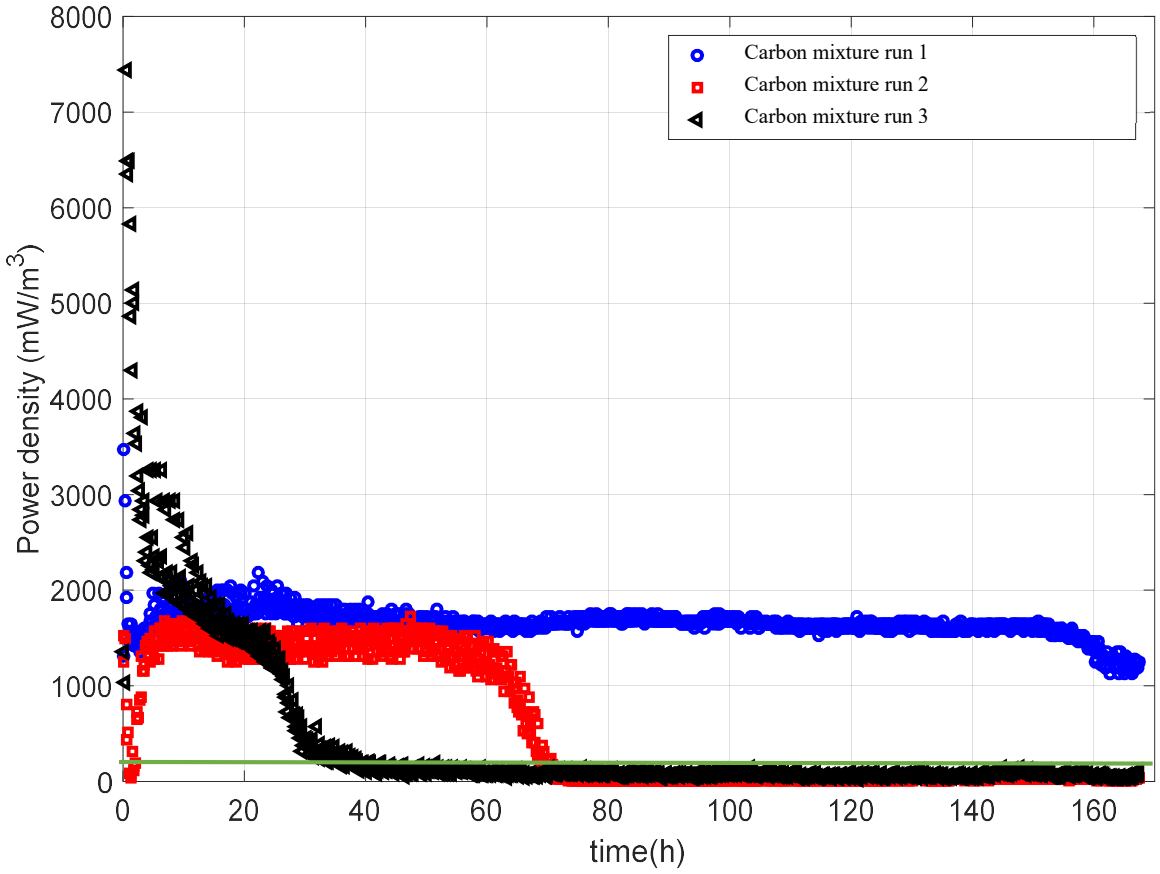

Figure 4-29: Power density (mW/m^3) generated by G. sulfurreducens grown on a mixture of graphite and GAC particles to a ratio of 1:1 after a 4 month growth period (3 runs). Blank cell average (—).

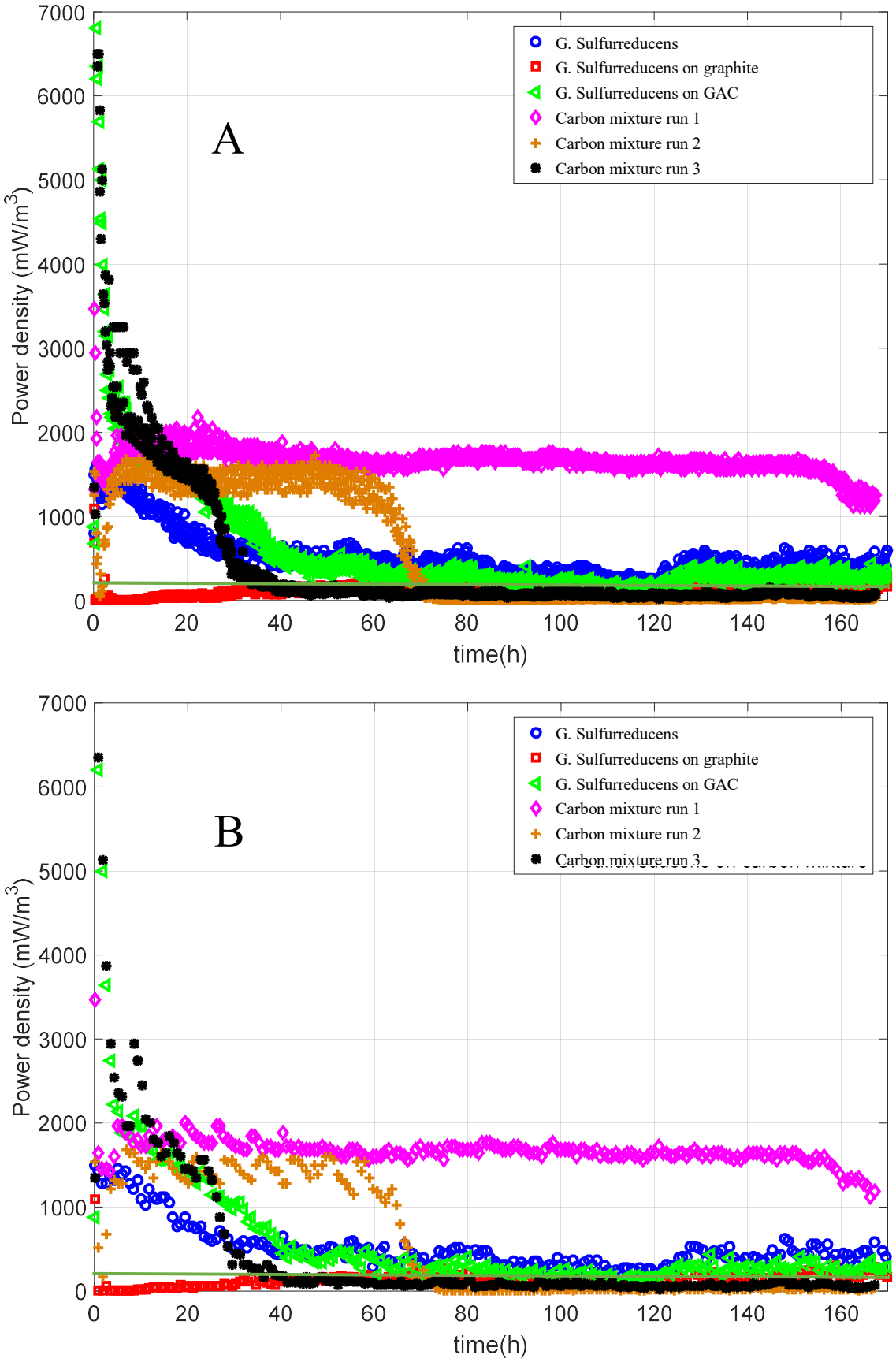

Figure 4-30: Power density (mW/m^3) generated by all different MFC setups with 4 months growth period. A: all data points; B: every 5th data point plotted. Blank cell average (—).

Using the data, one can compare each individual MFC performance to the growth period – i.e. how does the growth period influence the performance of the MFC. As can be seen from the previous figures the different growth periods investigated were selected to be 1 month, 3 months and 4 months. Figure 4-31 illustrates the power density generated by pure *G. sulfurreducens* compared at the different growth periods. Figure 4-32 represents the power density generated by *G. sulfurreducens* grown on graphite particles and Figure 4-33 represents the power density generated by *G. sulfurreducens* grown on GAC particles.

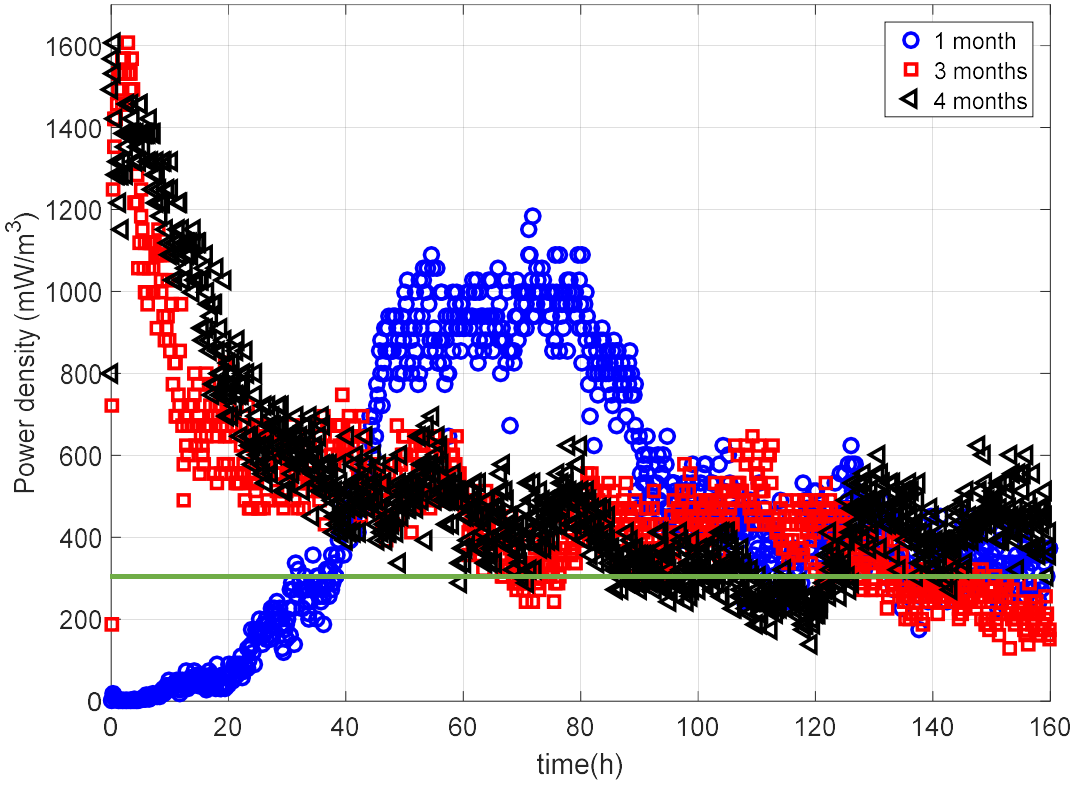

Figure 4-31: Power density (mW/m^3) generated by pure G. sulfurreducens after different growth periods. Blank cell average (—).

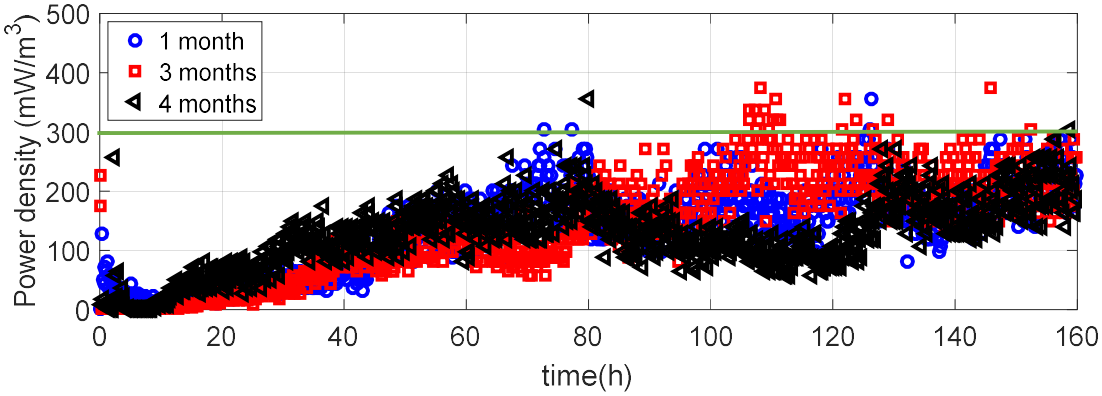

Figure 4-32: Power density (mW/m^3) generated by G. sulfurreducens with graphite particles after different growth periods. Blank cell average (—).

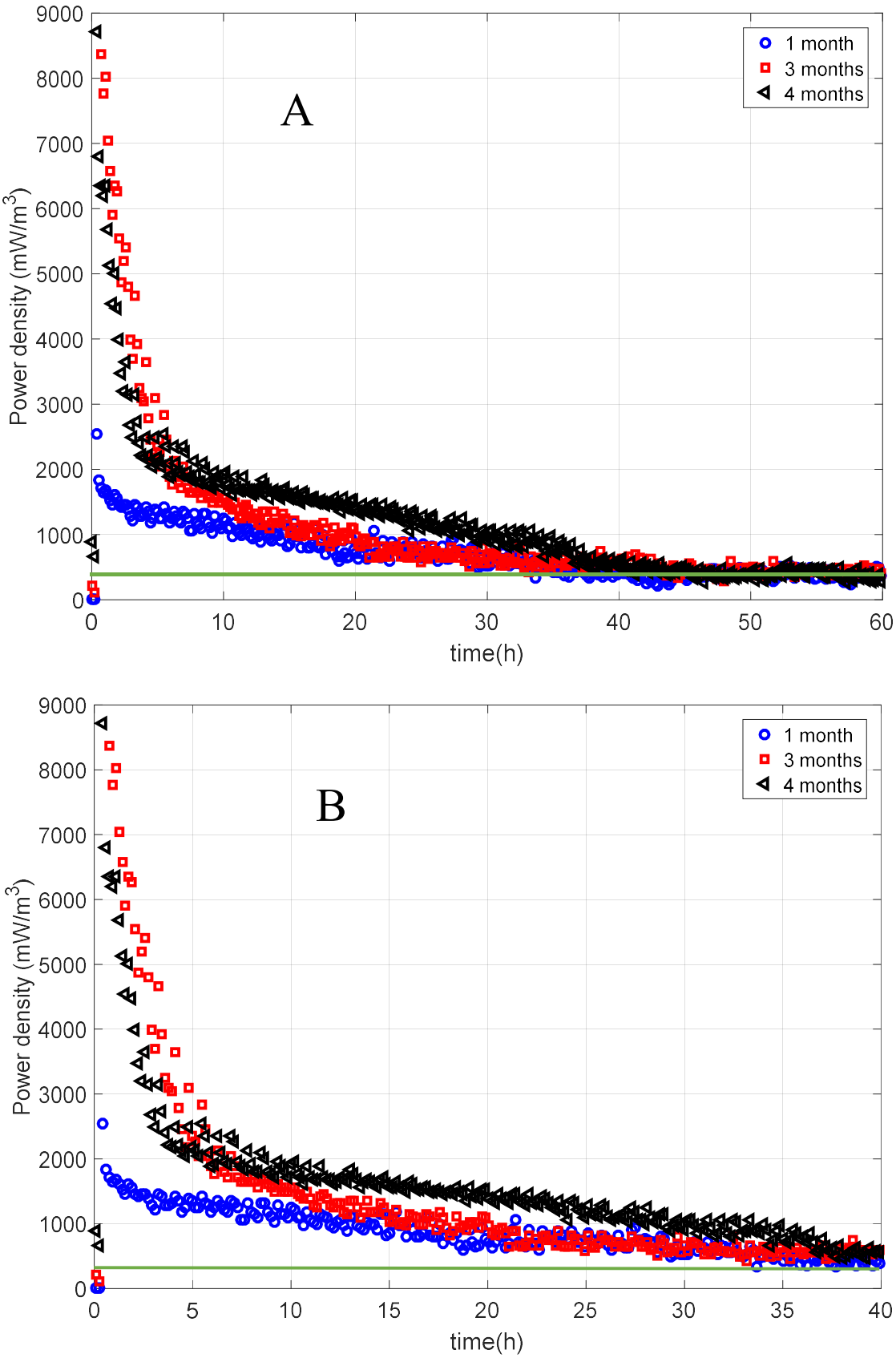

Figure 4-33: Power density (mW/m^3) generated by G. sulfurreducens with GAC particles after different growth periods. A: First 60 h; B: first 40 h. Blank cell average (—).

The maximum power densities obtained by the various configurations normalised to the anodic compartment volume, as well as average power densities are summarised in Table 4-4. It is difficult to compare the power densities to other MFC configurations from the literature due to the depletion rates and other factors contributing to the power outputs.

Table 4-4: Summary of power density normalised to anodic chamber volume.

		Power density (W/m^3)	
Growth period	**Growth substrate**	**Maximum**	**Average**
1 month	*G. sulfurreducens*	2.2	1.15
	Graphite particles	0.6	0.43
	GAC particles	4.0	1.49
3 months	*G. sulfurreducens*	3.2	0.95
	Graphite particles	0.6	0.29
	GAC particles	17.0	1.57
4 months	*G. sulfurreducens*	3.2	1.13
	Graphite particles	0.6	0.29
	GAC particles	17.0	1.49
	1:1 carbon mixture run 1	3.6	4.85
	1:1 carbon mixture run 2	3.2	1.32
	1:1 carbon mixture run 3	15.0	1.43
Average	*G. sulfurreducens*	2.9	1.08
	Graphite particles	0.6	0.34
	GAC particles	12.7	1.52
	1:1 carbon mixture	7.3	2.53
	BLANK CELL	0.6	0.47

The total energy generated by the various systems were determined using the method explained in Section 3.3.4 and is summarised in Table 4-5. All energy densities were calculated for a total of 160 h, to ensure comparable results.

Table 4-5: Energy density (MJ/m^3) generated by the various systems.

		Energy density (MJ/m^3)	
Growth period	**Growth substrate**	**250 Ω**	**Total**
1 month	*G. sulfurreducens*	0.348	0.665
	Graphite particles	0.128	0.249
	GAC particles	0.350	0.859
3 months	*G. sulfurreducens*	0.288	0.550
	Graphite particles	0.085	0.167
	GAC particles	0.401	0.902
4 months	*G. sulfurreducens*	0.322	0.648
	Graphite particles	0.082	0.169
	GAC particles	0.366	0.857
	1:1 ratio of GAC and graphite	1.001	2.792
	1:1 ratio of GAC and graphite	0.340	0.759
	1:1 ratio of GAC and graphite	0.265	0.825
Average	*G. sulfurreducens*	0.319	0.621
	Graphite particles	0.098	0.195
	GAC particles	0.372	0.873
	1:1 ratio of GAC and graphite	0.535	1.459
	BLANK CELL	0.194	0.196

5. Discussion

5.1 Microbial community

According to the DNA sequencing (Figure 4-1 and Figure 4-2), the results from the absorbance measurements (Table 4-1 and Table 4-2), and the PCR analysis, it can be concluded with great certainty that throughout the entire investigation the microbial community was pure *Geobacter sulfurreducens* without any contamination. It is important to specify the microbial community since any alteration will influence the structure and properties of the electrochemical characteristics and losses in the MFCs (Alterman et al., 2006). Substantially greater power densities have been achieved by utilising mixed communities or diverse microbial cultures rather than pure cultures (Logan, 2009, Cheng et al., 2006, Logan et al., 2005), which is why it is worth noting that the bioelectrogenesis is due to the inoculation of a pure culture.

5.2 Microbial growth

One of the objectives from this study was to investigate the effect of the addition of inorganic carbon particle in the growth media acting as "growth substrates" on the growth of *Geobacter sulfurreducens*. This effect is illustrated by the growth curves, Figure 4-4, and the various FE-SEM images.

In Figure 4-4 depicting the microbial growth of *Geobacter sulfurreducens* on GAC particles (illustrated by the '◊'), the lag and growth phases are clearly visible. The stationary phase seems to be approaching. The curve has an apparent "S-shape", typical for microbial growth. The curve in Figure 4-4 illustrating growth of pure *Geobacter sulfurreducens* (illustrated by the '○') seems to have a trend, if the first data point is considered an outlier, the growth seems to be slowly increasing. Figure 4-5 illustrating the turbidity progression of pure *Geobacter sulfurreducens* clearly shows an S-curve profile, typical for microbial growth. In this curve the lag, growth and stationary phases are clearly visible. This curve confirms the growth of pure *Geobacter sulfurreducens* and validates the comparison of the growth on the carbon particles using Figure 4-4. Considering the data illustrating the growth of *Geobacter sulfurreducens* on graphite particles (represented by the 'x'), the data is scattered slightly, but a mean between the data points can be taken, showing a near constant trend of approximately 0.4 g/L from the 11th day 21st day.

Figure 4-4 provides clear evidence that GAC particles can be used as a growth substrate which is demonstrated to be advantageous for microbial growth. After a growth period of 3 weeks the biomass concentration of the *Geobacter sulfurreducens* cells was increased nearly 6 fold by the mere addition of GAC particles to the initial growth media.

By considering the BET analysis in Table 4-3, the BET surface area of GAC particles is 601 ± 9 m^2/g and the Langmuir surface area is 745 ± 4 m^2/g. This extremely large surface area is proven to be advantageous for microbial growth (Jiang et al., 2011, Kim et al., 2006). The surface of pure GAC particles is rough, and advantageous for microbial growth. The microbes can easily attach to the surface as there are ample ideal attachment and growth sites. This is seen in the FE-SEM images of the pure GAC particles, Figure 4-6 and Figure 4-7.

Figure 4-6A is an illustration of the macrostructure, consisting of numerous large pores throughout the material, increasing the surface area. Figure 4-6B magnifies the pores. Figure 4-7 magnifies the microstructure of the material. Here the rough, cracked surface is clearly visible, illustrating the uneven surface with impurities present on the material. All these characteristics of the GAC particles are known to be advantageous for improved microbial growth. The biofilm production is initiated on the flat, yet rough surface, with agglomeration taking place on the cracks and ridges enabling the thickening of the biofilm.

The BET analysis for the GAC particles indicates that after 2 weeks of microbial growth, the surface area has decreased. This is because the biofilm now covers the flat surface comprising of pores and cracks and ridges, thereby decreasing the porosity of the pure GAC particles. After 3 weeks of growth, a thick biofilm is formed (visible in Figure 4-20B); this results in an increase in surface area due to the “packing structure” of the biofilm, indicating that the microbial biofilm creates additional “voids” or pores on the surface. This phenomenon can be explained by the following illustration represented by Figure 5-1.

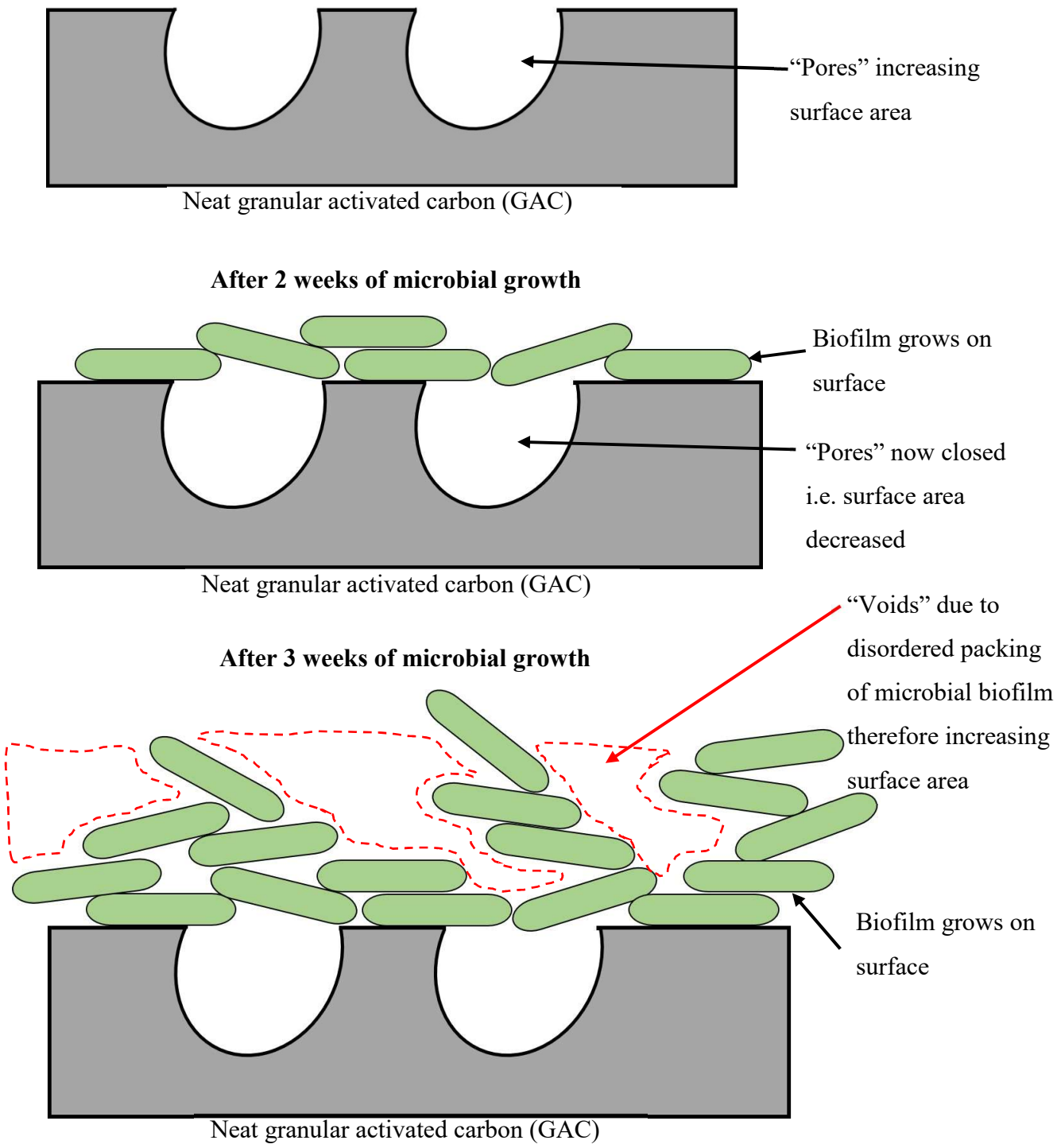

Figure 5-1: Illustration of surface area increase and decrease due to microbial growth.

The growth can also be qualitatively analysed and compared by the FE-SEM images of the GAC particles. Figure 4-11 to Figure 4-14 illustrate the surface after 2 weeks of microbial growth. Here one can observe that the biofilm starts to cover the surface of the GAC. There are ideal attachment sites where the microbial growth is enhanced, i.e. the cracks and the rough

edges, and a biofilm can start to form even after only 2 weeks of growth – visible in Figure 4-11. At 2 weeks of growth the microbial cells only sparsely cover the surface, with biofilm being visible in rare cases. In Figure 4-12 to Figure 4-14 the surface in observed to be covered by microbes.

It is indisputable from Figure 4-20 and Figure 4-21 that after 3 weeks of microbial growth, the biofilm that has formed is thick and dense. The biofilm-growth on the edges of the GAC particles is evident from Figure 4-20A, whereas Figure 4-20B represents the biofilm attached to the basal plane (parallel to lateral/horizontal axis) of the GAC particle. The thickness and irregularity are evident. Figure 4-21 magnifies the biofilm, showing the morphology of the microbes to be rod-shaped, and allows observation of the irregular packing, explaining the increase in surface area due to the creation of "voids" (Figure 4-21B).

By only taking Figure 4-4 into account there is not enough data to support a conclusion on the effect of graphite particles on microbial growth. According to the BET analysis in Table 4-3, the BET surface area of neat graphite particles is 0.13 ± 0.70 m^2/g and the Langmuir surface area is recorded as 0.16 ± 0.88 m^2/g. Although the error in both these cases are larger than the recorded values, rendering these values inconclusive, the order of magnitude compared to the neat GAC particles can be considered useful. The reason for this inaccurate value is due to the shape of the graphite particles. The analysis is done under the assumption of sphericity, but graphite particles are known for their large, thin and flat structures. The fact that the order of magnitude of the surface area of the pure graphite is 600 times smaller than that of the GAC particles, indicates the inefficiency in comparison.

The structure of the neat graphite particles can be investigated to attempt to explain the reason behind the poor microbial growth, and therefore why graphite is a poor choice for a growth substrate. In Figure 4-8 and Figure 4-10 the structure of neat graphite particles is represented. In Figure 4-8A and Figure 4-9A the basal plane can be observed as a smooth, crystalline glass-like surface. The damage on the edges are visible; these edge effects might enable attachment of microbial cells. Figure 4-8B and Figure 4-9B illustrates flakes with damaged basal planes, but with the crystallinity still observable – see Figure 4-9B with magnification insert of smooth basal plane. It is this smooth surface, however small, on which the microbial cells do not attach easily. Figure 4-9B is a magnification of the damaged basal plane, with the crystallinity intact. Figure 4-10, Figure 4-19 and Figure 4-23B represents the typical layered structure of graphite.

With 2 weeks of microbial growth, after extensive searching, microbial cells were not detected or found. Figure 4-15 to Figure 4-19 represent images of graphite after 2 weeks. All the images include crystals from the growth media due to the freeze dying process. The morphology of the microbial cells (observed in the FE-SEM images of growth on GAC particles – Figure 4-11 to Figure 4-14) is clearly different to that of these crystals; the microbes are rod-like or bacillus in shape whereas the crystals are clumped together forming a large structure and the magnification of the crystals. Figure 4-16B and Figure 4-18A illustrate that these crystals comprise more spherical or almost round particles.

It can be seen from all these images – Figure 4-15 to Figure 4-19 – that after an extensive search for microbial cells or biofilm, the basal planes are clearly without microbial growth. The basal plane crystallinity and smooth finish remain intact. Contrary to the flat plane of the GAC particles with growth, where the microbes were visible everywhere, on the graphite particles the basal plane seems to be clean in all images. Figure 4-18A is the only possible capture of a single microbial cell. Figure 4-19 is a magnification of the graphite structure, demonstrating the layers, crystallinity and glass-like surface of graphite very clearly on a magnified scale.

Figure 4-22 and Figure 4-23 represent the graphite growth substrate after a 3 week growth period. Even after 3 weeks of growth, and after an extensive search using the FE-SEM, microbial cells could not be located; this is evident form Figure 4-22 and Figure 4-23. The presence of the crystals in Figure 4-23A has already been explained. Note the red arrow in Figure 4-23A – this might be a single microbe; the morphology fits with that of the previous images, although this microbial cell is slightly large. Even if this is a single cell, it is an indication that the overall growth on graphite is extremely poor. Figure 4-23B is a perfect illustration of the microstructure of graphite; the layers are highly evident with a smooth basal plane (note blue arrow). In this image there are no microbial cells found either. All of these images, where no evidence of microbial growth could be observed, with the growth curve of *Geobacter sulfurreducens* on graphite particles in Figure 4-4 showing little to no increase in growth, lead to the conclusion that graphite inhibits growth due to poor attachment.

5.3 Bioelectricity generation

From Figure 4-24 it is noticeable that the blank cell produces a steady cell potential of 40 mV which is correlated to approximately 300 mW/m^3. This means that without any microbial cells, there is a redox reaction taking place between the components in the electrolyte (i.e. the growth media) and the electrode, however small – in a similar manner to the way that fuel cells operate. When analysing the performance of all the various MFC configurations, a "pseudo steady state" can be observed. In all the figures the "pseudo steady state" correlates to a cell potential and power density of approximately 40 mV and 300 mW/m^3 respectively. At the point where the MFC reaches its "pseudo steady state" it is as though the MFC behaves like the blank cell – i.e. in the absence of microbial cells – so this is correlated to the death of the *G. sulfurreducens.* In other words, this is the point where the lifetime of the MFC ends. This point, where the *G. sulfurreducens* stops influencing the performance of the MFC, will be considered for comparison.

The effect of the growth period on power density was investigated and clearly influences the performance of the MFC. There are two important parameters to consider when comparing the performance of MFCs. First the maximum power density generated by the MFC and second, the depletion rate of the maximum power density.

Figure 4-31 illustrates the power density produced by pure *G. sulfurreducens* during different growth periods. Figure 4-31 is redrawn with only every 5th data point given to enable a better view of the trends. This can be seen by Figure 5-2. It is, however, important to view both figures side by side to see the maximum power density obtained, which differs in the two figures due to the data points left out.

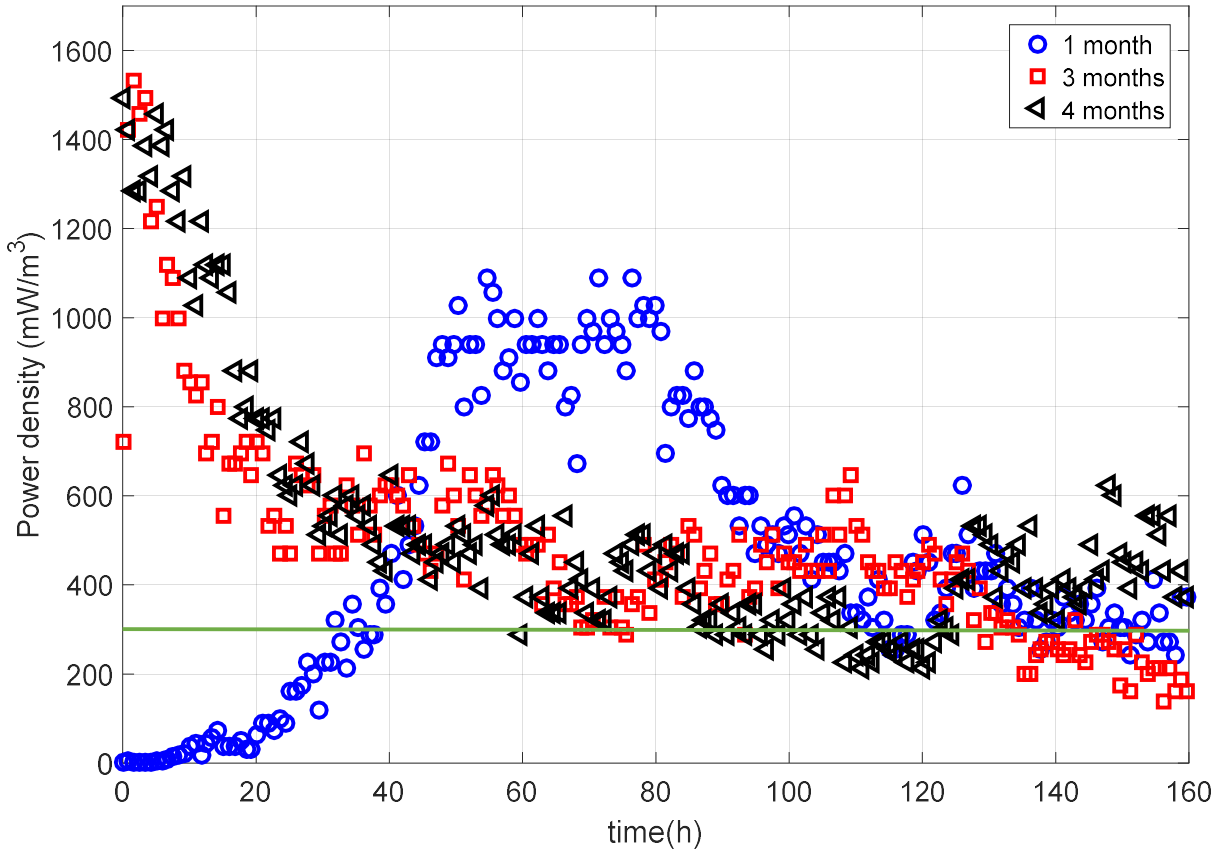

Figure 5-2: Power density (mW/m^3) generated by pure G. sulfurreducens after different growth periods (every 5th data point). Blank cell average (—).

The important difference observed in the investigation of the growth period is as follows. The microbial cells – *G. sulfurreducens* – are allowed to grow for the specified growth periods prior to inoculation into the MFC where after the power density or electricity can be harvested. It is also important to remember that all these experiments were batch operated; therefore, once inoculated the electrolyte (i.e. growth media) was not altered or enhanced with additional ingredients.

The most noticeable difference between the 1 month and both the other growth periods is that the 1 month curve exhibits an initial increase in power density until a maximum is reached, where it is maintained for approximately 30 h and then starts to decay. However, the 3 month and 4 month growth period curves start with the maximum power density at t = 0 and immediately start to decay. A reasonable explanation for this phenomenon is that the microbial cells are still in the growth phase or active phase during the 1 month period. Due to the cells not receiving additional nutrients, one can expect them to undergo the normal growth,

stationary and death phases. This profile can be seen for the 1 month curve. The 3 months and 4 months microbial cells are probably already in the death phase or at the end of the stationary phase. The "death" phase correlates to the depletion of nutrients. The reason for the lack of this initial increase leading to the maximum as exhibited by the 1 month curve, can be explained by the depletion of nutrients, as the batches are all inoculated on day t = 0, and merely transferred to the MFC under anoxic conditions, without altering the electrolyte. It has been concluded by several publications (Yost et al., 2012, Bond and Lovley, 2003) that the addition of nutrients mid-run increases power density. This can be further investigated to determine the effect of this on this set-up.

Figure 5-3 is a modification of Figure 4-31, where the 3 month and 4 month curves are moved to correlate with the 1 month death phase. Note that every 5th data point is plotted.

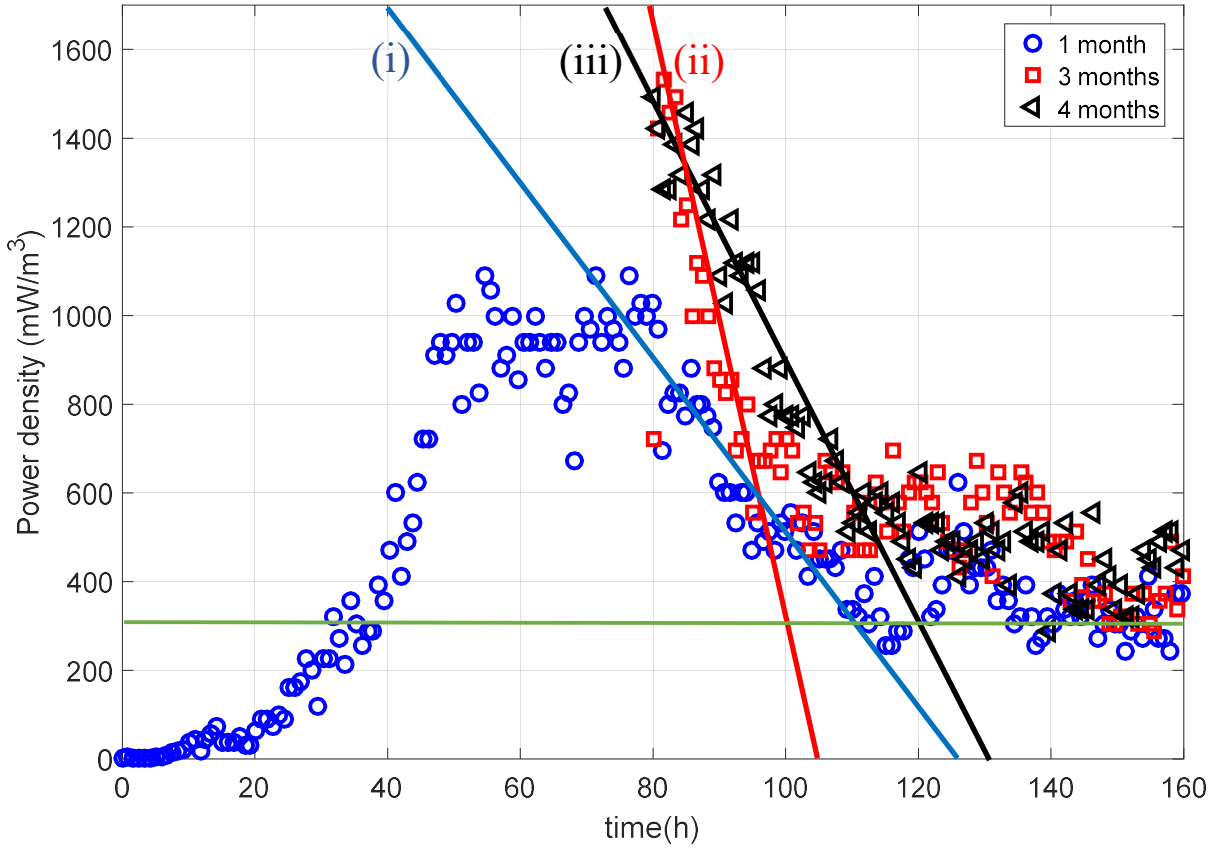

Figure 5-3: Modified power density (mW/m^3) generated by pure G. sulfurreducens after different growth periods (every 5th data point); The linear lines indicate power depletion rates. Blank cell average (—).

First the maximum power density of the 1 month curve is only 1100 mW/m^3 which is maintained for 30 h, whereas both the 3 month and 4 month curves have maximum power densities of 1600 mW/m^3 (clear from Figure 4-31) which immediately starts to decay. The depletion rate can be determined by the slope of the curve after the maxima. This is indicated by a linear line ((i) blue for 1 month (ii) red for 3 months and (iii) black for 4 months) drawn on each curve for visual purposes.

The depletion rates are as follow: 1 month yields 20 mW/m^{3}h for approximately 20 h; 3 months result in 70 mW/m^{3}h for approximately 20 h; and the 4 month curve shows 30 mW/m^{3}h for approximately 30 h.

From this analysis, it is obvious that the 3 month growth period leads to the least advantageous outcome with the highest depleting rate. Considering the 1 month versus the 4 month growth period, the decision resulting in the most advantageous growth period would depend on the required application. The 4 month MFC yields the highest power density (1.6 times higher than the 1 month MFC), with a depletion rate of 30 mW/m^{3}h over a period of 30 h. This MFC yields an energy density of 0.648 MJ/m^3 in total. The 1 month MFC yields a maximum of 1000 mW/m^3 obtained for 30 h, which is good if this is required, and then depletes at a rate of 20 mW/m^{3}h for 20 h. The energy density yielded by this MFC is slightly higher than the 4 months MFC, with a total of 0.665 MJ/m^3. The 1 month exhibits a power density which is maintained for a short while, but with a lower value, whereas the 4 months MFC delivers very high power (1.6 times the 1 month output) but is not maintained. The energy densities generated by these two are also similar.

Figure 4-32 illustrates the power density generated by *G. sulfurreducens* with graphite particles used as growth substrate. In order to see the data more clearly, Figure 4-32 is modified in such a way that every 5th data point is plotted. This is illustrated by Figure 5-4.

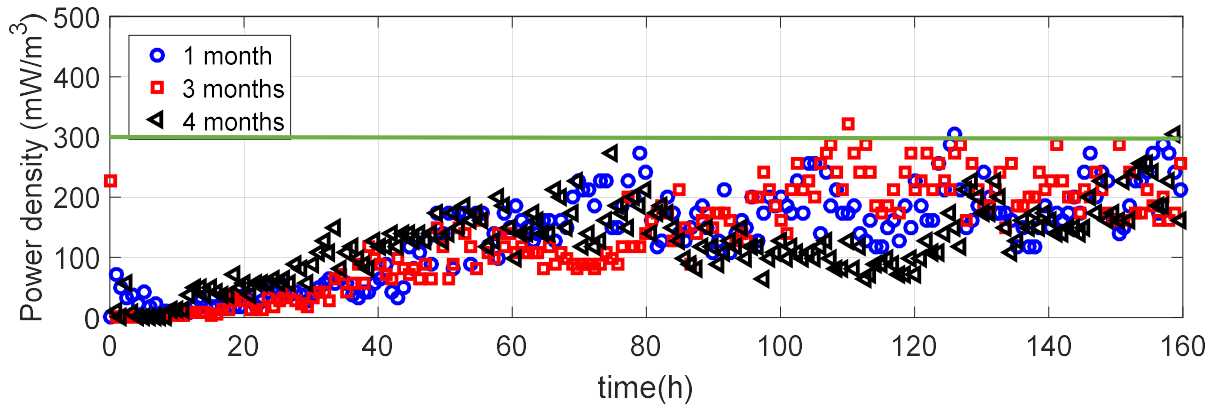

Figure 5-4: Power density (mW/m^3) generated by G. sulfurreducens with graphite particles after different growth periods (every 5th data point). Blank cell average (—).

As can be seen from Figure 5-4 the growth period did not affect the power density generated by the MFC containing graphite particles. The three curves follow the same trend; proving that the graphite particles inhibit growth; since the growth periods did not influence the power density to any extent, validating the findings in section 5.2 regarding the growth on graphite particles. For the entire experimental run time all three MFCs produce lower power density than the blank cell, rendering the pure graphite as growth substrate ineffective. Considering the average energy density generated from the *G. sulfurreducens* with graphite particles from Table 4-5 and comparing that to the blank cell energy density (calculated for a continuous 160 h) one can see that the values are the same, rendering the power generated by these MFCs moot.

Power density production by *G. sulfurreducens* on GAC particles at various growth periods are compared in Figure 4-33. Figure 4-33A illustrates the first 60 h. It can be observed that from 40 h the MFCs reach a “pseudo steady state” as explained at the beginning of this section. Therefore Figure 4-33B illustrating the first 40 h can be considered for the discussion. In order to compare the depletion rates, Figure 4-33B is modified into Figure 5-5.

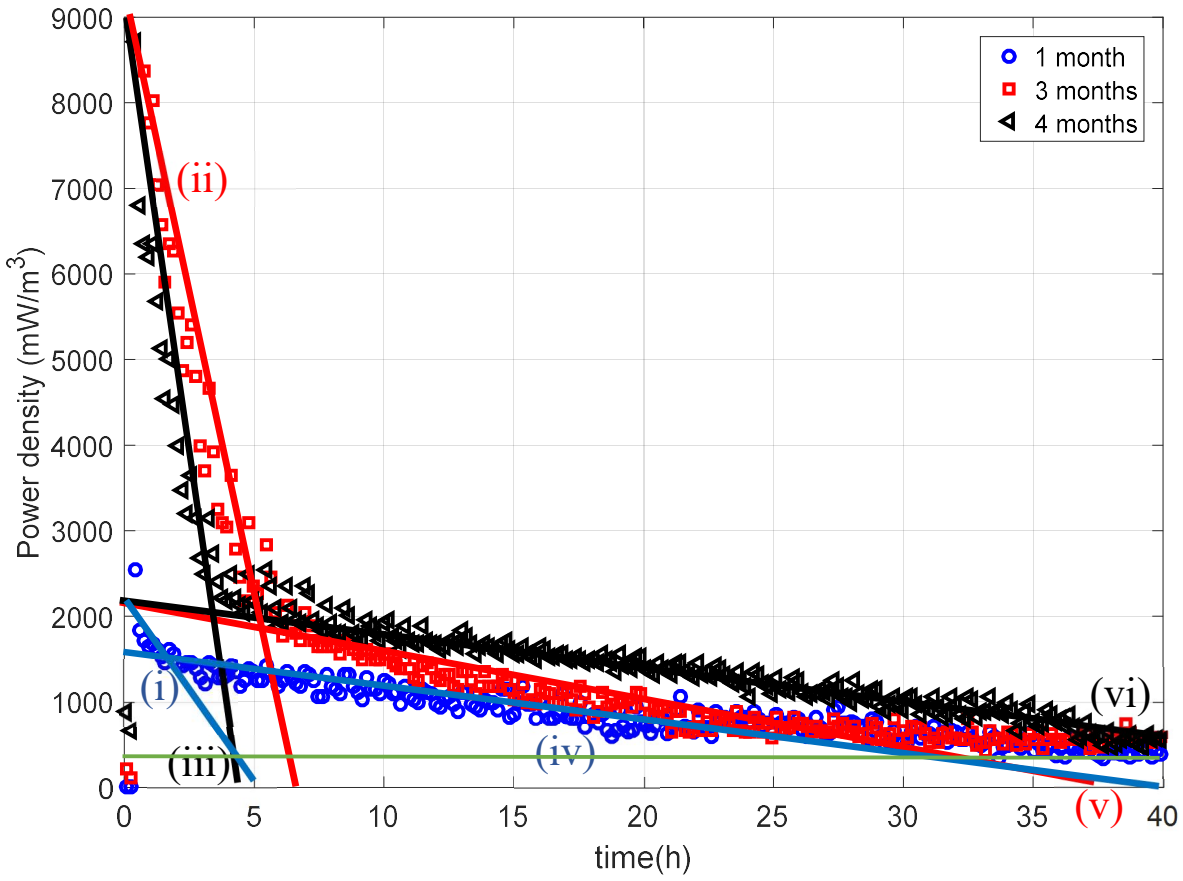

Figure 5-5: Power density (mW/m^3) generated by G. sulfurreducens with GAC particles after different growth periods (first 40 h). The linear lines indicate power depletion rates. Blank cell average (—).

The MFCs containing *G. sulfurreducens* with GAC particles demonstrate the same profile, with varying depletion rates. All the profiles have an initial maximum power density, followed by two distinct regions; the maximum is directly followed by a steep initial depletion rate (indicated by numbers (i), (ii) and (iii)), which is then followed by a less steep depletion rate (indicated by (iv), (v) and (vi)). The maximum power density produced by the 1 month MFC is approximately 2000 mW/m^3 whereas both the 3 month and 4 month MFCs generate a maximum power density of approximately 8500 mW/m^3.

The slope of each linear line is an indication of the depletion rate of each region. The blue lines indicate the depletion rates of the 1 month MFC, red the 3 month and black the 4 month MFC. As can be observed from Figure 5-5 the first set of depletion rates are estimated as: (i) 420 mW/m^{3}h; (ii) 1286 mW/m^{3}h; and (iii) 2000 mW/m^{3}h. The 1 month MFC depletes much more slowly compared to the MFCs comprising the longer growth cultures. The 3 month MFC

generates the “most power” for the longest period during this initial depletion rate, rendering it the most advantageous at this stage of the investigation.

The second depletion rate has a longer duration, lasting between 15 h and 35 h. The second set of depletion rates have the following estimated values: (iv) 30 mW/m^3h lasting approximately 25 h; (v) 56 mW/m^3h with a total duration of 15 h; and (vi) 40 mW/m^3h with the astonishing duration of 35 h before reaching the “death” stage. The 4 month MFC depletes rapidly initially, but the secondary depletion rate is the slowest which leads to it being the best choice.

Taking the energy density from these MFCs into account (Table 4-5) the 3 month MFC produces the most energy of 0.902 MJ/m^3 (total) and 0.401 MJ/m^3 (250 Ω), which is the highest of the 3 MFCs. The 1 month and 4 month MFCs both generate energy densities of 0.86 MJ/m^3, which is lower than the 0.9 MJ/m^3 generated by the 3 month MFC. However, taking all of these parameters into account, the 4 month growth period is the most advantageous for the MFCs containing GAC particles due to the longest lifespan of the MFC and the high maximum power density.

Considering the effect of the growth period on bioelectrogenesis, an increased growth period seems to be more advantageous; i.e. the 4 month growth period after *G. sulfurreducens* inoculation and incubation prior to MFC inoculation and energy harvesting proved to be the most advantageous for the GAC filled MFC and was tied with the 1 month MFC in the pure *G. sulfurreducens* filled MFC.

The next parameter to be investigated is the effect of the various growth substrates, GAC (amorphous carbon) and graphite (crystalline carbon) added to the ‘control’, i.e. pure *G. sulfurreducens* filled MFC.

Figure 4-26 represents the power density generated by all MFC-configurations after a growth period of 1 month. From this figure the maximum power density obtained from the control MFC can be taken as 1100 mW/m^3 which is maintained for 30 h. The MFC containing GAC particles reach a maximum of 1800 mW/m^3 at start-up after which the depletion starts. Figure 5-6 is a modification of Figure 4-26 to incorporate the power depletion rates.

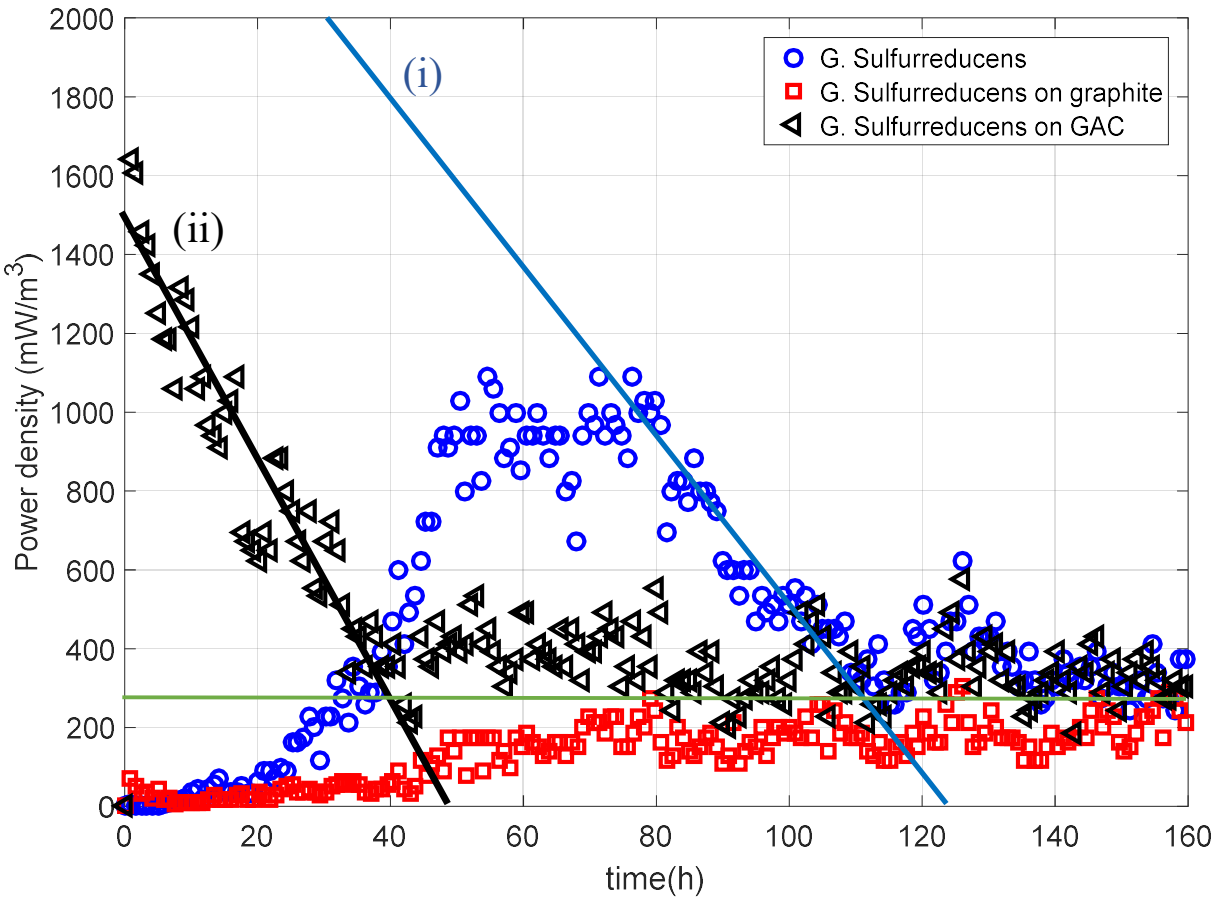

Figure 5-6: Power density (mW/m^3) generated after a growth period of 1 month (Every 5th data point plotted). The linear lines indicate power depletion rates. Blank cell average (—).

From the blue linear line (i), the depletion rate of the control MFC is 20 mW/m^3h for approximately 20 h. From the black linear line (ii), the MFC containing the GAC particles immediately starts to deplete at a rate of 30 mW/m^3h for 40 h. These configurations are comparable in the sense that the microbes all have the same growth time, although the pure *G. sulfurreducens* have the initial lag, growth and stationary phases, whereas the *G. sulfurreducens* grown on the GAC particles immediately starts to deplete. From the growth curve (Figure 4-4) it was observed that the addition of GAC particles increased the microbial growth nearly 6 fold compared to the growth of pure *G. sulfurreducens*. Due to the increased growth, the nutrients will deplete much faster in the MFC containing the GAC particles compared to the control MFC, therefor the "death phase" will commence earlier. The total energy generated by the control MFC was 0.648 MJ/m^3 (0.348 MJ/m^3 running only at 250 Ω load), whereas the GAC-MFC generated 33 % higher total energy density with a value of 0.859 MJ/m^3, but with a similar energy density at 250 Ω load of 0.350 MJ/m^3. This leads to the

conclusion that the GAC-containing MFC produces higher outputs compared to the control MFC at 1 month growth period.

Figure 4-27 illustrates the effect of the growth substrate on the power density at a growth period of 3 months. Figure 4-27B shows the initial 25 h of the experimental run. Here it is observed that the addition of GAC improves the power density immensely. Here the control MFC does not have the growth and stationary phases, both configurations have a maximum after which depletion starts. The addition of GAC improves the maximum power by 5.7 times. From Figure 5-3 the depletion rate of the control MFC after a 3 month growth period is 70 mW/m^3h for approximately 20 h, whereas from Figure 5-5 there are two distinct depletion rates in the GAC-MFC after a 3 month growth period. The first depletion rate is 1286 mW/m^3h for approximately 5 h and the second depletion rate 56 mW/m^3h for approximately 20 h. The total energy density of the GAC-MFC after 3 months is 64 % higher than the control MFC.

Figure 4-28 represents the power density generated by the different MFC configurations after a 4 month growth period. As can be observed from Figure 4-28B the maximum power density produced by the GAC filled MFC is increased by 5.9 times compared to the control MFC. The depletion rate of the control MFC is 30 mW/m^3h for approximately 30 h according to Figure 5-3, and according to Figure 5-5 the first depletion rate of the GAC-MFC is 2000 mW/m^3h for approximately 4 h; the secondary depletion rate is 40 mW/m^3h for a duration of 35 h. The total energy density generated by the GAC-MFC is 32 % higher than that produced by the control MFC.

It is evident that the addition of GAC particles is beneficial to both the microbial growth and the power and energy generation. The graphite particles, by contrast, inhibited microbial growth, as found from the growth curve in Figure 4-4 and multiple SEM images and therefore power generation, leading to the equivalent of a blank cell. Due to these contradictory effects on the outcome, a mixture of the substrates was investigated. Figure 4-29 shows the results of triplicate repeats of the power generation of *G. sulfurreducens* grown on a mixture of GAC and graphite in a ratio of 1:1 after a growth period of 4 months. As can be seen from Figure 4-29, the results from this repeated experiment are quite varied. Biological systems present difficulty in predicting their responses. This is an example of this unpredictability. Two of the three runs illustrated a constant power density output over a large period of time. An air bubble was observed in the cathodic chamber next to the PEM membrane during the run. Figure 5-7

illustrates a schematic of the mechanism involved in a normal MFC and the effect of a bubble on the MFC internal circuit.

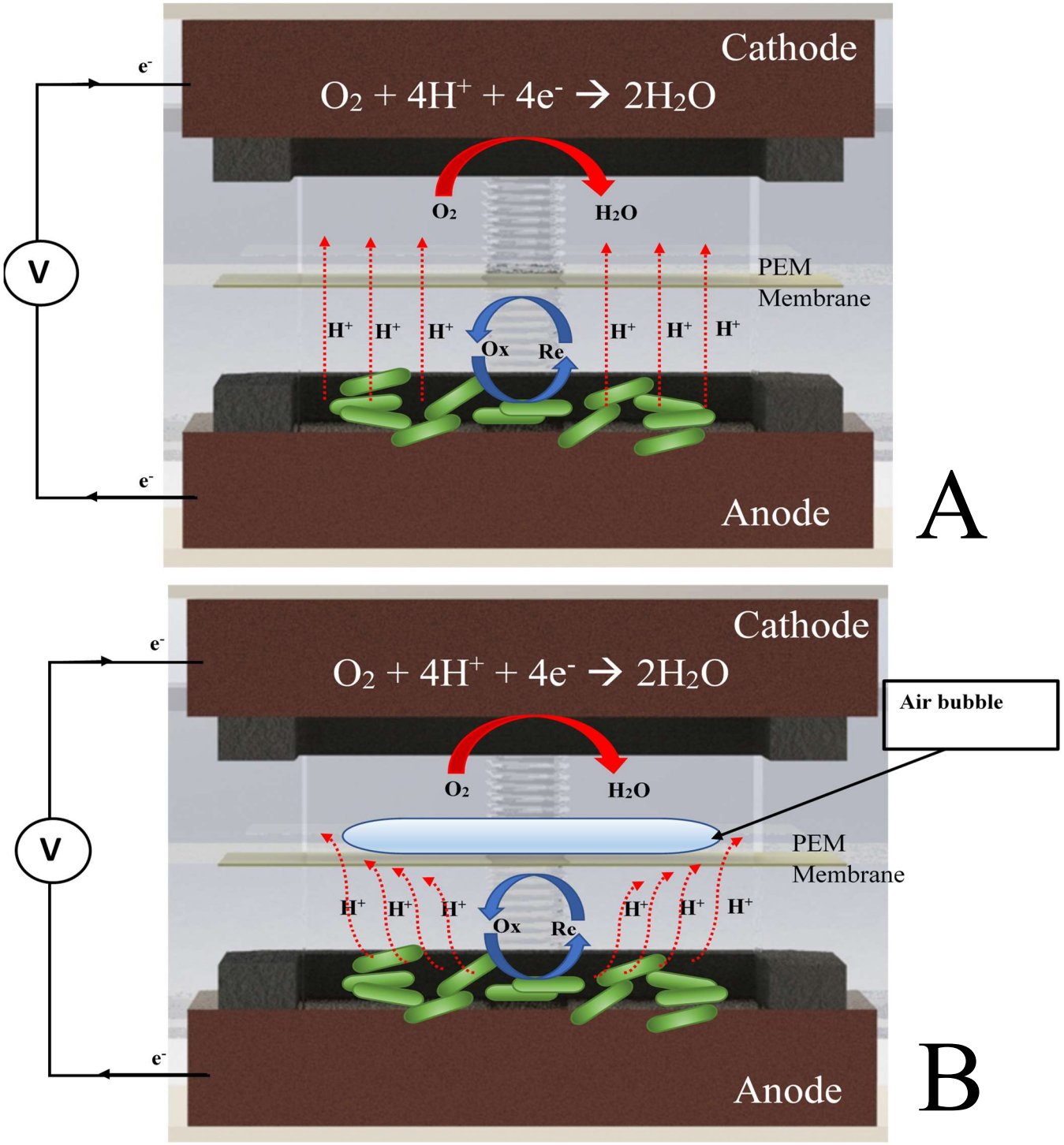

Figure 5-7: Schematic illustrating the mechanism of complete circuit (internal and external) (A); the result of bubble in cathodic chamber leading to broken internal ionic circuit (B).

As can be observed from the schematic in Figure 5-7A, the PEM membrane is permeable to the proton ions (H^+ ions) which react with the oxygen (O_2) on the surface of the cathode with

the following reaction: $O_2 + 4H^+ + 4e^- \rightarrow 2H_2O$. The larger the transfer surface, the higher the reaction activity will be. As soon as there is an object hindering the transfer path of the ions through the membrane, the activity of the MFC is lowered.

With the second repeat, (represented by '□' in Figure 4-29) containing the mixed carbon particles, a bubble was observed in the cathodic chamber. It is not clear when the bubble started to form, but it is certain that the entire PEM membrane surface was covered by the bubble after approximately 80 h. When a bubble covers the entire surface, there is no opening for the H^+ ions to move through, and so the internal ionic circuit is completely broken leading to a completely dead cell. This will result in the cell potential, and the power density, being zero as there is no reaction taking place inside the cell. With the blank cell there are reactions taking place from components in the electrolyte, leading to a small cell potential. If the circuit is broken, there can be no cell potential and therefore no power generation, i.e. a dead cell is the result.

If the bubble is small, only covering a small portion of the surface, it leads to reduced mass transfer, which leads to smaller reaction output, and so a lower cell potential. This is because the diffusion or mass transfer will need to be skewed around the bubble, leading to smaller number of ions being transferred through the membrane. The reaction activity is lowered due to delayed diffusion through a smaller area membrane. This phenomenon can be seen in Figure 5-7B.

Up until the bubble entered the system, the result was representative of the power density generated by *G. sulfurreducens* with the mixture of carbon substrates. Up to 60 h, the first and second repeats both maintained the maximum power density from start-up for a long period of time. The first repeat (represented by '○') maintained a power density of approximately 1800 mW/m^3 for 160 h before slowly starting to deplete. The second repeat (represented by '□') maintained a power density of approximately 1600 mW/m^3 before, after 60 h, completely depleting to 0 mW/m^3. The lower maximum power density can be due to the fact that there is a leak in the system, which means that the anodic chamber is not completely anoxic as expected and desired. Once the leak allowed for the bubble to form and increase in size to cover the entire area of the membrane the internal ionic circuit was broken which led to a completely "dead" cell.

The third repeat (represented by '◀' in Figure 4-29) showed a completely different profile to the other two repeats, with a maximum power density of 7500 mW/m^3. However, compared to Figure 4-33A, the profile of the third repeat is similar the profiles of the power density generated by *G. sulfurreducens* on GAC particles. Figure 5-8 shows the profiles of the power density generated by GAC-MFC after a growth period of 4 months and the third repeat of the MIX-MFC.

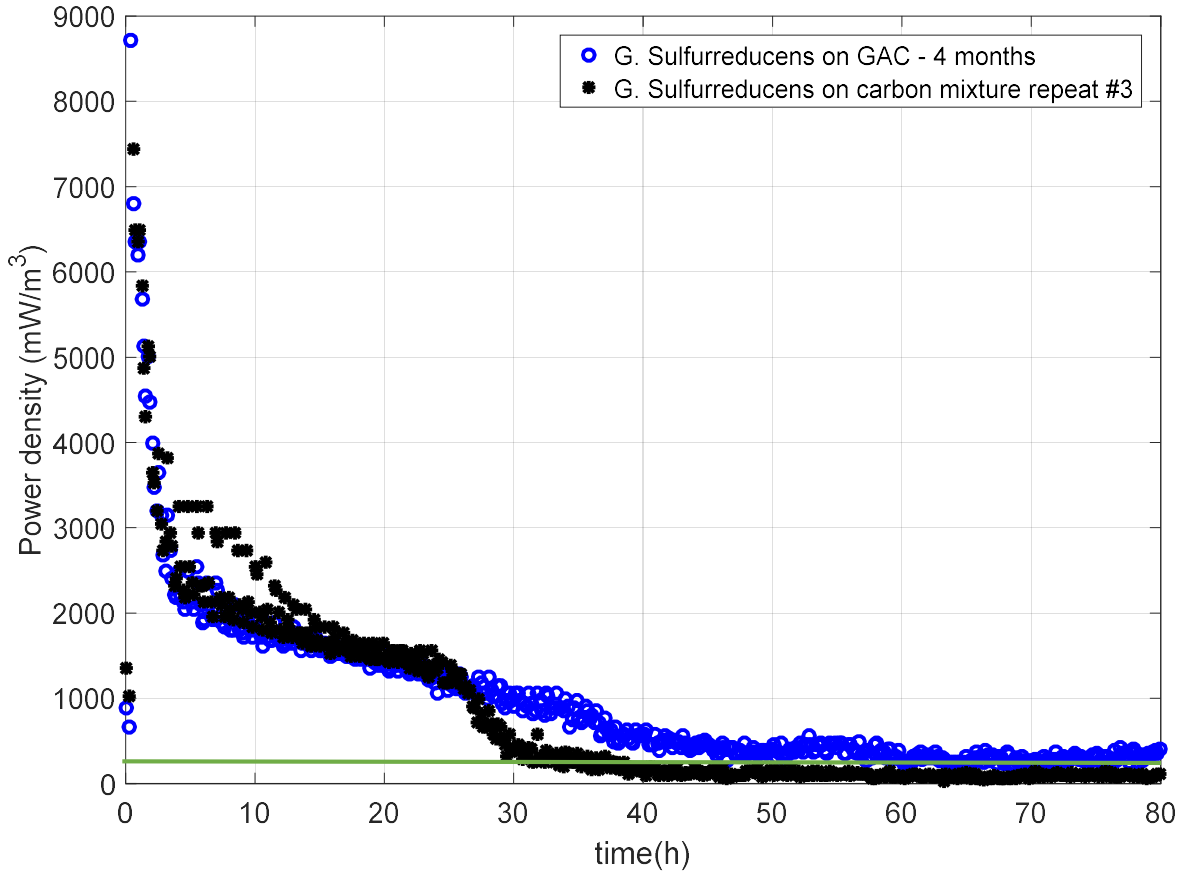

Figure 5-8: Power density (mW/m^3) generated by G. sulfurreducens on GAC particles ('○') and on a mixture of graphite and GAC particles to a ratio of 1:1 ('') after a 4 month growth period for the first 80 h. Blank cell average (—).*

As can be seen from Figure 5-8 the third repeated MIX-MFC illustrates the same profile as that from a pure GAC-MFC after a 4 month growth period. Both curves have an initial maximum at start-up, with distinct depletions rates. The GAC-MFC has two depletion rates whereas the MIX-MFC has three distinct depletion rates. One of the possible factors contributing to the MIX-MFC mimicking the GAC-MFC can be the packing of the bed. The carbon mixture particles are perhaps packed in such a way that the GAC particles contribute significantly more than the graphite particles, or that of the carbon mixture. The other reason for this response could be that the carbon mixture was not in a ratio of 1:1 as expected.

The energy density generated by these MFCs containing the carbon mixtures, especially the first two repeats (represented by the '○' and the '□') are very high compared to the other configurations. The first repeat MIX-MFC (represented by the '○') generated an astounding 1 MJ/m^3 energy density under an external load of 250 Ω, and a total energy density of 2.792 MJ/m^3. By the mere addition of graphite particles to the growth media containing GAC particles and *G. sulfurreducens*, and after a growth period of 4 months the total energy density was improved by 225% compared to the total energy density by the GAC-MFC with a growth period of 4 months. The second repeated MIX-MFC (represented by the '□') is representative of the energy density generated for 80 h, since the internal ionic circuit was broken in the middle of the experiment. It can be assumed that if the internal circuit was not broken the energy density could have doubled, leading to a total energy density of approximately 1.518 MJ/m^3. The total energy density of the third repeated MIX-MFC (represented by the '◀') is the same as the total energy density generated by the GAC-MFC with a 4 month growth period with a 4 % difference.

Figure 4-30 illustrates the power density generated by **all** MFC configurations after a growth period of 4 months for comparison purposes. A synergism can be observed from the use of the GAC and graphite mixture as growth substrate. The graphite particles alone inhibited microbial growth and consequently power generation, and with the addition of graphite to the GAC particles the power density generated by the *G. sulfurreducens* on the carbon mixture in the MFC is surpassed by the power generated by the MFC containing only GAC particles. As can be observed from this figure, the mixture of GAC and graphite particles as the growth substrate had a synergistic effect. This first and second repeats (represented by '◊' and '+') are the true representatives of a well-packed bed of carbon mixture filled MFC. The parameters required to ensure this synergistic outcome is a perfectly sealed, anoxic system to ensure that no bubbles disrupt the internal ionic circuit, and a well-distributed packed bed of carbon particles in the correct ratio. The ratio of graphite particles to GAC particles need to be investigated to find the optimum mixture ratio.

The summary of the maximum power density normalised to the anodic chamber volume of all configurations given in Table 5-4, can be compared to power densities achieved in the literature, given in Table 2-1. From this comparison, the maximum power output achieved by the MFCs in this investigation is larger (for pure microbial culture). On average, the pure *Geobacter sulfurreducens* MFC achieved a maximum power density of 2.9 W/m^3. With

addition of GAC particles to the initial growth media, the maximum power density was increased to an average of 17.0 W/m^3. The mixture of the two carbon substrates achieved an average maximum power density of 7.3 W/m^3. In Table 2-1 the MFC containing *Pseudomonas aeruginosa* using plain graphite as electrodes achieved a power density of 8.8 W/m^3. From Table 4-4 the average power density represents a value of power that is evenly distributed over the time-period. From this, the most successful mixed carbon MFC generated a power density of 4.85 W/m^3 in total, considering all external loads. This is extremely high compared to all pure community MFC systems from Table 2-1, even considering the average of the mixed carbon substrate MFCs the average power density is 2.53 W/m^3 which is high in comparison. The GAC filled MFC produces an average power density of 1.52 W/m^3 which is also relatively high compared to other systems.

However, as stated earlier, comparison of various MFCs are extremely difficult since there are many factors influencing the power outcome: continuous or batch; dual chamber vs single chamber or air-cathode cells; the total volume of the MFCs and more. It is therefore important only to compare MFCs with identical architecture, which is difficult to do. One also cannot merely consider the maximum power density as a performance rating. The MFCs in this investigation produce a maximum power at startup – mostly – and then display various depletion rates. It is therefore a better comparison to consider the total energy generated by the various cells. This data is not found in literature for comparison. It is important to consider the longevity of the power output, for instance. Considering only Table 4-4, the MFC containing only GAC particle performs better, by almost 75 %, than the mixed carbon substrate performance. This, however, does not consider the fact that with the mixed carbon substrates, the maximum power is maintained for a long period of time, unlike with the GAC where it depletes immediately. This is the reason why the energy density is considered.

The average total energy density for all configurations can be seen in Table 4-5. In this table it is again clear that the graphite-MFC delivers equivalent average total energy density to that of the blank cell, confirming the conclusion that this growth substrate inhibits growth and power generation. The addition of GAC particles to the control system, improved the average total energy density by 41 %. Using the data from the carbon MIX-MFC as generated (without modifying the second repeating MIX-MFC to the assumed value if the internal ionic circuit did not break and the cell did not die) the average total energy density was improved compared to the control MFC by 134 %, and 67 % improved compared to the GAC-MFC average. This

concludes that even with the flawed experimental MIX-MFCs, the results are improved immensely.

The energy density achieved by conventional fuels and batteries are summarised in Table 5-1.

Table 5-1: Energy densities of conventional sources.

Energy source	Energy Density (MJ/kg)	Density (kg/m^3)	Volumetric Energy Density (MJ/m^3)
Coal	32.5 [*1]	1345.68 [*3]	43700
CH_4 (Methane)	55.7 [*1]	161.74 [*3]	9010
Diesel	36 [*2]	815.9 [4]	29400
Methanol	18 [*2]	787 [*4]	14200
Li-ion Batteries	0.432 [*2]	2.34 [*5]	1011
NiCd batteries	0.144 [*2]	3.88 [*5]	558

[*1] (Rez, 2017)

[*2] (Kularatna, 2014)

[*3] (Perry and Green, 2008) – the density of bituminous coal is used

[*4] (Jia and Denbratt, 2018)

[*5] The density of the batteries was determined by measuring the mass and volume of two batteries and using an average – See Appendix D.

Most of the conventional energy sources are non-renewable sources. The energy density generated by the conventional energy sources, such as coal and fuels are high. However, there is a rapid fuel depletion and continued climate changes and focus on the carbon emissions and greenhouse gas emissions have shifted the attention to green or clean energy.

The conventional batteries produce high power densities compared to the bioelectrochemical cell investigated in this study. There are a few disadvantageous to the use of these conventional batteries. Because NiCd batteries contain cadmium, an environmentally hazardous substance, their disposal has become controversial. Alternative chemistries are therefore preferred. The newer lithium-based battery systems have overcome the safety and environmental obstacles set by previous battery systems and are the most efficient type of battery available (Kularatna, 2014).

Even though the power density of bioelectrochemical cells, i.e. microbial fuel cells, is much lower than that of conventional batteries there are many benefits to the utilisation of MFCs. These include the absence of harmful waste and the synergistic effect of utilising the MFC as a power source and a source to clean waste water. One can also increase the power density generated by connecting many MFCs in series or in parallel as illustrated by (Chouler et al., 2016). The power density produced in this investigation is only representative of one specific configuration; optimisation could increase the magnitude of power density, for example by using an inert cathode. The comparison is done to indicate where MFCs lie on the scale of energy density generation capabilities.

5.4 Modelling, prediction and up-scaling

A black box model was created to find the effect of each substrate on the various outcomes discussed in this investigation. A multivariable linear regression model was applied on the results obtained from the 4 months growth period with all the various MFC configurations. The data was found to be normally distributed and the linear relationship was found to be an adequate predictor. The outcomes investigated was the total energy density, both the average and maximum power density and the longevity of the MFC, in other words the length of time the cell generates power before reaching the "death" state or the equivalent power of the blank cell power density. The prediction models for the various outcomes are summarised in Table 5-2.

Table 5-2: Summary of models from linear regression.

Outcome	Model
Energy density	$E = 0.65 + (0.21\ x_{GAC}) - (0.48\ x_{graphite}) + (3.79\ x_{GAC} \cdot x_{graphite})$
Longevity	$t = 0.67 - (0.10\ x_{GAC}) - (0.67\ x_{graphite}) + (2.47\ x_{GAC} \cdot x_{graphite})$
Average power density	$P_{Ave} = 0.56 + (0.18\ x_{GAC}) - (0.42\ x_{graphite}) + (3.28\ x_{GAC} \cdot x_{graphite})$
Maximum power density	$P_{Max} = 1.60 + (6.90\ x_{GAC}) - (1.30\ x_{graphite}) - (3.07\ x_{GAC} \cdot x_{graphite})$

The models given in Table 5-2 represent all substrates as additives as well as a constant representing the MFC with no carbon substrate added. The models were modified to use the constant representing no carbon substrates as a base line, and the other constants were scaled in a range between 1 and -1 to compare the impact of the variable parameters to one another. To visually interpret the contribution of the substrates or additives to the outcomes, all scaled constants are plotted in Figure 5-9.

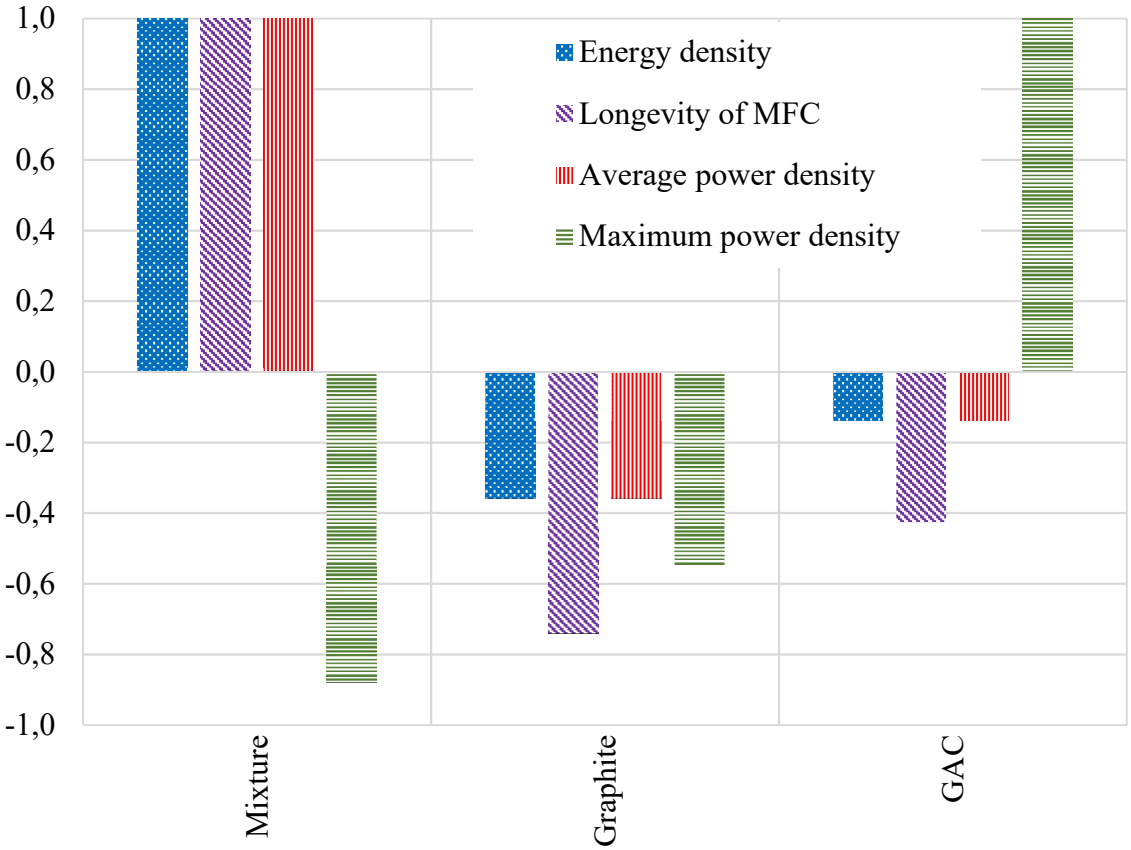

Figure 5-9: Constants using linear regression to express the effect of carbon substrates and their mixtures on the various outcomes described in this investigation.

Here it is clear that the mixed carbon contributes most favourably to all the overall outcomes. From this figure it is clear that the addition of GAC particles to the MFC leads to the best maximum power density, but as soon as graphite is added, the maximum power density is lowered, indicated by the negative green bar at the mixture section. The difference between these two additives is the longevity of the cells. One notices that the longevity of the GAC-MFC is negative, whereas the MIX-MFC is the best according to the graph. Although the addition of graphite negatively influences the maximum power, i.e. lowers the maximum power density achieved, this power is maintained for much longer once graphite is added. Graphite alone does not benefit the MFC in any regard. But as soon as graphite is added to the GAC particles, a synergistic effect is observed. This model was developed for a mixture of 50:50 graphite to GAC particles. The question now is, what ratio would be the optimum? By using the model created, it is possible to predict the outcomes with variable ratios of GAC and graphite in the MFC configuration. For all models described above, except for maximum power density model, the optimum ratio was determined to be 60:40 for GAC: graphite. With the

larger amount of GAC in the system, microbial growth is enhanced, ensuring sufficient growth in the system; then by adding the graphite particles, the conductivity is increased with an optimum ratio which enhances electron transfer.

The prediction models for the various parameters are represented in the Figure 5-10 to Figure 5-13. Since the objective was to compare the outcomes of MFCs after carbon substrates were added to the control MFC, the control MFC, with no carbon and only microbial cells, is indicated as the baseline (with a red square dotted line) in all the figures to enable easy comparison. The x-axis indicates the fraction of carbon mixtures, with the left margin indicating pure GAC and the right margin pure graphite. All possible mixtures lie between these points. If the mixing rule applies, then the outcome of all parameters (y-axis) will follow the mixing rule, indicated by the green long dash dot line. Anything above the baseline is an indication of an improvement to the normal control MFC.

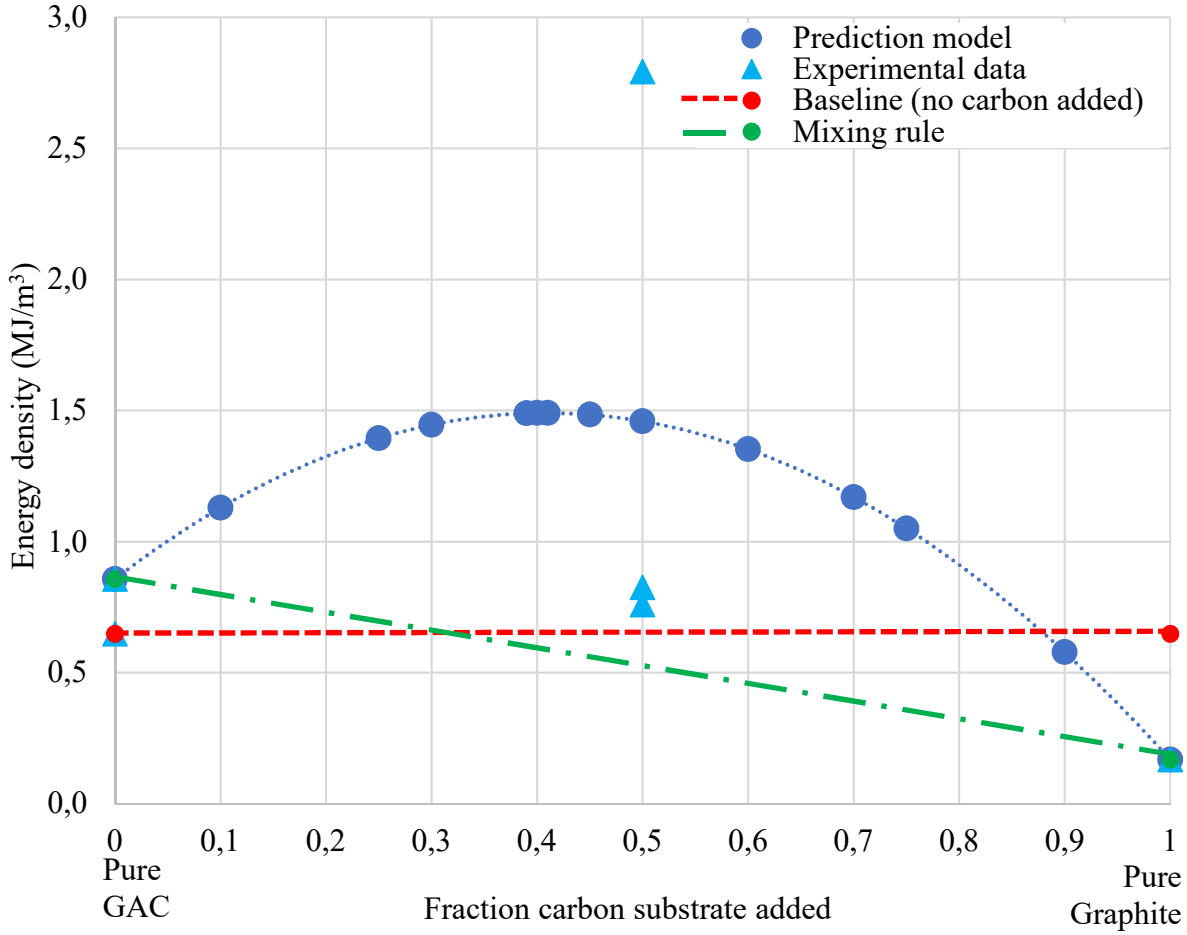

Figure 5-10: Prediction model for energy density from system.

Although the experimental data points have a large standard deviation due to the one cell not being properly sealed and the internal ionic circuit being broken, and the other cell had improper distribution of the carbon substrates (already discussed), the mixture of the two carbon substrates do not follow the mixing rule since there is a deviation from the linear line in the positive direction. This indicates and confirms that there is a synergistic effect.

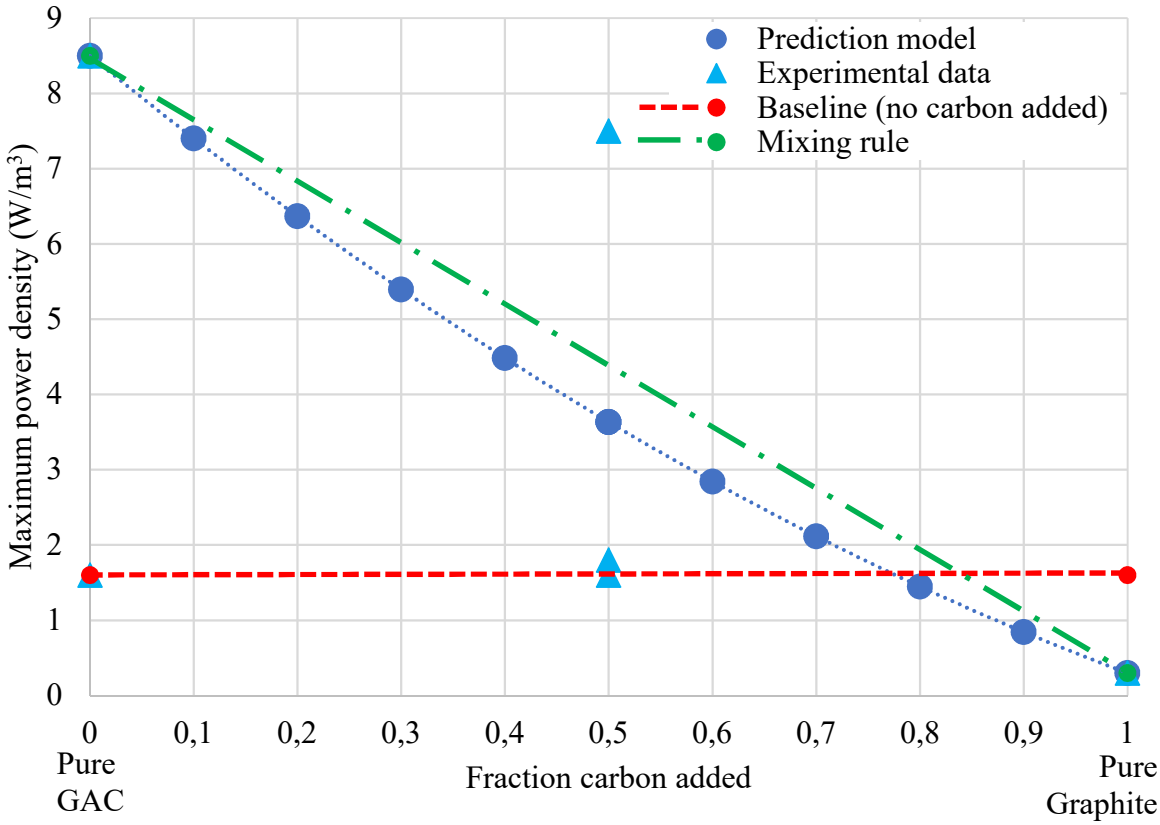

Figure 5-11: Prediction model for maximum power density from system.

From Figure 5-11 the significance of the effect of GAC addition to the control system is undeniable. The addition of pure graphite to the control MFC is unfavourable, and from the downward deviation from the mixing rule, it can be concluded that the mixture of the carbon substrates has an antagonistic effect on the maximum power density. However, from the figure it is clear that even with 70 % graphite and only 30 % GAC the mixture will still deliver higher maximum power densities than the control MFC.

The prediction models for the average power density and the longevity of the cells are described in Figure 5-12 and Figure 5-13, respectively. These profiles are similar to that of the energy density represented in Figure 5-10. The synergism of the mixture is clearly visible in these figures as well.

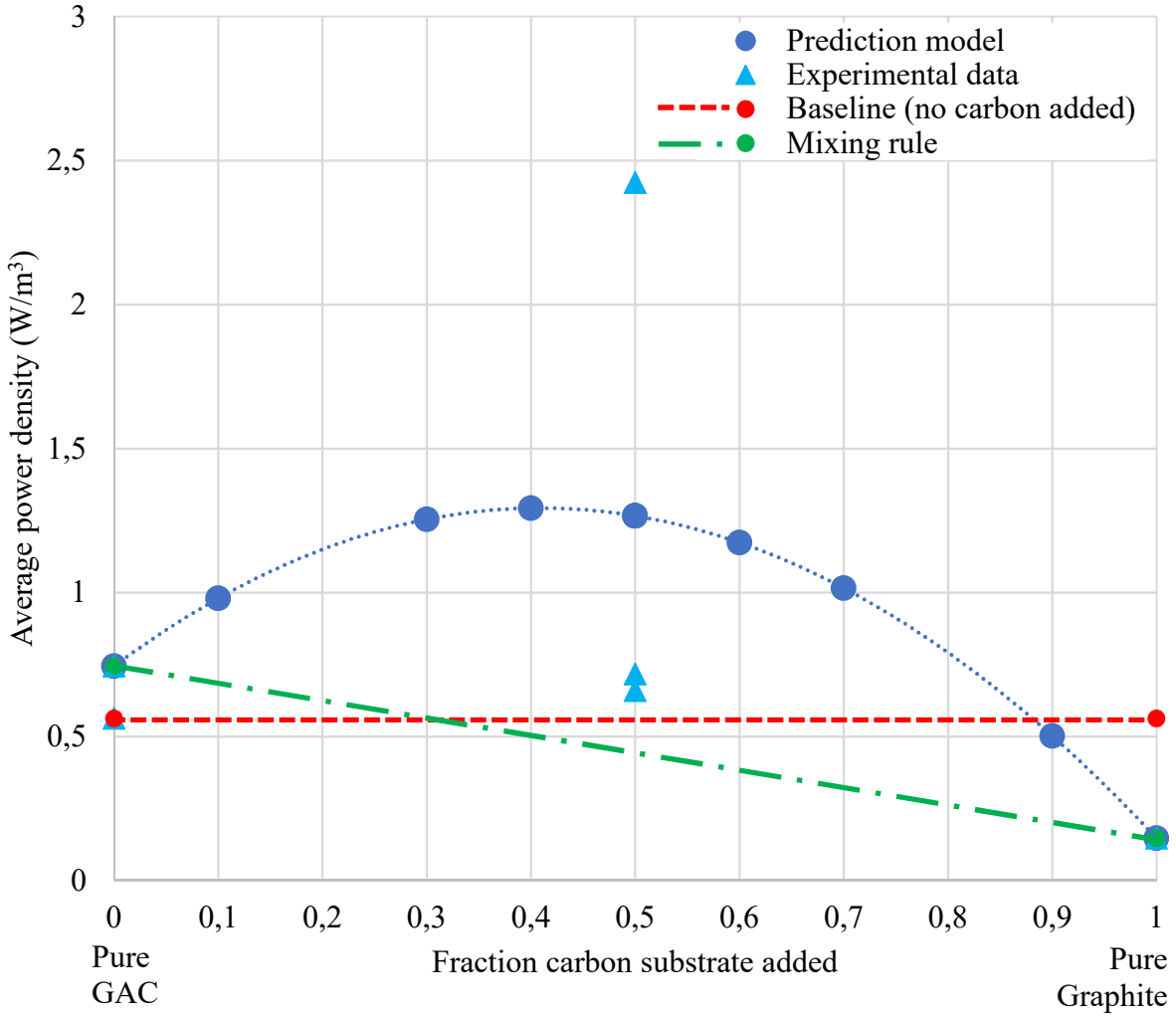

Figure 5-12: Prediction model for average power density from system.

Even though the mixture has a negative effect on the maximum power, the maximum is not the important parameter if it is not maintained. That is why the longevity and energy are the more important parameters to consider. The longevity is the length of time it takes for the cell before being completely depleted. From Figure 5-13 it is clear that the control MFC has a better longevity than when either GAC or graphite is added, individually. Once the mixture is introduced to the system, the synergism is significant. The longevity can be increased by almost 40 % according to the prediction if the optimum ratio is used.

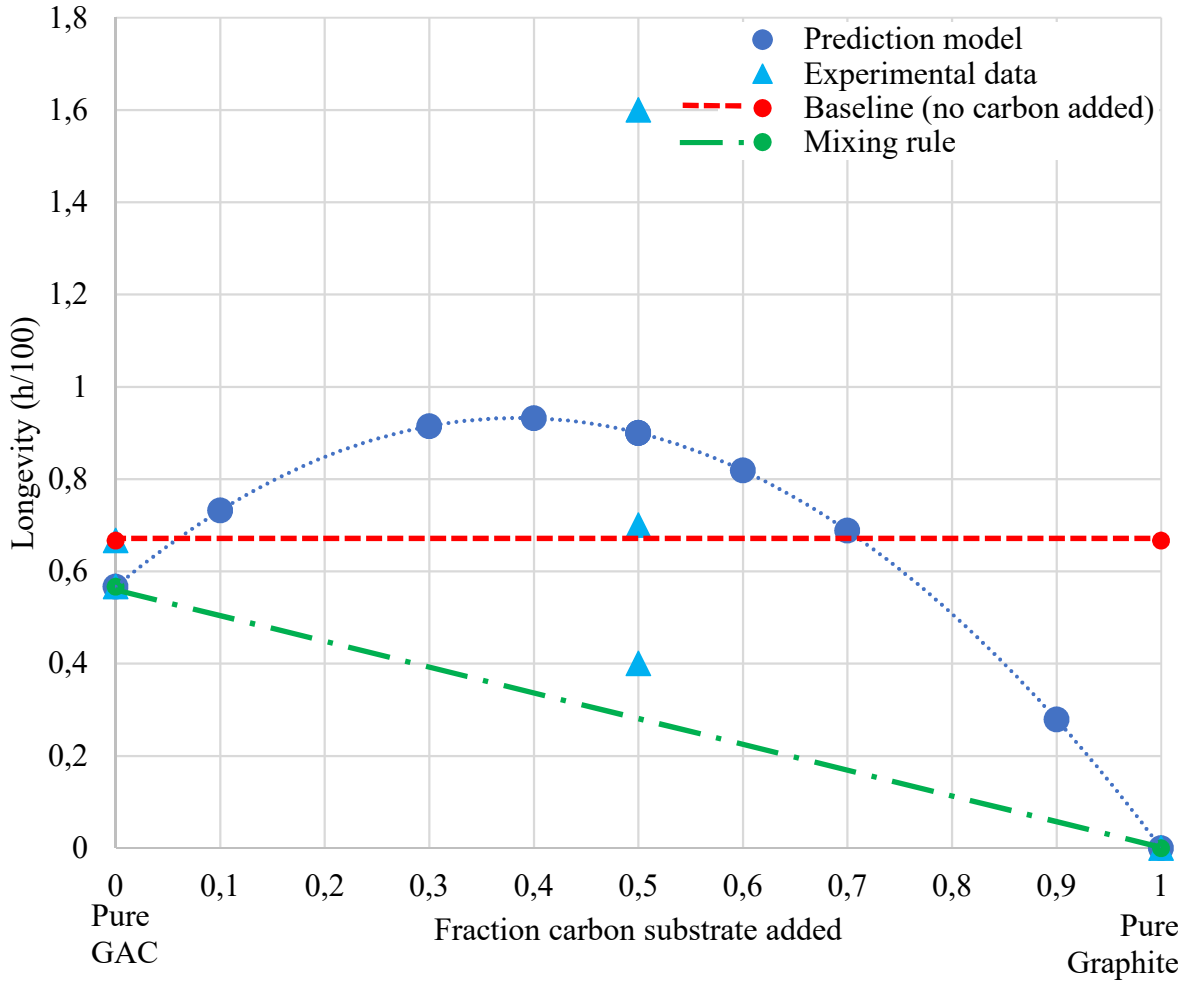

Figure 5-13: Prediction model for longevity from system.

All the prediction models are plotted in Figure 5-14. It is very important to notice that the data points used in this figure are predicted values from the models and not true experimental data points. In this one figure depicting all models, the overall synergism and deviation from the mixing rule is illustrated beautifully. Future work will be on the validation of the shape of the prediction models. The synergism is confirmed but the shape of the model needs more investigation and experimental data points, which will form part of future work.

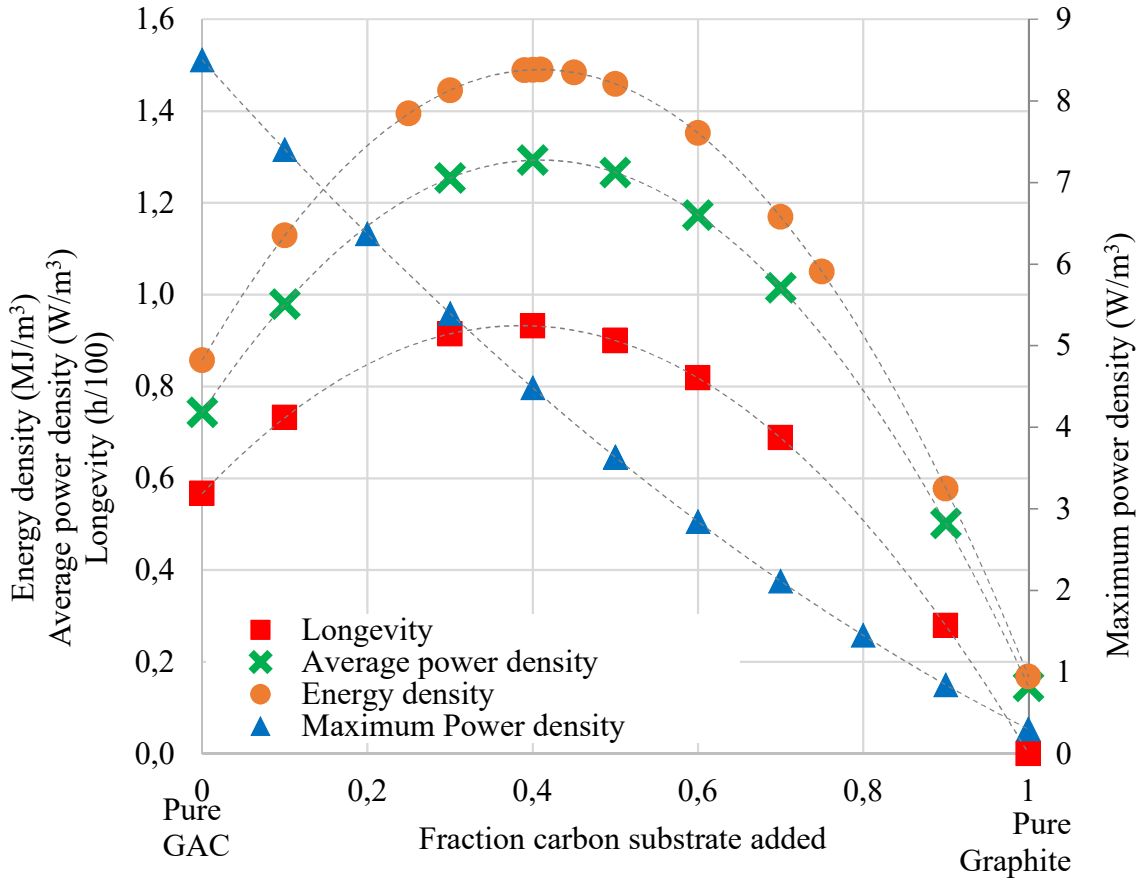

Figure 5-14: All prediction models of carbon substrates on various parameters. Data points are predicted values, not true experimental data points.

From the results obtained, one can investigate the possibility of utilising the MFCs found in this study in real-world applications. One scenario is to determine the number of MFCs connected in series required to generate enough power to light a 5 W LED bulb (assuming the bulb delivers a 250 Ω resistance) for one night, i.e. approximately 8 h. Considering the MFC with the carbon mixture as substrates, that delivered the highest energy density with a 250 Ω external load, 76 cells need to be connected in series to allow a 5 W LED light bulb to shine for a continuous 8 h.

Now one can optimise the cell by changing a few parameters, and consequently lower the number of cells required. If the electrode material is replaced with platinum, the cell potential can be increased with up to 15 % (Chouler et al., 2016, Logan et al., 2005). Using the optimum ratio of carbon substrates, i.e. 60 % GAC and 40 % graphite, the energy output can be increased by approximately 3 %. By continuously or periodically dosing the cells with nutrients as the microbial culture, the energy output can be increased. By finding the optimum ratio of electrode

surface area to chamber volume, i.e. increasing the surface area to chamber volume ratio which will decrease the average distance for electron transfer, decreasing internal resistance therefore increasing the power output (Ringeisen et al., 2006).

The optimum cell will have platinum electrodes (Watt-Smith et al., 2008a), with 60 % GAC particles and 40 % graphite particles, with a dosing system introducing fumarate as electron donor into the system periodically and aerating the cathodic chamber with oxygen as electron acceptor. It will have a larger ratio of surface area to chamber volume. This will increase the cell potential by at least 25 %, reducing the number of cells connected in series from 76 to approximately 60 cells in order to light a 5 W LED bulb for 8 h.

To save cost, one can also stack the cells on top of one another, utilising the one electrode as both the cathode for the one cell and the anode for the next, reducing material cost by eliminating the top and bottom plates for the intermediate cells; especially if the chosen electrode material is platinum, it would cut the cost of electrodes in half. These cells can then also be connected in series as required.

6. Conclusions and recommendations

The energy density of the MFC that uses a mixture of graphite and GAC particles as growth substrate is 134 % higher than that of the control MFC – containing only pure *Geobacter sulfurreducens*. The addition of the mixture of the two carbons results in a synergistic effect. The addition of only GAC to the MFC increased the average energy density by 41 % only, while the addition of pure graphite particles to the MFC had a negative effect, producing a lower energy density than the control MFC. The synergistic carbon mixture thus more than triples the power density of the MFC containing only pure GAC.

Even though MFCs deliver much lower power densities that conventional energy sources, there are many benefits to the utilisation of MFCs. These include the absence of harmful waste and the synergistic effect of utilising the MFC as a power source and a source to clean wastewater.

It was evident that the addition of GAC particles to the system was beneficial for bioelectrogenesis, since the maximum power density of the MFC containing GAC particles after a 4 months growth period was increased 6 fold, compared to the control MFC. The growth of *Geobacter sulfurreducens* was improved nearly 6 fold compared to the growth of *Geobacter sulfurreducens* in the absence of a growth substrate.

The graphite particles inhibited growth as well as bioelectrogenesis and it can be concluded that the MFC containing pure graphite as a growth substrate mimics the behaviour of the blank MFC, in the absence of any microbial culture.

It can also be concluded that longer growth periods of the growth media containing *G. sulfurreducens* and the desired carbon substrate before being inoculation into the MFC increases the overall outputs of the systems. A 4 month growth period in this investigation was concluded to be the most advantageous.

From the results it is abundantly clear that optimal growth plays a significant role in bioelectrogenesis. This is a vital parameter to prioritise when optimising the MFCs. The addition of GAC particles did not increase conductivity in the MFC. Since GAC is an amorphous carbon, it merely improved microbial growth which had a positive effect on the

system. It still needs to be investigated when in the growth cycle, i.e. when in the 4 months of growth, is the optimal time to start the harnessing of power generated by the microbial culture.

The increased conductivity in the absence of sufficient microbial growth proved to be moot, since there cannot be bioelectrogenesis in the absence of bio-organisms. It was however extremely well demonstrated that with the combination of sufficient microbial growth and increased conductivity – by the addition of both GAC particles for growth and graphite particles for conductivity – the performance of the MFCs was improved. It is now important to find an optimum ratio of carbon substrates.

The growth of the electricigen needs to be prioritised since the mechanism for power production relies on the oxidation and reduction of organic molecules that takes place due to microbial respiration. Therefor if there is a lack in sufficient microbial growth, bioelectrogenesis will be lowered due to the inactivity of the microbial community. Conductivity is, of course also important within the MFC. The microorganism chosen for this study is capable of producing highly conductive nanowires (Logan, 2009), therefor by increasing the conductivity in the MFC, the electrons will be transferred to the electrodes much easier with less resistance. Thus, it can be concluded that with sufficient microbial growth – by the addition of GAC particles – and with increased conductivity in the MFC – by the addition of graphite particles – bioelectrogenesis will be increase.

It can be concluded that the addition of a mixture an amorphous carbon to enhance growth and a crystalline carbon to enhance conductivity is beneficial to MFC bioelectrogenesis.

It is also imperative to acknowledge the possible practical issues one can encounter with running MFCs. In the event of an air-bubble entering an MFC, the internal ionic circuit can be hindered or broken, depending on the size and position of the bubble. This has many negative effects. In this investigation a large bubble entered the MFC covering the entire PEM surface, leading to the ultimate “death” of one of the MFCs filled with the mixture of the carbon substrates.

Another practical issue regarding the use of a mixed carbon substrate is the distribution of the packed bed of inorganic particles. The packed bed has an influence on the bioelectrogenesis since the particles settle out and lie on the surface of the electrode. In this investigation, the

mixed substrates were inoculated into the growth media at t = 0, where the growth increased with the substrates already in the media. Once the growth media is inoculated into the MFC the packed bed settles out and lies on the electrode. Depending on the distribution of the particles in the packed bed, the bed can have variable conductivity. If most of the GAC particles lie at the bottom in connection with the electrode surface and the graphite particles merely form a layer on the GAC particles, the MFC will mimic the performance of a pure GAC filled MFC. It is assumed that a well-distributed bed is ideal, since the microbial cells attach to the GAC particles easily, and the electron transfer will be aided with graphite particles in the vicinity. Therefore, if the entire bed is well-distributed, all GAC/microbial cells are surrounded by graphite particles to aid with the electron transfer, and the power harnessed will be larger. It is suspected that if the graphite particles formed a bed at the bottom with the GAC on top of the graphite, the conduction will be lower due to the lack of growth on the graphite particles which are in direct contact with the electrode. It is recommended that variable packing distributions be investigated.

It is also recommended that the effect of varied ratios of carbon substrates and the effect of various packing distributions of the carbon mixtures be investigated. The results suggest that microbial growth needs to be prioritised, but once growth has been established, increased conductivity improves bioelectrogenesis. From the model it can be predicted that a mixture with a ratio of 60:40 (GAC: graphite) is required to increase growth and conductivity and consequently improve the overall energy output from the MFC. This, however, needs to be investigated and proved.

It has been established from the literature that dosing the MFC with continuous or periodic substrate (acetate or fumarate in this system) will increase bioelectrogenesis. Therefore, another recommendation is to operate the system under continuous conditions and dosing the MFC periodically to observe the effect of increased nutrients for the microbial culture on the power output (Ringeisen et al., 2006).

By optimising the MFC architecture, one can improve the power output. By replacing the copper electrodes with graphite or platinum electrodes (Watt-Smith et al., 2008a) the power will increase due to increase conductivity and the inertness of the material. The power output has shown to improve by 15.6 % by replacing a Pt-free cathode with a Pt cathode (Chouler et al., 2016, Logan et al., 2005). The voltages and currents produced by MFCs can be increased

by connecting stacked MFCs in series or parallel. By connecting cells in series, the voltages over the stacked MFC system can be added, with one common current flowing through each MFC. By connecting the MFCs in parallel, the currents of the stacked MFCs can be added, while the voltage will be an average of the system. Using this configuration, a desired voltage or current can be obtained by combining the appropriate amount of connected MFCs in either series or parallel. The electricity production will be influenced by external conditions such as the electrical circuit (Alterman et al., 2006, Logan et al., 2006). By stacking MFCs, the theoretical thermodynamic limitations can be overcome (Chouler et al., 2016). This is another way to increase the power output from the system investigated in this study.

It is well documented that numerous microbial fuel cells generate power by oxidation of compounds in wastewater (Davis and Higson, 2007). This is one application where impact can be maximised since the outcomes include bioelectrogenesis along with the removal of organic compounds from waste streams. It has been calculated that the wastewater from a town of 150 000 people could be used to generate approximately 2.3 MW of power, assuming 100 % efficiency. A power output of 0.5 MW is more realistic (Logan, 2005). From this review it is mentioned that up to 80 % of the chemical oxygen demand of the wastewater can be removed by using an MFC and that the power generated could be used on site to power additional wastewater treatment.

Numerous implanted biomedical devices require power which is currently mostly supplied from batteries. These batteries need to be recharged or replaced in patients which necessitates additional surgeries. Finding a method of continual electricity generation within the body would revolutionise biomedical devices. The use of MFCs as power sources for implantable devices in humans is a promising focus point. MFCs offer advantages over existing technologies, like lithium-ion batteries in current implantable devices such as the heart pacemakers. The MFC would ideally use a biological metabolite fuel source (i.e. glucose or lactate) which is available in physiological fluids such as blood. It is unlikely that MFCs can replace the enzymatic glucose sensors that are currently used, but (Bettin, 2006) found that if a well-designed MFC system, operating in continuous flow, is implanted into the large intestines and uses the natural flora of microbes within, it could provide adequate power for cardiac pacing. This is one of the most promising future research areas. There are several variables that impact MFC power outputs, therefore intense research is still required. The one major problem that needs to be addressed is the longevity of many types of MFCs, most of

which would be capable of meeting demands for biomedical devices implanted for short-term applications only (Davis and Higson, 2007, Bettin, 2006).

Comparing conventional batteries to MFCs, it is clear that conventional energy sources produce high power densities compared to the typical bioelectrochemical cells. The use of conventional batteries has a few disadvantageous. For instance, NiCd batteries contain cadmium, which is an environmentally hazardous substance, so their disposal has become controversial. Therefore alternative chemistries are preferred. Although the newer lithium-based battery systems have overcome the safety and environmental obstacles set by previous battery systems and are the most efficient type of battery available (Kularatna, 2014), there is still interest in finding more environmentally friendly, waste-free energy sources. Even though MFCs deliver much lower power densities that conventional energy sources, there are many benefits to the utilisation of MFCs. These include the absence of in harmful waste and the synergistic effect of utilising the MFC as a green power source and a source to clean wastewater.

The first priority of future work is the validation of the prediction models by investigating a range of carbon substrate ratios. Additional future work should include the upscaling and architecture-optimisation of the MFC configuration. Thus far a relationship between the electrochemical parameters of a MFC and the evolution or growth of the microbial community has not yet been established (Alterman et al., 2006). Future work will be directed at finding a correlation between the growth culture and bioelectrogenesis.

7. References

ALTERMAN, P., RABAEY, K., THE PHAM, H., BOON, N. & VERSTRAETE, W. 2006. Continuous electricity generation at high voltages and currents using stacked microbial fuel cells. *Environmental Science & Technology Letters,* 40**,** 8.

ALYAMANI, A. & LEMINE, O. 2012. FE-SEM characterization of some nanomaterial. *Scanning Electron Microscopy.* InTech.

AMEND, J. P. & SHOCK, E. L. 2001. Energetics of overall metabolic reactions of thermophilic and hyperthermophilic Archaea and Bacteria. *FEMS Microbiology Reviews,* 25**,** 175-243.

ARENAS, L., DE LEÓN, C. P. & WALSH, F. 2017. Engineering aspects of the design, construction and performance of modular redox flow batteries for energy storage. *Journal of Energy Storage,* 11**,** 119-153.

AVILES, C., DEAN, W. & GOBBURI, B. 2017. Brewery Water and Process Water Management: The Golden, Green Opportunity Found in Anaerobic Treatment Solutions. *Master Brewers Association of the Americas,* 54**,** 41 - 44.

BARD, A. J., PARSONS, R. & JORDAN, J. 1985. *Standard potentials in aqueous solution,* New York, CRC press.

BARRET, C. 2000. Aerobots and hydrobots for planetary exploration. *38th Aerospace Sciences Meeting and Exhibit.* American Institute of Aeronautics and Astronautics.

BETTIN, C. 2006. *Applicability and Feasibility of Incorporating Microbial Fuel Cell Technology into Implantable Biomedical Devices.* Honors Thesis, The Ohio State University.

BOND, D. R. & LOVLEY, D. R. 2003. Electricity Production by Geobacter sulfurreducens Attached to Electrodes. *Applied and Environmental Microbiology,* 69**,** 1548-1555.

BRUNAUER, S., EMMET, P. & TELLER, E. 1938. S. Brunauer, PH Emmett, and E. Teller, *J. Am. Chem. Soc.,* 60**,** 309.

BULLEN, R. A., ARNOT, T. C., LAKEMAN, J. B. & WALSH, F. C. 2006. Biofuel cells and their development. *Biosensors and Bioelectronics,* 21**,** 2015-2045.

CHAUDHURI, S. K. & LOVLEY, D. R. 2003. Electricity generation by direct oxidation of glucose in mediatorless microbial fuel cells. *Nature Biotechnology,* 21**,** 1229.

CHENG, S., LIU, H. & LOGAN, B. E. 2006. Increased performance of single-chamber microbial fuel cells using an improved cathode structure. *Electrochemistry Communications,* 8**,** 489-494.

CHOULER, J., PADGETT, G. A., CAMERON, P. J., PREUSS, K., TITIRICI, M.-M., IEROPOULOS, I. & DI LORENZO, M. 2016. Towards effective small scale microbial fuel cells for energy generation from urine. *Electrochimica Acta,* 192**,** 89-98.

DAVIS, F. & HIGSON, S. P. J. 2007. Biofuel cells—Recent advances and applications. *Biosensors and Bioelectronics,* 22**,** 1224-1235.

DEVAL, A. & DIKSHIT, A. K. 2013. Construction, working and standardization of microbial fuel cell. *APCBEE Procedia,* 5**,** 59-63.

DUDLEY, R. & DALE, S. 2017. *BP Statistical Review of World Energy June 2017* [Online]. London UK. Available: https://www.bp.com/content/dam/bp/en/corporate/pdf/energy-economics/statistical-review-2017/bp-statistical-review-of-world-energy-2017-full-report.pdf [Accessed 3 June 2018].

FAN, Y., HU, H. & LIU, H. 2007. Enhanced Coulombic efficiency and power density of air-cathode microbial fuel cells with an improved cell configuration. *Journal of Power Sources,* 171**,** 348-354.

GHASEMI, M., DAUD, W. R. W., HASSAN, S. H. A., OH, S.-E., ISMAIL, M., RAHIMNEJAD, M. & JAHIM, J. M. 2013. Nano-structured carbon as electrode material in microbial fuel cells: A comprehensive review. *Journal of Alloys and Compounds,* 580**,** 245-255.

GILEADI, E. 1993. *Electrode kinetics for chemists, chemical engineers, and materials scientists*, Capstone.

JIA, Z. & DENBRATT, I. 2018. Experimental investigation into the combustion characteristics of a methanol-Diesel heavy duty engine operated in RCCI mode. *Fuel,* 226**,** 745-753.

JIANG, D., CURTIS, M., TROOP, E., SCHEIBLE, K., MCGRATH, J., HU, B., SUIB, S., RAYMOND, D. & LI, B. 2011. A pilot-scale study on utilizing multi-anode/cathode microbial fuel cells (MAC MFCs) to enhance the power production in wastewater treatment. *International Journal of Hydrogen Energy,* 36**,** 876-884.

KIM, B. C., POSTIER, B. L., DIDONATO, R. J., CHAUDHURI, S. K., NEVIN, K. P. & LOVLEY, D. R. 2008. Insights into genes involved in electricity generation in Geobacter sulfurreducens via whole genome microarray analysis of the OmcF-deficient mutant. *Bioelectrochemistry,* 73**,** 70-5.

KIM, H. J., PARK, H. S., HYUN, M. S., CHANG, I. S., KIM, M. & KIM, B. H. 2002. A mediator-less microbial fuel cell using a metal reducing bacterium, Shewanella putrefaciens. *Enzyme and Microbial Technology,* 30**,** 145-152.

KIM, J., JIA, H. & WANG, P. 2006. Challenges in biocatalysis for enzyme-based biofuel cells. *Biotechnology Advances,* 24**,** 296-308.

KULARATNA, N. 2014. *Energy Storage Devices for Electronic Systems: Rechargeable Batteries and Supercapacitors,* London, Academic Press.

LIN, W., COPPI, M. V. & LOVLEY, D. 2004. Geobacter sulfurreducens can grow with oxygen as a terminal electron acceptor. *Applied and Environmental Microbiology,* 70**,** 2525-2528.

LOGAN, B. E. 2005. Simultaneous wastewater treatment and biological electricity generation. *Water Science and Technology,* 52**,** 31-37.

LOGAN, B. E. 2009. Exoelectrogenic bacteria that power microbial fuel cells. *Nature Reviews Microbiology,* 7**,** 375.

LOGAN, B. E., HAMELERS, B., ROZENDAL, R., SCHRODER, U., KELLER, J., FREGUIA, S., AELTERMAN, P., VERSTRAETE, W. & RABAEY, K. 2006. Microbial Fuel Cells Methodology and Technology. *Environmental Science & Technology Letters,* 40**,** 12.

LOGAN, B. E., MURANO, C., SCOTT, K., GRAY, N. D. & HEAD, I. M. 2005. Electricity generation from cysteine in a microbial fuel cell. *Water Research,* 39**,** 942-952.

LOGAN, B. E. & REGAN, J. M. 2006. Electricity-producing bacterial communities in microbial fuel cells. *Trends Microbiol,* 14**,** 512-8.

LOGAN, B. E., WALLACK, M. J., KIM, K.-Y., HE, W., FENG, Y. & SAIKALY, P. E. 2015. Assessment of Microbial Fuel Cell Configurations and Power Densities. *Environmental Science & Technology Letters,* 2**,** 206-214.

MANO, N., MAO, F. & HELLER, A. 2003. Characteristics of a miniature compartment-less glucose− O2 biofuel cell and its operation in a living plant. *Journal of the American Chemical Society,* 125**,** 6588-6594.

MATLOCK, B. 2015. Assessment of nucleic acid purity. *Thermo Fisher Scientific.[verkkojulkaisu].[Viitattu 2017-11-23.] Saatavissa: https://tools. thermofisher. com/content/sfs/brochures/TN52646-E-0215M-NucleicAcid. pdf.*

MCMILLAN, W. & TELLER, E. 1951. The assumptions of the BET theory. *The Journal of Physical Chemistry,* 55**,** 17-20.

MINTEER, S. D., LIAW, B. Y. & COONEY, M. J. 2007. Enzyme-based biofuel cells. *Current Opinion in Biotechnology,* 18**,** 228-234.

OSMAN, M., SHAH, A. & WALSH, F. 2010. Recent progress and continuing challenges in bio-fuel cells. Part II: Microbial. *Biosensors and Bioelectronics,* 26**,** 953-963.

OSMAN, M., SHAH, A. & WALSH, F. 2011. Recent progress and continuing challenges in bio-fuel cells. Part I: Enzymatic cells. *Biosensors and Bioelectronics,* 26**,** 3087-3102.

PERRY, R. H. & GREEN, D. W. 2008. Perry's chemical engineers' handbook. 8th ed. ed. New York: McGraw-Hill.

RABAEY, K., BOON, N., HÖFTE, M. & VERSTRAETE, W. 2005a. Microbial phenazine production enhances electron transfer in biofuel cells. *Environmental Science & Technology,* 39**,** 3401-3408.

RABAEY, K., CLAUWAERT, P., AELTERMAN, P. & VERSTRAETE, W. 2005b. Tubular microbial fuel cells for efficient electricity generation. *Environmental Science & Technology,* 39**,** 8077-8082.

RABAEY, K. & VERSTRAETE, W. 2005. Microbial fuel cells: novel biotechnology for energy generation. *TRENDS in Biotechnology,* 23**,** 291-298.

REZ, P. 2017. *The simple physics of energy use,* Oxford, Oxford University Press.

RINGEISEN, B. R., HENDERSON, E., WU, P. K., PIETRON, J., RAY, R., LITTLE, B., BIFFINGER, J. C. & JONES-MEEHAN, J. M. 2006. High power density from a miniature microbial fuel cell using Shewanella oneidensis DSP10. *Environmental Science & Technology,* 40**,** 2629-2634.

STEWART, J. 2011. *Calculus,* Belmont, USA, Brooks/Cole Cengage Learning.

THAUER, R. K., JUNGERMANN, K. & DECKER, K. 1977. Energy conservation in chemotrophic anaerobic bacteria. *Bacteriological Reviews,* 41**,** 100.

UCAR, D., ZHANG, Y. & ANGELIDAKI, I. 2017. An overview of electron acceptors in microbial fuel cells. *Frontiers in microbiology,* 8**,** 643.

VAN HEERDEN, X. 2015. *The influence of three different intercalation methods on the properties of exfoliated graphite.* MEng Chemical Engineering, University of Pretoria.

WALSH, F. C., ARENAS, L. F. & PONCE DE LEÓN, C. 2018. Developments in Electrode Design: Structure, Decoration and Applications of Electrodes for Electrochemical Technology. *Journal of Chemical Technology & Biotechnology*.

WALSH, F. C. & DE LEÓN, C. P. 2018. Progress in electrochemical flow reactors for laboratory and pilot scale processing. *Electrochimica Acta*.

WATT-SMITH, M., FRIEDRICH, J., RIGBY, S., RALPH, T. & WALSH, F. 2008a. Determination of the electrochemically active surface area of Pt/C PEM fuel cell electrodes using different adsorbates. *Journal of Physics D: Applied Physics,* 41**,** 174004.

WATT-SMITH, M., RIGBY, S., RALPH, T. & WALSH, F. 2008b. Characterisation of porous carbon electrode materials used in proton exchange membrane fuel cells via gas adsorption. *Journal of Power Sources,* 184**,** 29-37.

YOST, A. E., CHRISTY, A. D., ZHAO, L. & TUOVINEN, O. H. 2012. Impact of Increased Surface Area Cathodes Using Nanostructures in Microbial Fuel Cells for Electricity Production. *2012 Dallas, Texas, July 29 - August 1, 2012*.

8. Appendix A

8.1 Mechanical design

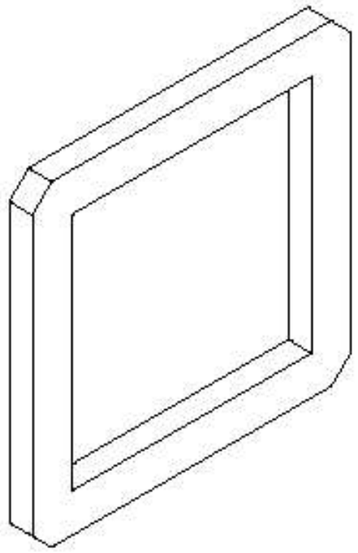

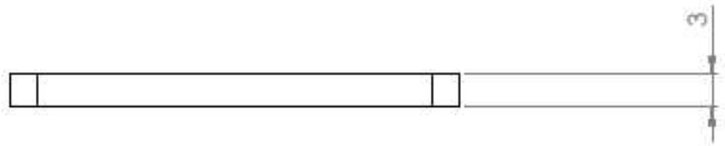

UNLESS OTHERWISE SPECIFIED: DIMENSIONS ARE IN MILLIMETERS SURFACE FINISH: TOLERANCES: LINEAR: ANGULAR:	Copyright University of Pretoria			DEBURR AND BREAK SHARP EDGES	DO NOT SCALE DRAWING	REVISION
NAME	DATE				TITLE: Cell gasket	
Xandra van Heerden						
		MATERIAL: Viton			DWG NO. vtGasket	A3
		WEIGHT:			SCALE:2:1	SHEET 1 OF 1

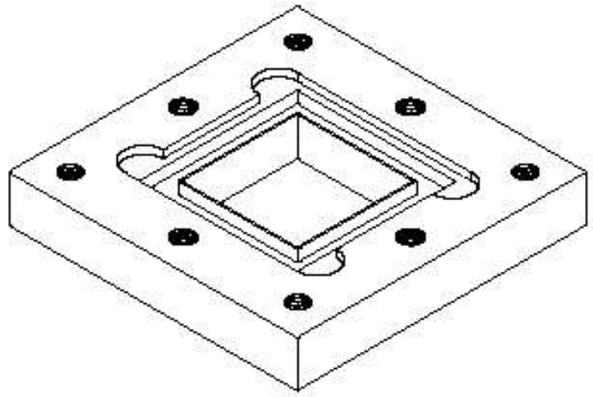

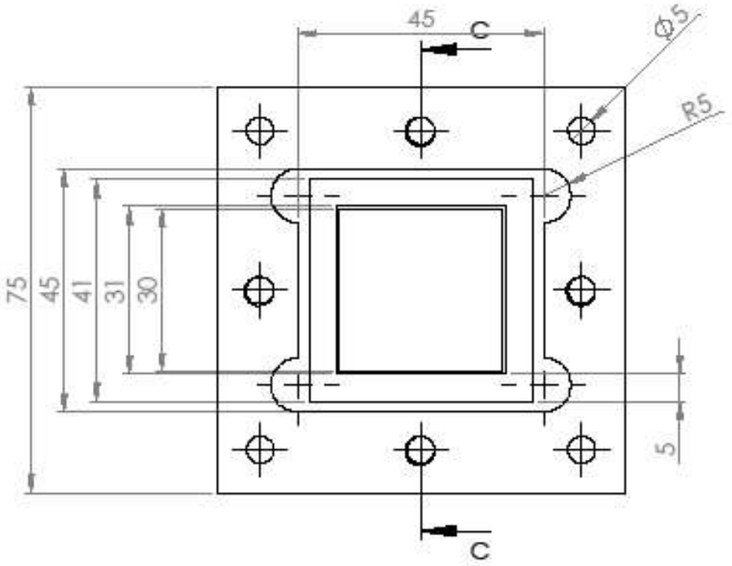

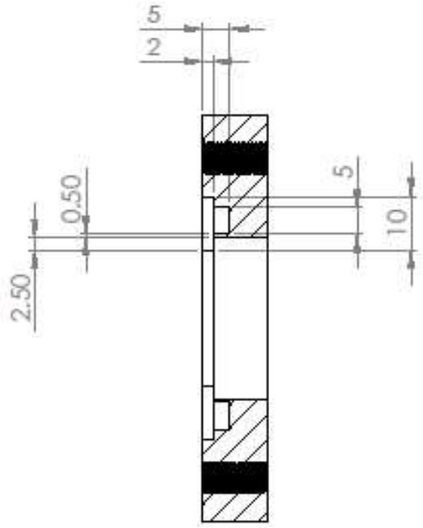

SECTION C-C

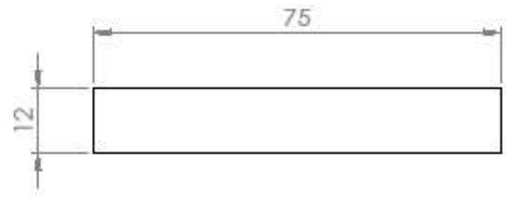

UNLESS OTHERWISE SPECIFIED: DIMENSIONS ARE IN MILLIMETERS SURFACE FINISH: TOLERANCES: LINEAR: ANGULAR:	Copyright University of Pretoria	DEBURR AND BREAK SHARP EDGES	DO NOT SCALE DRAWING / REVISION
NAME: Xandra van Heerden	DATE:		TITLE: Cell, mid plate, bottom
MATERIAL: Polycarbonate			DWG NO. pcMPB / A3
WEIGHT:			SCALE:1:1 / SHEET 1 OF 1

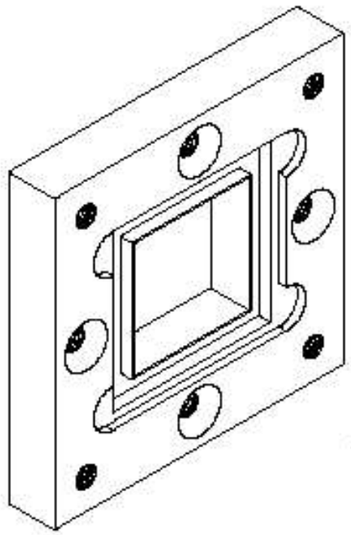

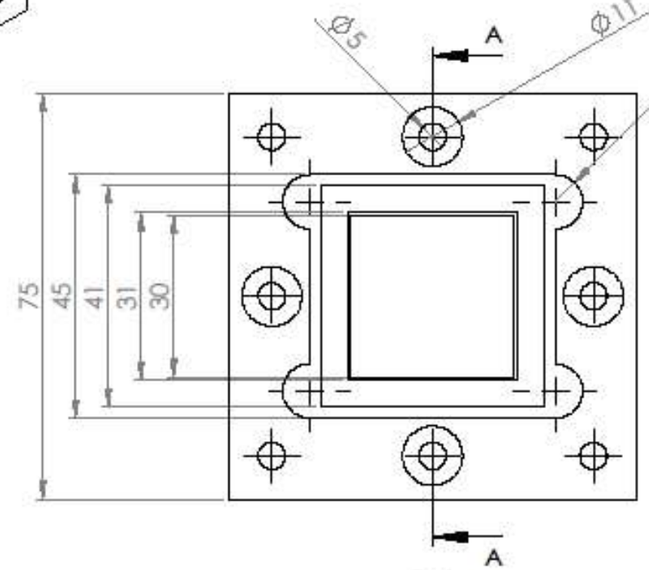

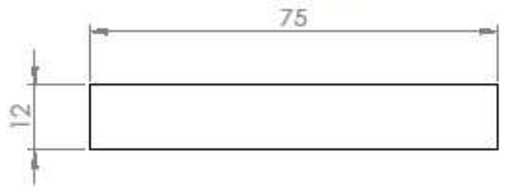

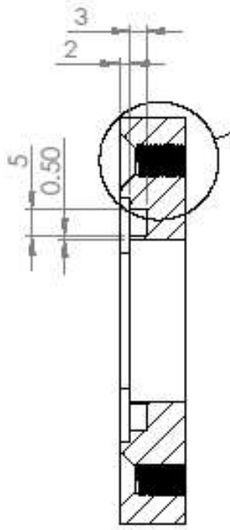

SECTION A-A

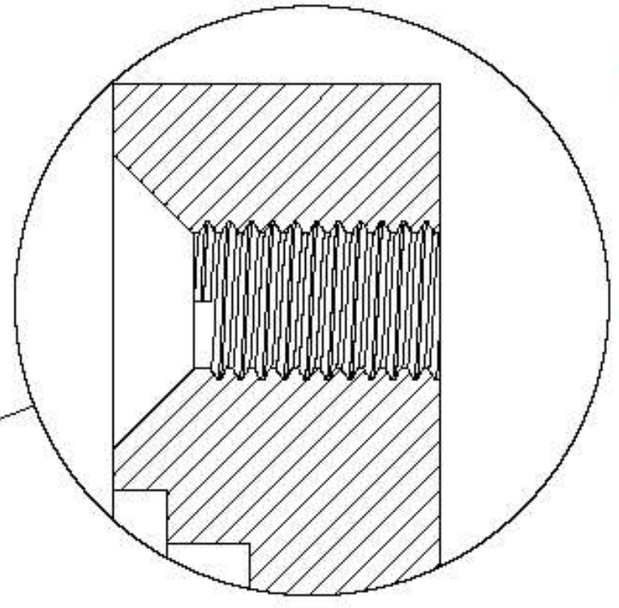

DETAIL B
SCALE 5 : 1

UNLESS OTHERWISE SPECIFIED: DIMENSIONS ARE IN MILLIMETERS SURFACE FINISH: TOLERANCES: LINEAR: ANGULAR:	Copyright University of Pretoria	DEBURR AND BREAK SHARP EDGES	DO NOT SCALE DRAWING / REVISION
NAME: Xandra van Heerden	DATE:	TITLE:	Cell, mid plate, top
MATERIAL:	Polycarbonate	DWG NO.	pcMPT / A3
WEIGHT:		SCALE:1:1	SHEET 1 OF 1

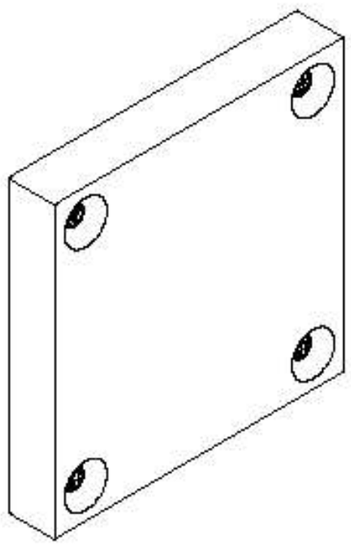

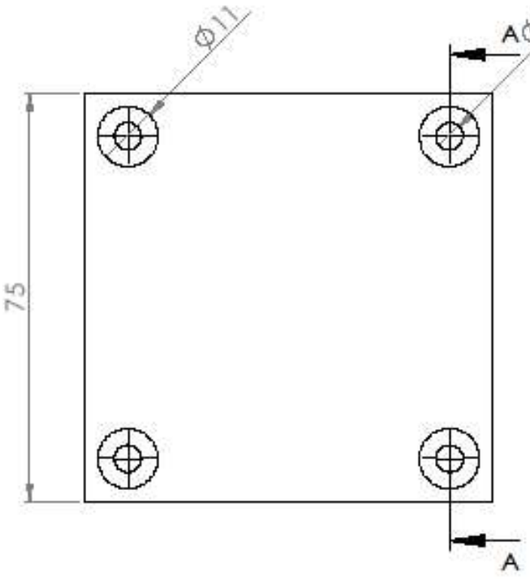

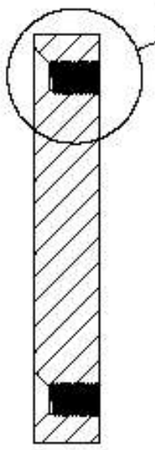

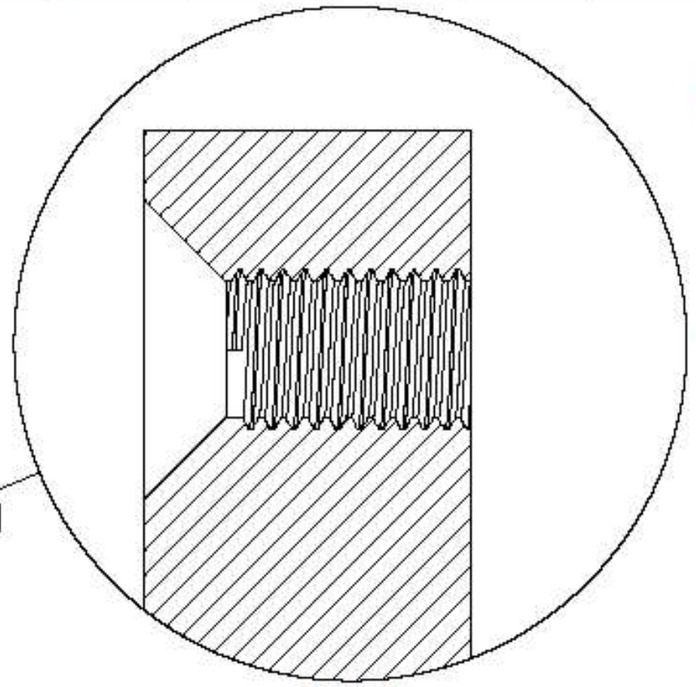

DETAIL B
SCALE 5 : 1

SECTION A-A

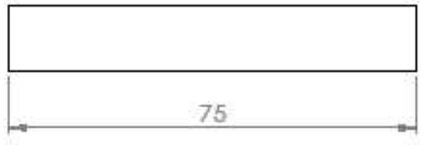

UNLESS OTHERWISE SPECIFIED: DIMENSIONS ARE IN MILLIMETERS SURFACE FINISH: TOLERANCES: LINEAR: ANGULAR:	Copyright University of Pretoria	DEBURR AND BREAK SHARP EDGES	DO NOT SCALE DRAWING / REVISION
NAME: Xandra van Heerden	DATE		TITLE: Cell outer plate
MATERIAL: Polycarbonate			DWG NO. pcTop / A3
WEIGHT:			SCALE:1:1 / SHEET 1 OF 1

9. Appendix B

9.1 Product sheet

ATCC

Product Sheet

Geobacter sulfurreducens
(ATCC® 51573™)

Please read this FIRST

Storage Temp.
Frozen: -80°C or colder
Freeze-Dried: 2°C to 8°C
Live Culture: See Propagation Section

Biosafety Level
1

Intended Use

This product is intended for research use only. It is not intended for any animal or human therapeutic or diagnostic use.

Citation of Strain

If use of this culture results in a scientific publication, it should be cited in that manuscript in the following manner: *Geobacter sulfurreducens* (ATCC® 51573™)

American Type Culture Collection
PO Box 1549
Manassas, VA 20108 USA
www.atcc.org

800.638.6597 or 703.365.2700
Fax: 703.365.2750
Email: Tech@atcc.org

Or contact your local distributor

Description

Designation: PCA
Deposited Name: *Geobacter sulfurreducens* Caccavo et al.
Product Description: Type strain. Genome sequencing strain.

Propagation

Medium
ATCC® Medium 1957: Geobacter medium

Growth Conditions
Temperature: 26°C to 30°C
Atmosphere: Anaerobic gas mixture, 80% N2-10% CO_2-10% H2 or 80% N_2-20% CO_2

Propagation Procedure

1. Keep vial frozen until ready to use.
2. To reduce media before inoculation, use 5% coenzyme M (0.1 mL per 10 mL). 1 M Fumarate (0.2 mL per 10 mL of broth and 0.2 mL per plate) needs to be added before inoculation. If needed, exchange the gas in the test tube for 80% N_2-20% CO_2 or 80% N_2-10% CO_2-10% H_2.
3. Under anaerobic conditions, thaw vial and then quickly transfer into a single tube of #1957 broth. A second tube of #1957 broth can also be inoculated with 0.5 mL from the original broth.
4. Incubate at 26°C to 30°C for 5 to 6 days. Subsequent transfers will grow faster following the initial recovery period.
5. Growth is evident by turbidity and an accumulation of cells at the bottom of the broth that are an orange/pink coloration.

ANAEROBIC CONDITIONS:
Anaerobic conditions for transfer may be obtained by either of the following:

- Use of an anaerobic gas chamber, or
- Placement of test tubes under a gassing cannula system hooked to anaerobic gas.

Anaerobic conditions for incubation may be obtained by any of the following:

- Loose screw caps on test tubes in anaerobic chamber,
- Loose screw caps on test tubes in an activated anaerobic gas pack jar, or
- Use of sterile butyl rubber stoppers on test tubes so that an anaerobic gas headspace is retained.

Notes

This culture grows well in broth. Incubation of up to 20 days may be required for growth on agar. Add 0.2 mL of 1M Fumarate to each plate prior to inoculation. Colonies on #1957 agar are pinpoint, circular, entire, low convex, pale orange and are best observed with a microscope.

No growth should occur on nonselective media. We strongly suggest obtaining reference Caccavo *et al.* Appl. Environ. Microbiol. 60: 37523759 (1994) for further information.

Purified genomic DNA of this strain is available as ATCC® 51573D-5™.
Additional information on this culture is available on the ATCC® web site at www.atcc.org.

References

References and other information relating to this product are available online at www.atcc.org.

Biosafety Level: 1

Appropriate safety procedures should always be used with this material. Laboratory safety is discussed in the current publication of the *Biosafety in Microbiological and Biomedical Laboratories* from the U.S. Department of Health and Human Services Centers for Disease Control and Prevention and National Institutes for Health.

ATCC Warranty

The viability of ATCC® products is warranted for 30 days from the date of shipment, and is valid only if the

10. Appendix C

10.1 Certificate of analysis: Granular activated carbon

Weck Laboratories, Inc.
Analytical Laboratory Service - Since 1954

Report Date: Wednesday, April 20, 2013
Received Date: Wednesday, March 30, 2013
Received Time: 9:00 am
Turnaround Time: Normal

Client: Activated Carbon Innovations cc.
P O Box 17990 Sunward Park, 1470
Boksburg South Africa

Phone: 072-880-8840
FAX: 2786-509-2741

Attn: Malcolm Bland
Project: Ref. 110322M
P.O.#:

Certificate of Analysis

Work Order No: 1D07028-01 **Sample ID:** Carbon Sample **Matrix:** Carbon
Sampled by: Client **Sampled:** 03/30/13 00:00 **Sample Note:**

Analyte	Result	Qualifier	Units	RL	Dilution	Method	Prepared	Analyzed	Batch
Apparent Density	0.388	A-01	g/cc		1x1	ASTM D2854	04/11/13 10:19	04/15/13 12:55	W1D0367
Ash Content %	1.66		% by Weight	0.0100	1x1	ASTM 2866	04/11/13 10:20	04/11/13 18:11	W1D0368
Ball-Pan Hardness Number	88		Units		1x1	ASTM D3802	04/12/13 11:38	04/20/13 10:30	W1D0427
Iodine, Triple Point	879		mg I2/g GAC		1x1	ASTM D4607	04/12/13 11:39	04/19/13 11:46	W1D0428
Moisture @ ASTM D2867	8.63		% by Weight	0.0100	1x1	ASTM D2867	04/11/13 17:47	04/12/13 15:22	W1D0399
Water Solubles	0.88		%	0.010	1x1	ASTM D5029	04/12/13 11:39	04/20/13 14:25	W1D0429

Case Narrative:

14859 East Clark Avenue, City of Industry, California 91745-1396 (626) 336-2139 FAX (626) 336-2634
www.wecklabs.com

10.2 Certificate of analysis: Graphite

Graphit Kropfmühl GmbH Langheinrichstraße 1 94051 Hauzenberg

University of Pretoria
Pretoria 0002
South Africa

CERTIFICATE OF ANALYSIS 3.1
EN 10204:2004

Material	Natural Crystalline Graphite
Grade	RFL 99.9
Delivery Date	January 2010
Quantity	1 small canister
Produced by	Graphit Kropfmühl GmbH Langheinrichstr. 1 94051 Hauzenberg

Carbon content:		99,9 %
Ash-Content		0,1 %
Particle Size	315 µm	24,1 %
	200 µm	54,3 %
	160 µm	15,7 %
	100 µm	4.0 %
	71 µm	0,6 %
	-71 µm	1,3 %

We confirm that the above-mentioned delivery has been produced in a continuous batch and tested according to the conditions valid for this grade. Goods are in conformity with quality specification relevant to grade ordered by you.

Document Date 10.04.2018

Graphit Kropfmühl GmbH
Langheinrichstr. 1
94051 Hauzenberg

Inspection representative

Graphit Kropfmühl GmbH
Langheinrichstraße 1
94051 Hauzenberg
Germany
Tel.: +49 8586 634-0
Fax: +49 8586 634-111
E-Mail: info@gk-graphite.com

Bankverbindung
HypoVereinsbank
BLZ 740 200 74
Kto. 8 725 180
IBAN DE47 7402 0074 0008 7251 80
SWIFT (BIC): HYVEDEMM448

Geschäftsführer
Thomas Junker, Torben Mölle
Aufsichtsrat (Vorsitzender)
Dr. Heinz Schimmelbusch
Amtsgericht Passau HRB 7432

WWW.GK-GRAPHITE.COM

11. Appendix D

Density of batteries:

NiCd battery 1:

Measuring mass of cylinder: m = 13.05 g

Volume of cylinder: V = 3.38 cm^3

Density: $\rho = m/V = 3.861$ g/cm^3

NiCd battery 2:

Measuring mass of cylinder: m = 13.17 g

Volume of cylinder: V = 3.38 cm^3

Density: $\rho = m/V = 3.896$ g/cm^3

NiCd Average:

Density: $\rho = m/V = 3.879$ g/cm^3

Li-ion battery 1:

Measuring mass of cylinder: m = 52.56 g

Volume of cylinder: V = 23.52 cm^3

Density: $\rho = m/V = 2.235$ g/cm^3

Li-ion battery 2:

Measuring mass of cylinder: m = 46.45 g

Volume of cylinder: V = 19.00 cm^3

Density: $\rho = m/V = 2.445$ g/cm^3

Li-ion Average:

Density: $\rho = m/V = 2.340$ g/cm^3

DNA sequencing

1. BioEdit Seq Alignment Editor = Notepad, nucleotide
2. NCBI – Blast database:

Blast result:

1. Geobacter sulfurreducens PCA chromosome, complete genome:
   Max score: 1083, Total score: 2166, Query cover: 100%, Identification: 100%,
   Accession: NC_002939.5

Full DNA Sequence:

>A_E9F

TCCTTCGGGGTGGTGAAAGTGGCGCACGGGTGAGTAACGCGTGGATAATCTGCC
CGAGGATTTGGGATAACATCTCGAAAGGGGTGCTAATACCGAATAAGCCCACGG
GGTCTACGGATCTTGCGGGAAAAGGGGGGGACTTTCGGGCCTCCTGTCTTCGGAT
GAGTCCGCGTACCATTAGCTAGTTGGTAGGGTAATGGCCTACCAAGGCGACGAT
GGTTAGCTGGTCTGAGAGGATGATCAGCCACACTGGAACTGAGACACGGTCCAG
ACTCCTACGGGAGGCAGCAGTGGGGAATTTTGCGCAATGGGGGAAACCCTGACG
CAGCAACGCCGCGTGGGTGATGAAGGCCTTCGGGTCGTAAAGCCCTGTCGGGAG
GGAAGAAATGATTGAGAGCTAATACCTCTTGGTCTTGACGGTACCTCCGAAGGA
AGCACCGGCTAACTCCGTGCCAGCAGCCGCGGTAATACGGAGGGTGCAAGCGTT
GTTCGGAATTATTGGGCGTAAAGCGCGTGTAGGCGGTCTTTTAAGTCTGATGTGA
AAGCCCCGGGCTCAACCTGGGAAGTGCATTGGAAACTGGGAGAC

Length: 3814128 Identities: 586/.586 (100%) Gaps: 0/586 (0%)

Geobacter sulfurreducens PCA chromosome, complete genome

Sequence ID: NC_002939.5 Length: 3814128 Number of Matches: 2

Range 1: 684763 to 685348 GenBank Graphics ▼ Next Match ▲ Previous Match

Score	Expect	Identities	Gaps	Strand
1083 bits(586)	0.0	586/586(100%)	0/586(0%)	Plus/Plus

```
Query  1       TCCTTCGGGGTGGTGAAAGTGGCGCACGGGTGAGTAACGCGTGGATAATCTGCCCGAGGA  60
               ||||||||||||||||||||||||||||||||||||||||||||||||||||||||||||
Sbjct  684763  TCCTTCGGGGTGGTGAAAGTGGCGCACGGGTGAGTAACGCGTGGATAATCTGCCCGAGGA  684822

Query  61      TTTGGGATAACATCTCGAAAGGGGTGCTAATACCGAATAAGCCCACGGGGTCTACGGATC  120
               ||||||||||||||||||||||||||||||||||||||||||||||||||||||||||||
Sbjct  684823  TTTGGGATAACATCTCGAAAGGGGTGCTAATACCGAATAAGCCCACGGGGTCTACGGATC  684882

Query  121     TTGCGGGAAAAgggggggACTTTCGGGCCTCCTGTCTTCGGATGAGTCCGCGTACCATTA  180
               ||||||||||||||||||||||||||||||||||||||||||||||||||||||||||||
Sbjct  684883  TTGCGGGAAAAGGGGGGGACTTTCGGGCCTCCTGTCTTCGGATGAGTCCGCGTACCATTA  684942

Query  181     GCTAGTTGGTAGGGTAATGGCCTACCAAGGCGACGATGGTTAGCTGGTCTGAGAGGATGA  240
               ||||||||||||||||||||||||||||||||||||||||||||||||||||||||||||
Sbjct  684943  GCTAGTTGGTAGGGTAATGGCCTACCAAGGCGACGATGGTTAGCTGGTCTGAGAGGATGA  685002

Query  241     TCAGCCACACTGGAACTGAGACACGGTCCAGACTCCTACGGGAGGCAGCAGTGGGGAATT  300
               ||||||||||||||||||||||||||||||||||||||||||||||||||||||||||||
Sbjct  685003  TCAGCCACACTGGAACTGAGACACGGTCCAGACTCCTACGGGAGGCAGCAGTGGGGAATT  685062

Query  301     TTGCGCAATGGGGGAAACCCTGACGCAGCAACGCCGCGTGGGTGATGAAGGCCTTCGGGT  360
               ||||||||||||||||||||||||||||||||||||||||||||||||||||||||||||
Sbjct  685063  TTGCGCAATGGGGGAAACCCTGACGCAGCAACGCCGCGTGGGTGATGAAGGCCTTCGGGT  685122

Query  361     CGTAAAGCCCTGTCGGGAGGGAAGAAATGATTGAGAGCTAATACCTCTTGGTCTTGACGG  420
               ||||||||||||||||||||||||||||||||||||||||||||||||||||||||||||
Sbjct  685123  CGTAAAGCCCTGTCGGGAGGGAAGAAATGATTGAGAGCTAATACCTCTTGGTCTTGACGG  685182

Query  421     TACCTCCGAAGGAAGCACCGGCTAACTCCGTGCCAGCAGCCGCGGTAATACGGAGGGTGC  480
               ||||||||||||||||||||||||||||||||||||||||||||||||||||||||||||
Sbjct  685183  TACCTCCGAAGGAAGCACCGGCTAACTCCGTGCCAGCAGCCGCGGTAATACGGAGGGTGC  685242

Query  481     AAGCGTTGTTCGGAATTATTGGGCGTAAAGCGCGTGTAGGCGGTCTTTTAAGTCTGATGT  540
               ||||||||||||||||||||||||||||||||||||||||||||||||||||||||||||
Sbjct  685243  AAGCGTTGTTCGGAATTATTGGGCGTAAAGCGCGTGTAGGCGGTCTTTTAAGTCTGATGT  685302

Query  541     GAAAGCCCCGGGCTCAACCTGGGAAGTGCATTGGAAACTGGGAGAC  586
               ||||||||||||||||||||||||||||||||||||||||||||||
Sbjct  685303  GAAAGCCCCGGGCTCAACCTGGGAAGTGCATTGGAAACTGGGAGAC  685348
```

2. Geobacter sulfurreducens_Strain AM-1 genome:
   Max score: 987, Total score: 1974, Query cover: 100%, Identification 100%,
   Accession: CP010430.1

Full DNA Sequence:

>B_E9F_

GTGGCGCACGGGTGAGTAACGCGTGGATAATCTGCCCGAGGATTTGGGATAACA
TCTCGAAAGGGGTGCTAATACCGAATAAGCCCACGGGGTCTACGGATCTTGCGG
GAAAAGGGGGGGACTTTCGGGCCTCCTGTCTTCGGATGAGTCCGCGTACCATTAG
CTAGTTGGTAGGGTAATGGCCTACCAAGGCGACGATGGTTAGCTGGTCTGAGAG
GATGATCAGCCACACTGGAACTGAGACACGGTCCAGACTCCTACGGGAGGCAGC
AGTGGGGAATTTTGCGCAATGGGGGAAACCCTGACGCAGCAACGCCGCGTGGGT
GATGAAGGCCTTCGGGTCGTAAAGCCCTGTCGGGAGGGAAGAAATGATTGAGAG
CTAATACCTCTTGGTCTTGACGGTACCTCCGAAGGAAGCACCGGCTAACTCCGTG
CCAGCAGCCGCGGTAATACGGAGGGTGCAAGCGTTGTTCGGAATTATTGGGCGT
AAAGCGCGTGTAGGCGGTCTTTTAAGTCTGATGTGAAAGCCCCGGG

Download GenBank Graphics Sort by: E value

Geobacter sulfurreducens strain AM-1 genome

Sequence ID: CP010430.1 Length: 4566144 Number of Matches: 2

Range 1: 2780488 to 2781021 GenBank Graphics ▼ Next Match ▲ Previous Match

Score	Expect	Identities	Gaps	Strand
987 bits(534)	0.0	534/534(100%)	0/534(0%)	Plus/Plus

```
Query  1        GTGGCGCACGGGTGAGTAACGCGTGGATAATCTGCCCGAGGATTTGGGATAACATCTCGA  60
                ||||||||||||||||||||||||||||||||||||||||||||||||||||||||||||
Sbjct  2780488  GTGGCGCACGGGTGAGTAACGCGTGGATAATCTGCCCGAGGATTTGGGATAACATCTCGA  2780547

Query  61       AAGGGGTGCTAATACCGAATAAGCCCACGGGGTCTACGGATCTTGCGGGAAAAgggggggg  120
                ||||||||||||||||||||||||||||||||||||||||||||||||||||||||||||
Sbjct  2780548  AAGGGGTGCTAATACCGAATAAGCCCACGGGGTCTACGGATCTTGCGGGAAAAGGGGGGGG  2780607

Query  121      ACTTTCGGGCCTCCTGTCTTCGGATGAGTCCGCGTACCATTAGCTAGTTGGTAGGGTAAT  180
                ||||||||||||||||||||||||||||||||||||||||||||||||||||||||||||
Sbjct  2780608  ACTTTCGGGCCTCCTGTCTTCGGATGAGTCCGCGTACCATTAGCTAGTTGGTAGGGTAAT  2780667

Query  181      GGCCTACCAAGGCGACGATGGTTAGCTGGTCTGAGAGGATGATCAGCCACACTGGAACTG  240
                ||||||||||||||||||||||||||||||||||||||||||||||||||||||||||||
Sbjct  2780668  GGCCTACCAAGGCGACGATGGTTAGCTGGTCTGAGAGGATGATCAGCCACACTGGAACTG  2780727

Query  241      AGACACGGTCCAGACTCCTACGGGAGGCAGCAGTGGGGAATTTTGCGCAATGGGGGAAAC  300
                ||||||||||||||||||||||||||||||||||||||||||||||||||||||||||||
Sbjct  2780728  AGACACGGTCCAGACTCCTACGGGAGGCAGCAGTGGGGAATTTTGCGCAATGGGGGAAAC  2780787

Query  301      CCTGACGCAGCAACGCCGCGTGGGTGATGAAGGCCTTCGGGTCGTAAAGCCCTGTCGGGA  360
                ||||||||||||||||||||||||||||||||||||||||||||||||||||||||||||
Sbjct  2780788  CCTGACGCAGCAACGCCGCGTGGGTGATGAAGGCCTTCGGGTCGTAAAGCCCTGTCGGGA  2780847

Query  361      GGGAAGAAATGATTGAGAGCTAATACCTCTTGGTCTTGACGGTACCTCCGAAGGAAGCAC  420
                ||||||||||||||||||||||||||||||||||||||||||||||||||||||||||||
Sbjct  2780848  GGGAAGAAATGATTGAGAGCTAATACCTCTTGGTCTTGACGGTACCTCCGAAGGAAGCAC  2780907

Query  421      CGGCTAACTCCGTGCCAGCAGCCGCGGTAATACGGAGGGTGCAAGCGTTGTTCGGAATTA  480
                ||||||||||||||||||||||||||||||||||||||||||||||||||||||||||||
Sbjct  2780908  CGGCTAACTCCGTGCCAGCAGCCGCGGTAATACGGAGGGTGCAAGCGTTGTTCGGAATTA  2780967

Query  481      TTGGGCGTAAAGCGCGTGTAGGCGGTCTTTTAAGTCTGATGTGAAAGCCCCGGG  534
                ||||||||||||||||||||||||||||||||||||||||||||||||||||||
Sbjct  2780968  TTGGGCGTAAAGCGCGTGTAGGCGGTCTTTTAAGTCTGATGTGAAAGCCCCGGG  2781021
```